

Development of Smart Skimming Technologies

**Dr. Gregory W. Johnson, Chris Grayson, Ken Dykstra, Adam Stromlund, Mark Wiggins,
Dr. Michele Fitzpatrick, and Dr. Peter Swaszek**

Alion Science & Technology, 1 Chelsea St., Ste. 200, New London, CT 06320

Contract No. E14PC00035

Deliverable 7 – Final Report

29 June 2016

Prepared for:

U.S. Department of the Interior, Bureau of Safety and Environmental Enforcement
45600 Woodland Road
Sterling, VA 20166

COR: Kristi McKinney

This final report has been reviewed by the BSEE and approved for publication. Approval does not signify that the contents necessarily reflect the views and policies of the BSEE, nor does mention of the trade names or commercial products constitute endorsement or recommendation for use.



This study was funded by the Bureau of Safety and Environmental Enforcement (BSEE), U.S. Department of the Interior, Washington, D.C., under Contract E14PC00035.

EXECUTIVE SUMMARY

Alion Science and Technology (Alion) proposed an Autonomous Oil Skimmer (AOS) to the Bureau of Safety and Environmental Enforcement (BSEE) in a white paper in January 2014. This concept was approved and funded for development by BSEE under Contract E14PC00035. Under this contract, Alion developed a skimmer system that can maneuver autonomously and skim the oil from a given area with automatic tracking and reporting of progress and performance. This AOS consists of a commercial-off-the-shelf (COTS) oil skimmer and vessel, a COTS autopilot system, a high precision navigation package, oil sensors and custom control software (see Figure ES-1). The result is a mobile and mountable navigation, sensor, and computer control system that can be used with a variety of skimmer and vessel systems for maximum oil spill response flexibility.



Figure ES-1: AOS attached to test vessel.

The oil sensor in the AOS is used to measure the thickness of the oil so the system can monitor the oil being skimmed in real-time and track oil thickness verses position as it is skimming. Based on the oil thickness gradients, the tracking algorithm directs the skimmer to head in the direction of thickest oil concentration while also monitoring the skimming coverage to ensure all areas are checked. The tracking algorithm communicates the desired direction of travel to the autopilot system, which controls the vessel's steering system to maneuver the AOS in the desired direction. As the AOS recovers the oil, statistics on oil thickness and oil recovery rate as a function of position are tabulated for real-time performance monitoring as well as stored for post-event evaluation.

One of the key enabling technologies for the AOS concept is a sensor to determine where the thickest oil is located. Alion surveyed the market and located only two companies with *potentially* viable products on the market; neither product was specifically designed for this application. Both COTS sensors (two different technologies used to detect and measure the

thickness of oil) were tested at Ohmsett in March 2015 with some success. They were both able to detect the oil-water transitions although the dynamic thickness measurements were less clear.

Both sensors suffered from poor hydrodynamic performance of their stock enclosures, which obscured raw sensor performance. As a result of the initial testing, Alion developed a new sensor mount based upon a buoyant hydrofoil attached to the end of a hinged outrigger beam, allowing vertical movement for wave-following capabilities (see Figure ES-2). While this new design improved the hydrodynamics of the sensors, the form factor of the sensors still induces flow problems that cannot be alleviated. These sensors were designed to be installed in tanks with either standing water or vertically moving water.

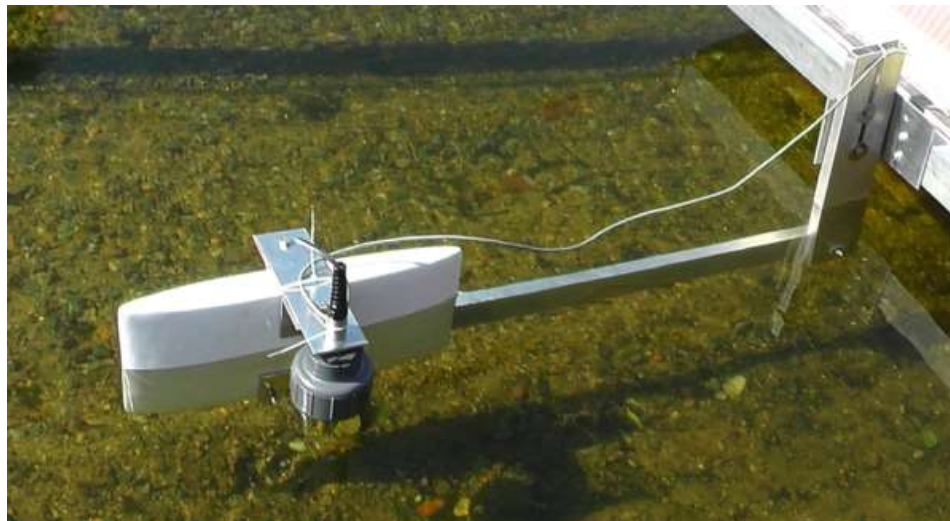


Figure ES-2: Alion-designed sensor float.

Alion then developed a complete AOS system prototype, including the new sensor mount with stand-alone sensor heads, and tested this on Gardner Lake in Salem, CT in September 2015. This system integrated the AOS system with a skimmer and vessel from Clean Venture. An autopilot control system for the outboard motor was installed by Three Belles Marina. The complete system performed well and demonstrated the concept of autonomous skimming. The original skimming algorithm used for the demonstration was a simple “lawn mower” pattern to recover the oil. During the testing it was discovered that the vessel’s operational characteristics did not match original assumptions with regards to turning rate, resulting in a lot of time being spent outside the oil slick area. Since the goal was to maximize the time in ideally the thickest oil, additional time was spent after the testing in investigating alternative algorithms in order to improve performance.

Seven different options were developed and tested in simulation. These were tested repeatedly to optimize the performance of each algorithm across the parameter space of each individual algorithm. These optimized algorithms were then contrasted to each other across a range of oil recovery time (0 – 60 hours) on three different oil spill patterns (oblong, round, and long thin). The looping (with flip) pattern (see Figure ES-3) seemed to perform the best of the seven across all times and patterns, although the absolute differences were not that great.

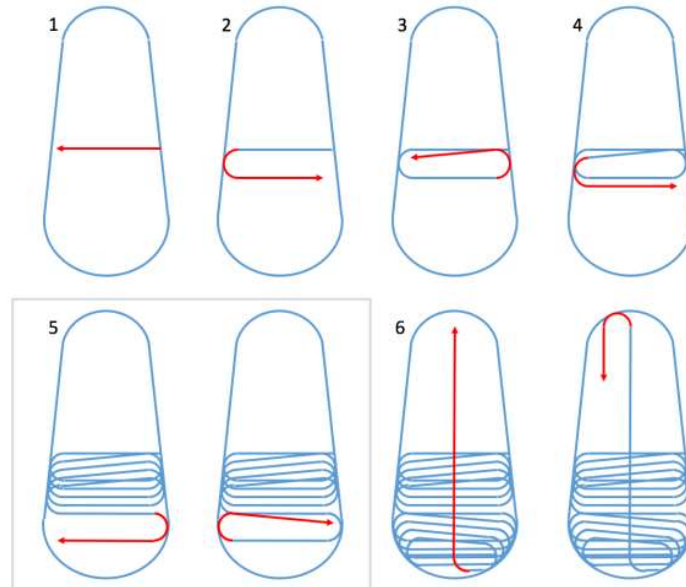


Figure ES-3: Looping algorithm pattern.

Both sensors were tested again at Ohmsett in March 2016 using the new sensor mount as part of the complete system. The new sensor mount performed much better and enabled the sensor heads to track very well in calm water and long period waves. Performance dropped off in short period waves as the combined motion of the boat, skimmer, and sensor float moving at different points on the wave train would cause the sensor head to lift out of the water or submerge at times. Both sensors again tracked oil-water transitions, although there was about a 4 second delay in one sensor's response due to the sensor electronics. Oil thicknesses of 5, 10, and 15 mm were tested and both sensors showed slight differences in response to the different thickness. There is no absolute calibration for either sensor, so absolute thickness to determine from the sensor reading alone is not possible without manufactures assistance and further testing. It would probably be difficult in a real world environment to accurately track thickness gradients other than very extreme gradients.

As an additional option that had not been identified initially, Alion investigated the use of infrared (IR) sensor imagery to determine oil thickness. An IR camera was procured and testing was conducted in Alion's lab and also concurrently with the Ohmsett system testing in March 2016. The initial exploratory efforts in this direction show great promise that IR imagery can perform as well as, if not better than, the other sensors tested without the disadvantages inherent in sensors that need to track the surface of the water in a dynamic situation (see Figure ES-4). There *are* environmental consideration such as sun glare and scintillation that need to be investigated more fully, but it appears that these affects can be filtered out. The IR imagery also cannot determine absolute thickness without some external reference or calibration; however, it is much more sensitive to thickness gradients.

In addition, the IR sensor provides a field of measurements (the sensor has 640x480 sensor points) as opposed to a point source like the other sensors, which provides the ability to see thickness gradients across a larger area instantly. This could provide look-ahead capability to the AOS algorithm as opposed to using just measurements where the skimmer is currently located.

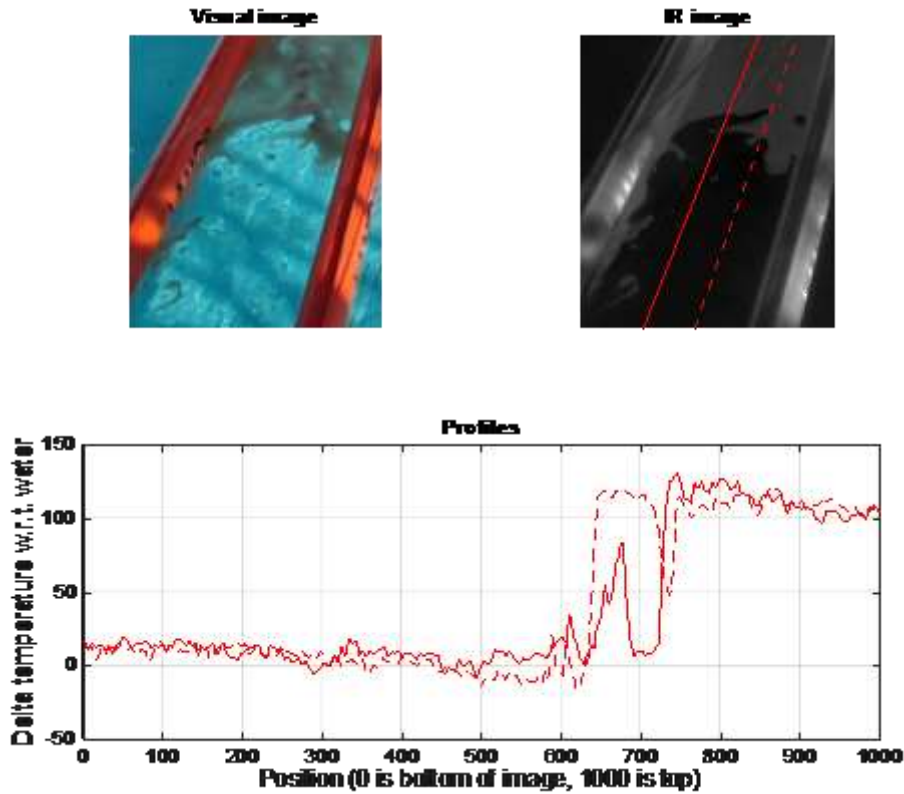


Figure ES-4: Data for a 5mm oil layer in calm water. Each graph line represents the thermal measurements along the respective line in the IR image.

The final sensor tested was an inline sensor to measure the percent water-in-oil in the discharge hose. The goal was to have a sensor to be able to measure the effectiveness of skimming operations in real-time. Only one COTS sensor was identified that might work for this. This sensor was tested during the March 2015 Ohmsett sensor testing and showed some promise. One of the test procedures of attempting to mix specific amounts of oil and water did not seem to yield a fully-mixed solution leading to erratic measurements. Measurements made using the discharge from skimmer yielded much better results; however, only limited samples were taken. Further samples were taken using this methodology during the March 2016 testing. Results show that this sensor appears to give reasonable estimates of oil percentage in the discharge line, as long as the oil concentration is better than 70%. Since most skimmers are designed to provide recovery efficiencies of 80% or more this should provide a capability that has some usefulness; coupled with a flow meter it could provide real-time tracking of recovery rates and efficiency.

Table of Contents

1. Introduction	1
2. Background.....	2
3. Sensor Selection and Initial Testing.....	3
3.1. Floating Sensors.....	3
3.1.1. GE Leakwise ID-227 Oil Sheen Monitoring System.....	3
3.1.2. Arjay 2852 HCF and 2852-PCD	4
3.2. Floating Sensor Calibration	5
3.3. Floating Sensor Tests.....	6
3.3.1. GE without Flow Diverter	6
3.3.2. GE with Flow Diverter.....	7
3.3.3. Arjay Sensors	8
3.4. Floating Sensor Results.....	8
3.5. In-Line Sensor.....	10
4. System Design	13
4.1. Navigation and Computer Systems.....	13
4.2. Oil Sensor Mounting.....	14
4.3. Autopilot System	14
4.4. Computer Control System.....	15
5. Open Water System Test	18
5.1. Vessel Installation.....	18
5.2. Gardner Lake Results.....	19
5.2.1. Initial Testing Results	19
5.2.2. Navigation System Test Results	21
5.2.3. Autopilot Test Results	21
5.2.4. PTZ IP Camera Test Results.....	22
5.2.5. Control Box issues identified in testing	22
6. Sensor Performance during Second Ohmsett Test	24
6.1. Oil Thickness Sensor Tests.....	24
6.1.1. Oil Slick Thickness Sensor - Setup.....	24
6.1.2. Oil Slick Thickness Sensor – Test Performed	26
6.1.3. Oil Slick Thickness Sensor Results	28
6.2. Discharge Line Oil Sensor Tests.....	33
6.2.1. Oil-in-Water Sensor – Setup	33
6.2.2. Oil-in-Water Sensor – Test Performed	35
6.2.3. Oil-in-Water Sensor – Results	37
7. Algorithm Performance	38
7.1. Algorithm Descriptions.....	39
7.1.1. Semi-random (Figure 38)	39
7.1.2. Star (Figure 39)	40
7.1.3. Figure-8 (Figure 40).....	40
7.1.4. Spiral (Figure 41)	41
7.1.5. Flower (Figure 42)	41

- 7.1.6. *Looping (Figure 43)*..... 42
- 7.2. Algorithm Simulation Methodology..... 42
- 7.3. Algorithm Simulation Results..... 43
- 8. Recommendations 47**
- 8.1. Thickness Sensors..... 47
- 8.2. Inline Sensor 47
- 8.3. Autopilot/vessel Integration..... 47
- 8.4. IR Sensor..... 48
- 8.5. Algorithm Development 50
- 8.6. Aerial Surveillance..... 50
- 8.7. Group Coordination / tracking..... 51
- 9. References 52**
- Appendix A. Initial Sensor Test Results A-1**
- A.1 GE Sensors..... A-1
- A.2 Arjay Floating Sensor A-3
- A.3 Arjay Flow Sensor A-6
- Appendix B. Alion Floating Sensor Mount B-1**
- Appendix C. Control Panel Schematic C-1**
- Appendix D. Arjay Sensor Results D-1**
- Appendix E. GE Sensor Results E-1**
- Appendix F. IR SENSING F-1**

Table of Figures

Figure ES-1: AOS attached to test vessel.	i
Figure 1: Autonomous Oil Skimmer Concept.	1
Figure 2: GE Leakwise ID-227.	3
Figure 3: Arjay 2852-HCF sensor (top) and sensor sled (bottom).	4
Figure 4: Bottom of sensor sled showing metal chute.	5
Figure 5: GE and Arjay calibration curves.	6
Figure 6: Picture of oil patches in lane, looking South (direction of travel).	7
Figure 7: GE sensor and flow diverter.	8
Figure 8: Example hydrodynamic issues present with GE sensor.	9
Figure 9: Example hydrodynamic issues with Arjay sensor.	10
Figure 10: Arjay 2852-IFA Oil in Water Sensor.	11
Figure 11: Raw sensor data from the first inline sensor test, using the combination of measured streams of water and oil (4-20 mA sensor data inverted to match other results).	11
Figure 12: Raw sensor data from the second inline sensor test, using the skimmer to mix the oil and water (4-20 mA sensor data inverted to match other results).	12
Figure 13: Arjay 2852-IFA inline sensor calibration curve (4-20 mA sensor data inverted to match other results).	12
Figure 14: AOS navigation and computer box block diagram.	13
Figure 15: Redesigned sensor float assembly.	14
Figure 16: Autopilot system block diagram.	15
Figure 17: Oil skimmer control software flowchart.	16
Figure 18: Oil Recovery Software Graphical User Interface.	17
Figure 19: Test location at Gardner Lake; boat launch indicated by yellow star.	18
Figure 20: Equipment layout on vessel for Gardner Lake test.	19
Figure 21: New skimmer float assembly in operation, note that the sensor and float remain perpendicular to front of skimmer.	20
Figure 22: Oil Recovery with limited turns.	21
Figure 23: Navigation/Control box on vessel.	23
Figure 24: AOS vessel.	25
Figure 25: Test diagram.	25
Figure 26: Example oil slick.	26
Figure 27: Arjay Sensor first run.	29
Figure 28: Screen capture of stray oil patch from Figure 27.	29

Figure 29: GE sensor example run.....	31
Figure 30: Screen capture of GE sensor entering oil patch.	31
Figure 31: Screen capture of GE sensor leaving oil patch.....	32
Figure 32: Screen capture of GE sensor prior to entering oil patch.....	32
Figure 33: Actual discharge sensor test setup.	34
Figure 34: Configuration for Discharge Line Sensor test (hydraulic lines not shown).	34
Figure 35: Example Oil-In-Water sensor output.	35
Figure 36: Oil-In-Water sensor results.	37
Figure 37: Oil spill patterns; oblong (top left), round (top right), and narrow (bottom).	38
Figure 38: Semi-random algorithm pattern.....	39
Figure 39: Star algorithm pattern.	40
Figure 40: Figure-8 algorithm pattern.....	40
Figure 41: Spiral algorithm pattern.....	41
Figure 42: Flower algorithm pattern.	41
Figure 43: Looping algorithm pattern.	42
Figure 44: Spill 1, oblong pattern.	44
Figure 45: Spill 2, Round Pattern.	45
Figure 46: Spill 3, Long and Narrow Pattern.....	46
Figure 47: LAMOR Oil Recovery Workboat.	48
Figure 48: FLIR Vue Pro Thermal Infrared Camera.	49
Figure 49: Drone Aviation Corporation WATT200 tethered drone.	51
Figure 50: Two vessels towing booms could be controlled autonomously by the master vessel.	52
Figure 51: GE sensor results without flow diverter.	A-2
Figure 52: GE sensor results with flow diverter.	A-3
Figure 53: Arjay initial floating sensor results.	A-4
Figure 54: Inline sensor raw data.....	A-7
Figure 55: Sensor mount - Arjay sensor version.	B-1
Figure 56: Sensor mount - GE sensor version.	B-1
Figure 57: Control panel schematic.	C-1
Figure 58: Arjay sensor graphs, tests 1-6.....	D-3
Figure 59: Arjay sensor graphs, tests 7-12.....	D-4
Figure 60: GE sensor graphs, tests 1-6.	E-3
Figure 61: GE sensor graphs, tests 7-12.	E-4

Figure 62: A first example showing that the oil/water interface is clearly reflected in the IR data. Each graph line represents the thermal measurements along the respective line in the IR image. F-1

Figure 63: An example showing that while waves make the IR data noisier, the oil/water interface is still evident. Each graph line represents the thermal measurements along the respective line in the IR image. F-2

Figure 64: Data for a 5mm oil layer in calm water. Each graph line represents the thermal measurements along the respective line in the IR image. F-3

Figure 65: Data for a 15mm oil layer in calm water. Each graph line represents the thermal measurements along the respective line in the IR image. F-4

Figure 66: An example with sun reflection. Each line in the graph represents measurements along the respective lines in the adjusted IR image. F-5

Figure 67: IR profiles versus distance for a relatively uniform oil layer. F-6

Figure 68: Time sequential data – comparing the normalized IR sensor data to that of the Arjay floating sensor. F-7

Figure 69: Time sequential data – comparing the normalized IR sensor to that of the GE floating sensor. F-7

Figure 70: IR image and temperature profile for different thicknesses of oil using IR lamps to heat surface of the tank. F-8

Figure 71: IR image and temperature profile for thick and thin oil at equilibrium. F-9

Figure 72: IR image and temperature profiles over time for thick and thin oil at equilibrium. .. F-9

Figure 73: IR image and temperature profile for different thicknesses of oil. F-10

Figure 74: Outdoor data showing typical results: top is visual, bottom is IR with profile location (dotted) and temperature (solid). As previously seen, the oil appears warmer than the water. F-11

Figure 75: Outdoor data showing (temperature) reversed results: top is visual, bottom is IR with profile location (dotted) and temperature (solid). In this case the water appears to be warmer than the oil due to the lack of solar radiation and cooler surrounding air and wind. F-12

List of Tables

Table 1: Arjay Oil Thickness Sensors Test Matrix.....	27
Table 2: GE Oil Thickness Sensors Test Matrix.	27
Table 3: Discharge Line Sensor Tests and Results.....	36
Table 4: Spill 1, Oblong Pattern, Percent Oil Recovered after N Hours for Each Algorithm.	44
Table 5: Spill 2, Round Pattern, Percent Oil Recovered after N Hours for Each Algorithm.	45
Table 6: Spill 3, Long and Narrow Pattern, Percent Oil Recovered after N Hours for Each Algorithm.....	46
Table 7: GE initial sensor results without flow diverter.	A-1
Table 8: GE initial results with flow diverter.	A-2
Table 9: Arjay initial sensor results.	A-5
Table 10: Arjay percentage oil sensor – pump test results.	A-6
Table 11: Arjay percentage oil sensor - skimmer test results.	A-6
Table 12: Arjay Sensor Results.....	D-1
Table 13: GE sensor results.	E-1

Acronyms

A/D	Analog to Digital
AOS	Autonomous Oil Skimmer
BSEE	Bureau of Safety and Environmental Enforcement
BS&W	Bottom Solids and Water
CAD	Computer Aided Design
CONOPS	Concept of Operations
COTS	Commercial of the Shelf
DC	Direct Current
DGPS	Differential GPS
DOI	Department of the Interior
ETA	Estimated Time of Arrival
FLIR	Forward Looking Infrared
GPS	Global Positioning System
GUI	Graphical User Interface
IP	Internet Protocol
IR	Infrared
L1/L2	1575.42 MHz/1227.60 MHz
mA	milliamper
MHz	megahertz
mm	millimeter
NMEA	National Marine Electronics Association
OCS	Outer Continental Shelf
Ohmsett	Oil Spill Response Research and Renewable Energy Test Facility
OSRO	Oil Spill Removal Organization
OSRR	Oil Spill Response Research
PSI	Pounds per Square Inch
PTZ	Pan, Tilt, and Zoom
ROV	Remotely Operated Vehicle
RPM	Revolutions per Minute
RTK	Real-Time Kinematic
SD	Secure Digital
TIFF	Tagged Image File Format
UAV	Unmanned Aerial Vehicle
USB	Universal Serial Bus
USCG	United States Coast Guard
V	Volt

I. Introduction

Alion has developed an automated skimmer system that can autonomously maneuver and skim the oil from a given area with automatic tracking and reporting of progress and performance. This Autonomous Oil Skimmer (AOS) consists of a commercial-off-the-shelf (COTS) skimmer and vessel, a COTS autopilot system, a high precision navigation package, oil sensors, and custom control software. The result is a portable and mountable navigation, sensor, and computer control system that can be used with a variety of skimmer and vessel systems for maximum oil spill response flexibility. A block diagram of the system is shown in Figure 1 (blue boxes were developed/ integrated by Alion, red boxes are COTS systems).

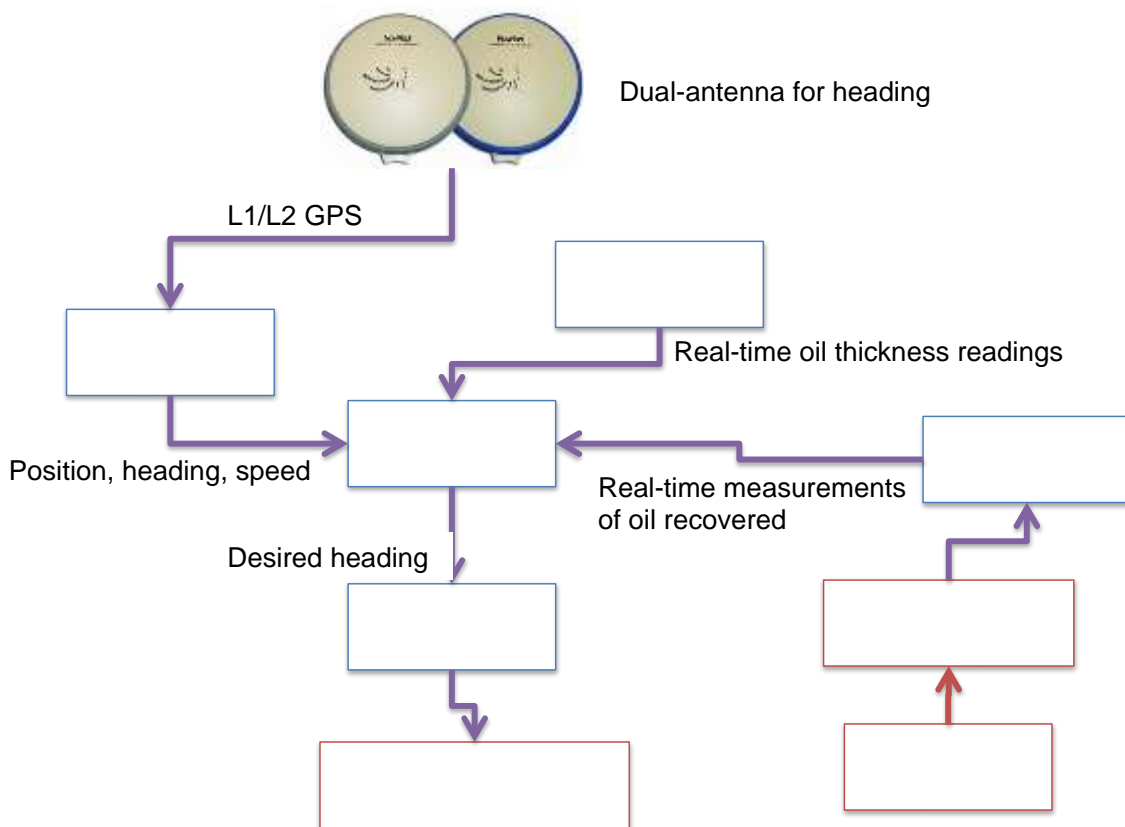


Figure 1: Autonomous Oil Skimmer Concept.

Development of the AOS included selection of thickness sensors with initial sensor tests at the Bureau of Safety and Environmental Enforcement's (BSEE's) Oil Spill Response Research and Renewable Energy Test Facility (Ohmsett) in March 2015. Based on these tests, Alion redesigned the sensor mount and conducted an open water test of the entire system (without oil) on Gardner Lake in Salem, CT in September 2015. Another test of the sensors mounted on the complete system (sans autopilot) was conducted at Ohmsett in March 2016. This report describes the integration and testing of the entire system.

2. Background

In December 2013 the BSEE solicited White Papers for specific areas of interest to the BSEE Oil Spill Response Research (OSRR) Program on Oil Spill Response Operations in the U.S. Outer Continental Shelf (OCS). One of the topics was the development of Smart Skimming Technologies, including:

- a) Develop technology packages to aid in the automation and optimization of oil skimmer performance. Technologies should aim to ultimately remove the skimmer operator entirely in order to maximize and normalize oil recovery efforts and results. Areas of investigation should include oil thickness measurement devices that can independently control skimmer operation to meet encountered oil thickness demands without operator input. Thickness measurement devices can use any kind of practical technology and ideally be able to retrofit to at least one type of commercial skimmer.
- b) Develop technology packages for real-time measurement of oil and water recovery, real-time calculation and reporting of recovery efficiency. Technologies should aim to retrofit to existing commercial skimmers but not hinder flow rate.
- c) Develop novel power generation technology to use recovered oil from onboard storage of either skimmer or vessel of opportunity. Power generation should be readily adaptable for electric, mechanical, pneumatic and/or hydraulic outputs.
- d) Development of other innovative technologies that could lead to automation and optimization of oil skimmer performance.

Alion's response was a proposal to develop a skimmer system that would autonomously maneuver and skim the oil from a given area with automatic tracking and reporting of progress and performance. This AOS would consist of a COTS skimmer and propulsion system, coupled with a COTS autopilot and high precision navigation package, oil thickness sensors, and some custom algorithm development. The goal would be to develop a field mountable navigation, sensor, and computer control system that could be used with a variety of skimmer systems for maximum oil spill response flexibility.

The AOS' oil sensor is used to measure the thickness of the oil so the system can monitor the oil being skimmed in real-time and track oil thickness verses position as it is skimming. Based on the oil thickness gradients, the tracking algorithm directs the skimmer to navigate in the direction of thickest oil concentration while also monitoring the skimming coverage to ensure all areas are checked. The tracking algorithm communicates the desired direction of travel to the autopilot system, which controls the vessel's steering system to maneuver the AOS in the desired direction. As the AOS recovers the oil, statistics on oil thickness and oil recovery rate as a function of position are tabulated for real-time performance monitoring as well as stored for post-event evaluation.

3. Sensor Selection and Initial Testing

3.1. Floating Sensors

One of the key components of the smart skimmer system is a sensor to enable the system to determine where the thickest oil is located. Three COTS floating oil sensors (one from General Electric Analytical Instruments and two variations of the same sensor technology from Arjay Engineering) were identified as potential candidates and tested at BSEE's Ohmsett facility (Leonardo, NJ) in March 2015. These were the only sensors that could be identified as commercially available and potentially feasible at the time of the market survey.

3.1.1. GE Leakwise ID-227 Oil Sheen Monitoring System

The Leakwise ID-227, manufactured by GE Analytical Instruments, is a floating sensor that detects the presence of and monitors the buildup of hydrocarbons on water. The ID-227 System consists of two main parts: a sensor head mounted on a wave rider buoy (see Figure 2) and a signal processor (SLC 220) for up to four sensors. The Leakwise sensor uses a high-frequency electromagnetic absorption technique.

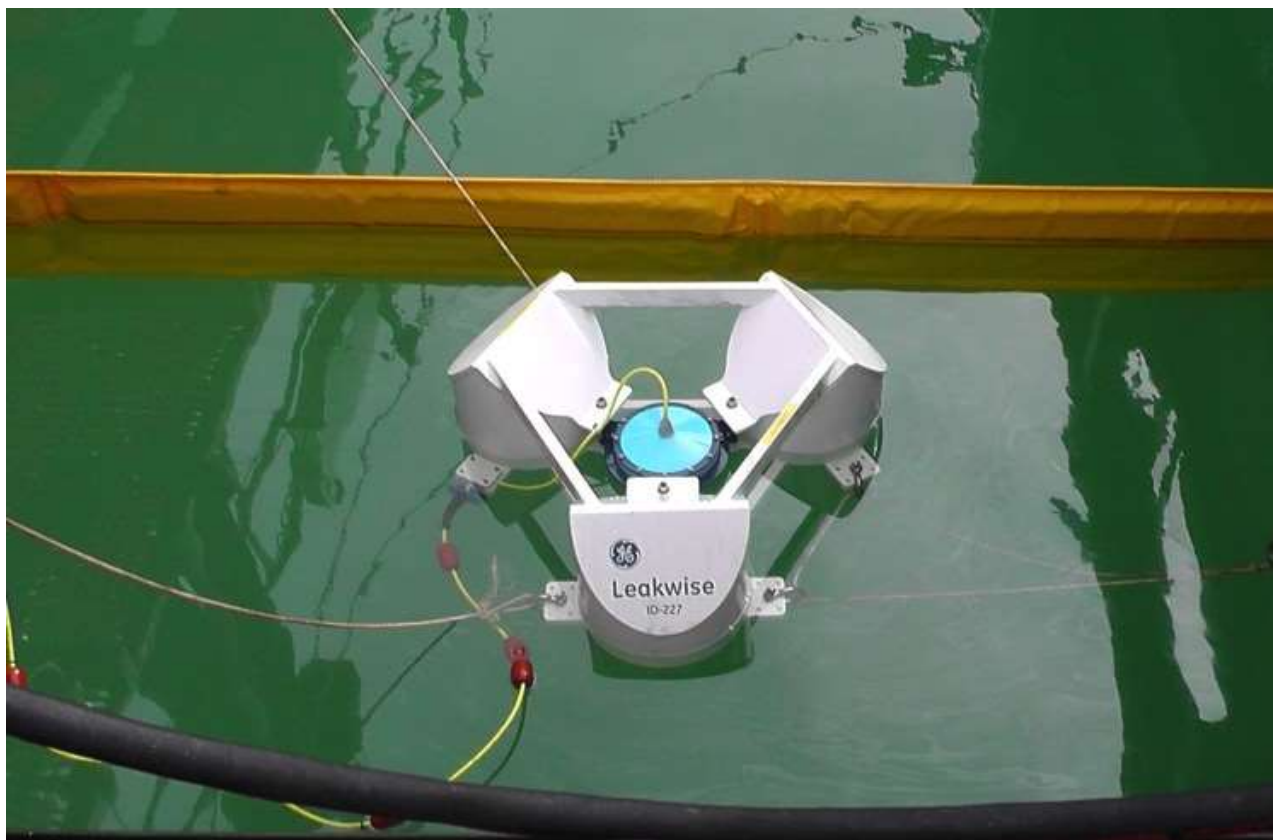


Figure 2: GE Leakwise ID-227.

The ID-227 sensor head, in the center of the three floats in Figure 2, is a high frequency transceiver with two antenna elements. One antenna is located at the water/air interface (internal to the sensor) and the second is underwater (external band around the circumference of the sensor). A high frequency signal is transmitted through the water between the antennas. The

higher energy absorption of water (dielectric constant about 80) results in increased loading on the transmitter and a higher output signal. An oil layer (dielectric constant about 3) on the water reduces this loading and the output signal drops since water absorbs more energy than hydrocarbons or air. When the upper antenna is surrounded by an oil layer or an oil/water mixture, the loading is reduced in proportion to the reduction in water content. The received sensor signal is processed by GE's PS-220 analog processor, which outputs a 4-20mA signal that is proportional to the oil thickness.

3.1.2. Arjay 2852 HCF and 2852-PCD

Arjay Engineering produces a number of probes designed for sensing and measuring oil on water. All of Arjay's sensors are based on the same technology – looking at the capacitance field. They measure the change in capacitance due to differences in the dielectric – the dielectric of oil is lower than water so the capacitance decreases as oil thickness increases.

One of the Arjay sensors tested was the 2852-HCF tri-float sensor. From discussions with Arjay, the floating sensor (see Figure 3 top) uses the water as the ground plane for the capacitance field. The oil on top of the water makes the distance between the “plates” grow, which decreases capacitance along with the decrease due to the dielectric nature of the oil to get an improved response. This off-the-shelf sensor is not really designed the smart skimmer application but was used to assess possible performance.



Figure 3: Arjay 2852-HCF sensor (top) and sensor sled (bottom).

The manufacturer also prepared a sensor sled (see Figure 3 bottom) using a similar sensor, the 2852-PCD. The 2852-PCD is used in commercial applications in a chute, where the metal chute provides the ground plane. The sled was designed to provide improved performance over that of

the 2852-HCF while being moved through the water. The sled incorporated a metal chute on the underside (Figure 4); this was cut off part-way through the testing to improve oil flow past the sensor. The manufacturer also incorporated a conductivity sensor for testing in case there was emulsification occurring during the drag tests.



Figure 4: Bottom of sensor sled showing metal chute.

3.2. Floating Sensor Calibration

Both the GE and Arjay sensors were tested in a controlled environment to try to determine a mapping between sensor output and oil thickness. The two sensors were tested simultaneously in separate tanks that were side-by-side. Oil was added in 1 mm allotments. The original plan was to start at 1 mm thickness and go up to 20 mm. However, due to the viscosity and surface tension of the Hydrocal, the minimum achievable thickness to cover the surface area of the tanks was 4 mm. The calibrations curves are shown in Figure 5. From a raw sensor performance perspective, both sensors work and show a response with increasing oil thickness. The GE sensor has a very compressed scale – especially at the thicker oils, which would make discerning differences at the high end of the scale difficult. The Arjay sensor uses more of the 4-20 mA scale with more distinction possible at the higher end, but is more compressed in the mid-range. All data points

are shown with error bars at ± 10 standard deviations. The GE data was much cleaner (low standard deviation), probably due to the averaging in the sensor processor. The Arjay sensor had much more noise in the measurements in the mid range (6-13 mm); during the measurements we had difficulty getting the sensor to reach equilibrium at those thicknesses.

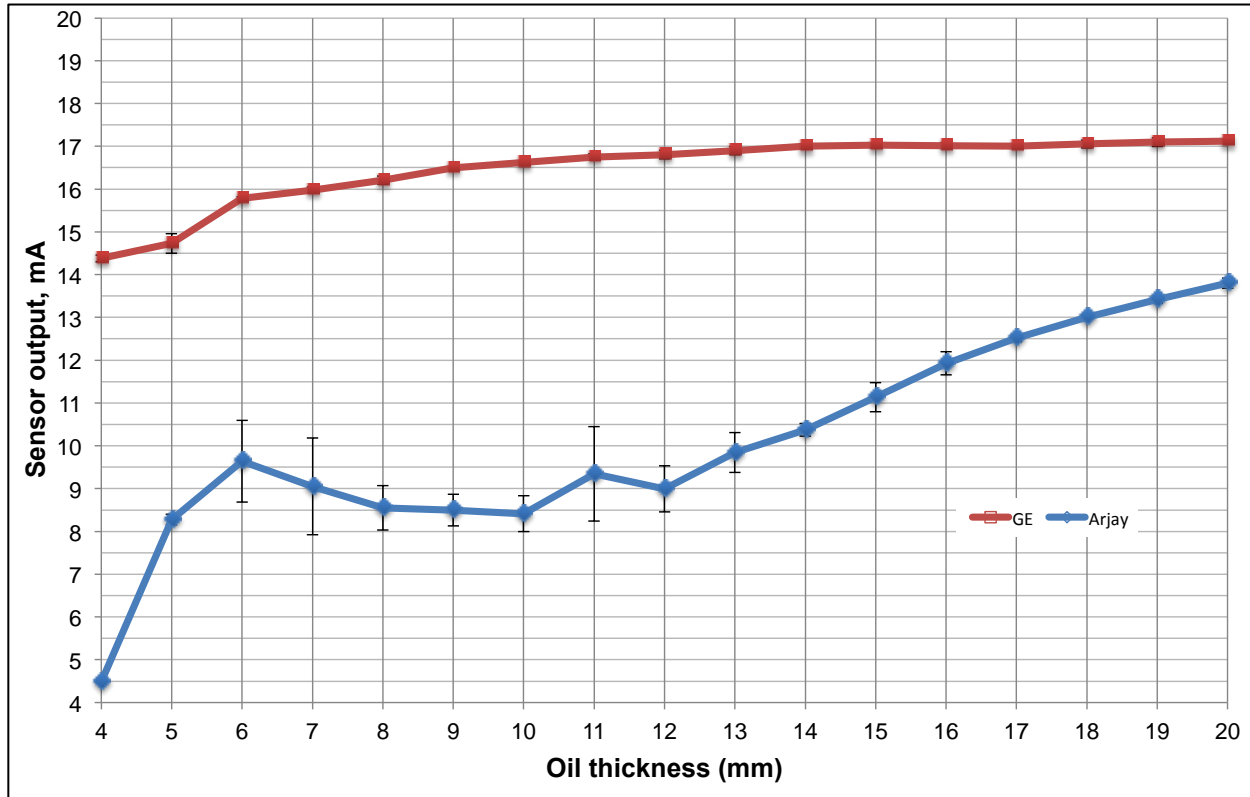


Figure 5: GE and Arjay calibration curves.

3.3. Floating Sensor Tests

The floating sensors were attached to the Ohmsett testing bridge and moved through oil patches to assess their performance with two oil thicknesses while moving at a variety of speeds. A 6 ft wide boomed test lane with four oil patches was set up. The oil patches were ~40 ft long separated by ~60ft. The oil was kept in the patches by an air bubbler system (see Figure 6). The tests were also used to assess sensor integration with the computer system.

3.3.1. GE without Flow Diverter

The GE sensor with the three floats was tested at speeds up to 3 kts. After running the 1.5 and 2 kt tests, it was observed that the tow point was creating a clear patch of water in the middle of the oil patch and the low tow point was causing the GE sensor to bog down. The tow point was raised for the remainder of the testing. At the lowest and highest speeds it did not work well at all, so the thicker oil patch test was only run at 1 and 1.5 kts. For the thicker oil test, additional oil was only added to patch number 2. No wave tests were conducted due to lack of time.

The test plan called for slicks of 5 mm and then 15 mm but due to the viscosity and surface tension of the Hydrocal, the oil volume required for 5 mm thickness would not spread over the

entire patch. Since the resulting patch size was deemed too small for the higher speeds, twice the oil was used, which would have been a 10 mm thickness; however, this also did not spread over the entire area so the actual thickness ranged from 11-14 mm (estimated by measuring the length of the patches). The table summarizing the test results can be found in Appendix A.



Figure 6: Picture of oil patches in lane, looking South (direction of travel).

3.3.2. GE with Flow Diverter

GE created a flow diverter which they thought would improve performance (see Figure 7). The GE sensor with flow diverter was only tested at 0.5 and 1.0 kts. After observing it at these speeds, it was clear that it was not working as intended: oil was very slow to enter the chamber, and once there did not leave. There was no clear response to entering and exiting the oil patches. It also dragged a considerable amount of oil out of the patches. It might have performed better at higher speeds, but given that the form factor was not compatible with the smart skimmer system design, it was decided to skip higher speeds and focus on the GE sensor alone. The results are summarized in Appendix A.



Figure 7: GE sensor and flow diverter.

3.3.3. Arjay Sensors

Since they were small enough to fit into the test lane side-by-side, the two Arjay floating sensors were tested simultaneously. This decreased the total testing time, allowing for more trial runs. Both sensors were tested at up to 3 kts using two different thicknesses of oil and then with waves added. After running the first set of tests, the tow points of both sensors were relocated higher to help keep the sensors from bogging down in the water at the higher speeds. Also, it was noticed that the metal chute seemed to restrict the oil flow to the sensor on the sled so this was cut off after the first set of tests, which improved the responsiveness. For the final set of tests with the waves added, only the medium speeds (1 - 2.5 kts) were used. Initially waves with small amplitude were used and then larger waves for the last run.

3.4. Floating Sensor Results

There were some difficulties in assessing the performance of the floating sensors. First of all, it turned out to be difficult to get an accurate ground truth of the actual oil patch thickness. The average thickness could be estimated from the area and the volume of oil; however, the oil was not spread uniformly due to the wind and the bubblers that were used for containment. Also, some unknown amount of oil was dragged out of the patches by the sensors each time they ran through them. An acoustic rover was used to measure the thickness of one of the patches, but it was not possible due to manpower, budget, and time constraints to use this to measure the thickness of **all** of the patches prior to each run. The only totally accurate indication available is the time mark into and out of each oil patch. Thus the assessment of sensor performance is really more of how responsive they were to the changes from water to oil and oil to water.

The second difficulty was that none of the sensors had the ideal hydrodynamic form factor. The performance of the sensor itself was hugely influenced by how well it could be pulled through the water. This was especially problematic with the GE sensor but to a lesser extent also with the Arjay (see Figure 8 and Figure 9). Some of the work going forward was to design a better mount for the sensors to enable better hydrodynamic performance. Also, restriction of the oil flow past the sensor caused long delays in the sensor registering the presence of oil and delays in getting back to a water response. The final mounting design needed to allow for the smooth flow of

oil/water past the sensor without causing a build-up of oil under the sensor (making for larger oil thickness readings). Due to anomalies in the calibration data, it is not clear if the sensor was floating on top of the entire oil layer. A sensor head that is convex like the GE sensor may work better for this.

From the towing tests, the biggest impact seems to be the hydrodynamic issues already discussed. The speed of the oil/water moving past the sensor head did not seem to be a factor. When the sensors were in the oil they registered oil and when in water (without having oil pulled along with the sensor) they registered water. The sled without the chute had the best response at all of the speeds, although it was not perfect either.



Figure 8: Example hydrodynamic issues present with GE sensor



Figure 9: Example hydrodynamic issues with Arjay sensor.

3.5. In-Line Sensor

The AOS Concept of Operations (CONOPS) also called for a sensor to monitor the oil recovery performance. The only COTS possibility identified was the Arjay Model 2852-IFA Percent Water in Oil Monitor (Figure 10). The 2852-IFA uses the same capacitance principle as the 2852-HCF but uses a different sensor head due to its mounting inside of a pipe. A probe approximately 6 inches long extends into a pipe tee and measures the capacitance along its length. Again, the lower dielectric constant of oil results in lower capacitance. The analog sensor signal is processed by a separate 2852-OWM controller and output as a 4-20mA to the DAQ mounted in the control box.

This sensor was tested at Ohmsett with two different tests: mixing measured amounts of oil and water directly and using a skimmer to pick up (and mix) oil and water. The results from the two different tests with the sensor were very different. The results using the pump test displayed very noisy sensor readings, indicating the incomplete mixing of oil and water except in the extreme cases of almost all oil or almost all water. This is shown in Figure 11; the green lines indicate the start of the mixture sampling and the red lines indicate the end; the blue line is the raw sensor measurement. Note that except for the left hand range (mostly oil) and the right hand range (mostly water), the sensor readings oscillate quite a bit. The skimmer however, seemed to mix the oil and water very well (as observed visually) and the results were much less noisy (see Figure 12) so these results are assumed to be more accurate. They are certainly more pertinent to

the smart skimmer system design, which will be using a similar skimmer. The range of values is such that it could be used to accurately assess whether there is a high concentration of oil coming from the skimmer or not.

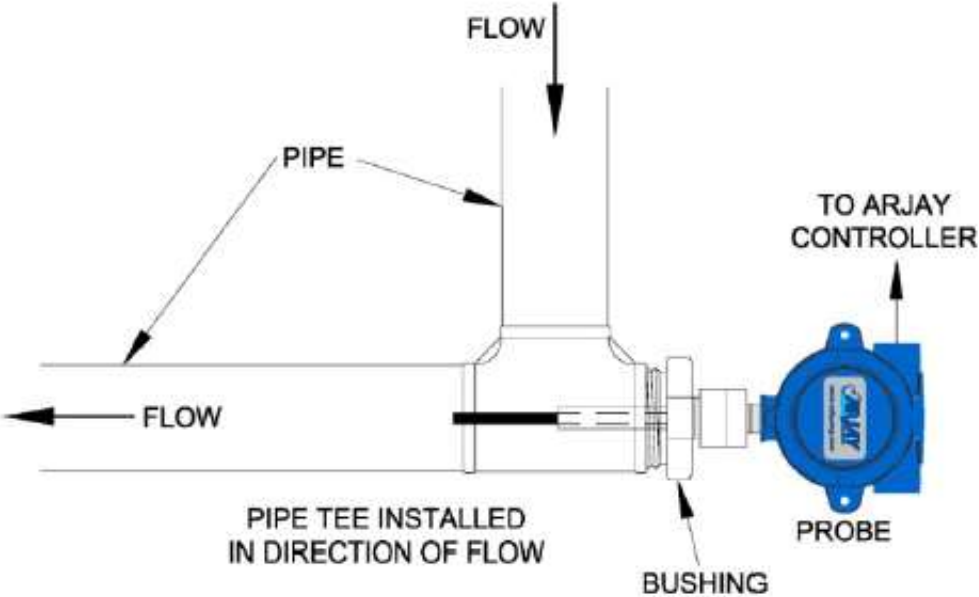


Figure 10: Arjay 2852-IFA Oil in Water Sensor.

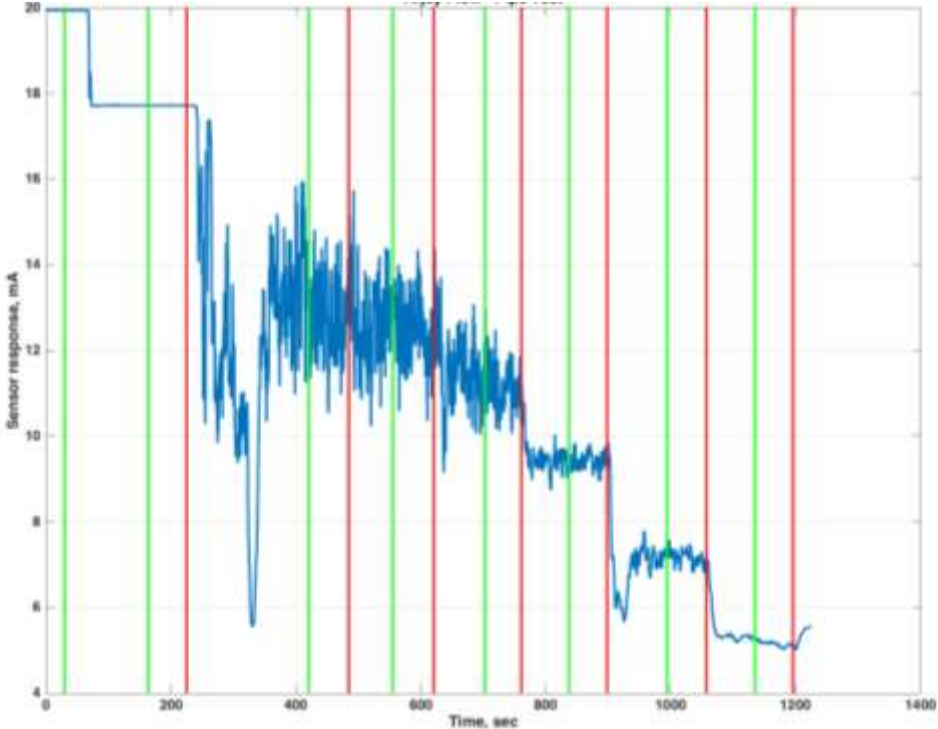


Figure 11: Raw sensor data from the first inline sensor test, using the combination of measured streams of water and oil (4-20 mA sensor data inverted to match other results).

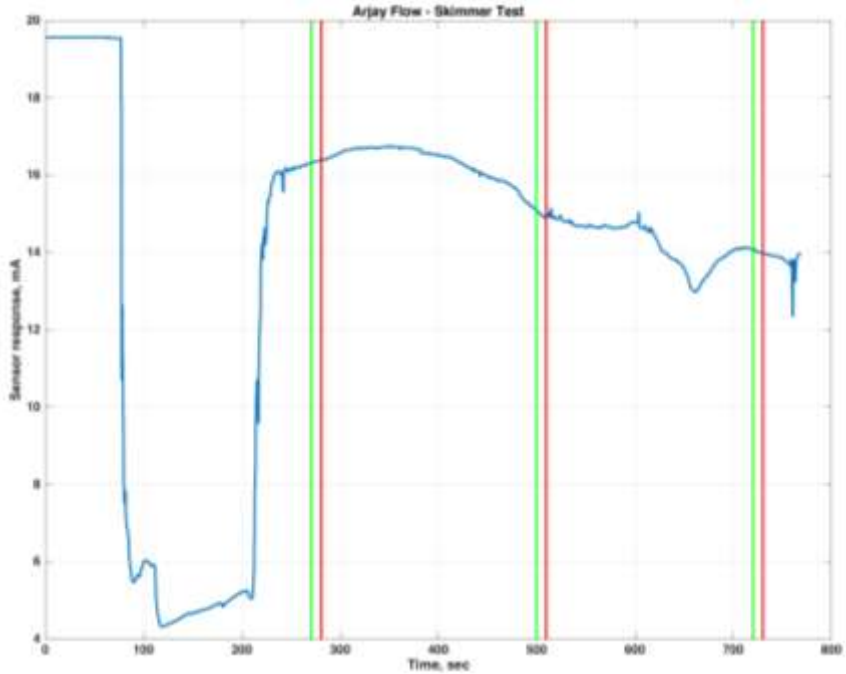


Figure 12: Raw sensor data from the second inline sensor test, using the skimmer to mix the oil and water (4-20 mA sensor data inverted to match other results).

The sensor readings during the sampling periods (green line to red line) were averaged. The sample was tested to determine the percentage oil and water. These values are plotted for both tests in Figure 13. For each data point the error bars are shown; at 2 standard deviations for the pump test, and at 10 standard deviations for the skimmer test. The larger noise in the pump test values is easily seen.

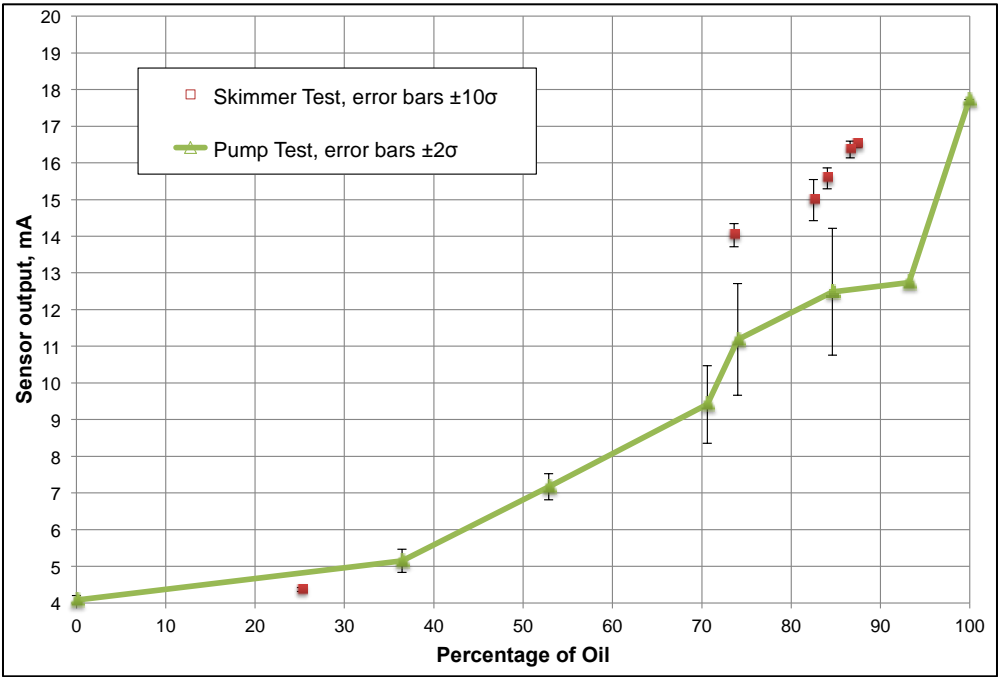


Figure 13: Arjay 2852-IFA inline sensor calibration curve (4-20 mA sensor data inverted to match other results).

4. System Design

The various components of the system as depicted in the block diagram in Figure 1, are described in the sub-sections below.

4.1. Navigation and Computer Systems

The navigation and computer system is packaged into a rugged rack mount box that contains the following main components (see block diagram in Figure 14):

- **DataQ DI-245 Data Acquisition:** This is a 4-channel, 14-bit analog to digital (A/D) device that is used to acquire data from the oil thickness sensor and from the skimmer discharge pipe oil/water sensor. The sensor data are provided via an analog 4-20 mA signal that is digitized by the DataQ and supplied to the control system algorithm.
- **Novatel Flex6 GPS ALIGN System:** This is a dual frequency (L1/L2 (1575.42 MHz / 1227.60 MHz)) GPS system that not only provides high-accuracy positions but also provides accurate heading measurements based upon signal phase differences between the two antennas.
- **Peplink Pepwave MAX BR1 4G LTE Mobile Router:** This is a combination cellular modem and WiFi router that is used to establish Internet connectivity to the computer. This is used along with LogMeIn software to allow remote monitoring and control of the entire system.
- **Twister 77E computer:** This is a fanless solid-state computer that runs all of the control software.
- **12V battery:** The box contains a battery to ensure the system stays operational through momentary power outages.

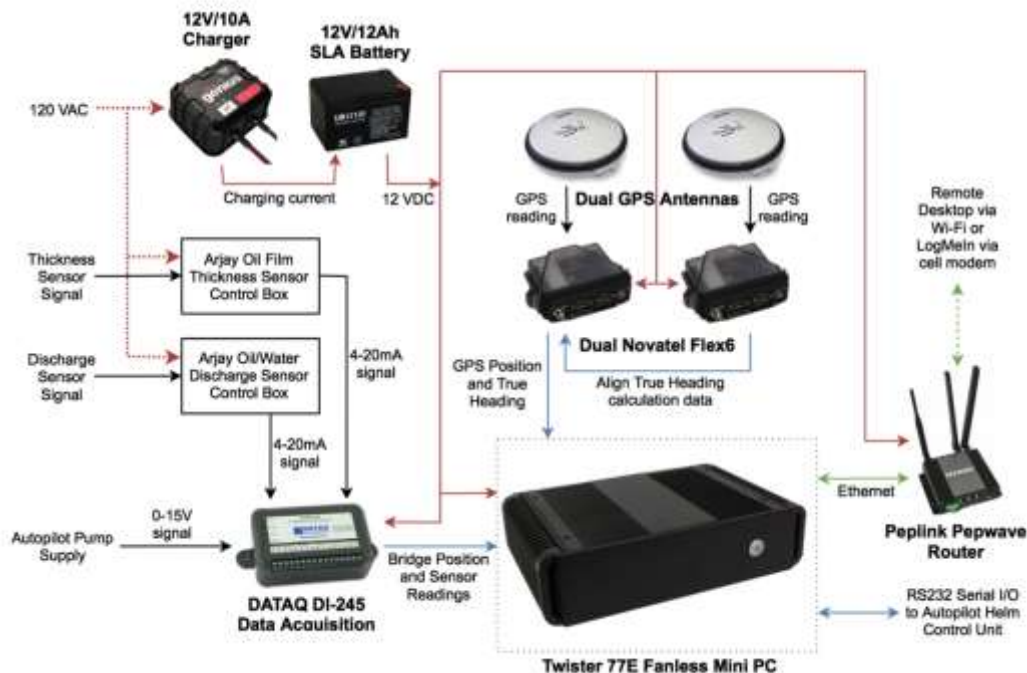


Figure 14: AOS navigation and computer box block diagram.

4.2. Oil Sensor Mounting

Based upon the results of the initial sensor testing described in Section 3, the Arjay and GE oil thickness sensors both worked to some extent; however, it was clear that a more hydrodynamic mounting system was needed. Using some Alion Naval Architecture expertise, a new mounting system was designed that could be attached to the skimmer and that would keep the sensor head on top of the water and minimize the tendency to lift or submerge in wave action. This design is shown for the Arjay sensor in Figure 15. The same float and arm assembly was used for both sensors with a different adaptor for attaching the sensor head. Computer Aided Design (CAD) drawings for both versions are in Appendix B.

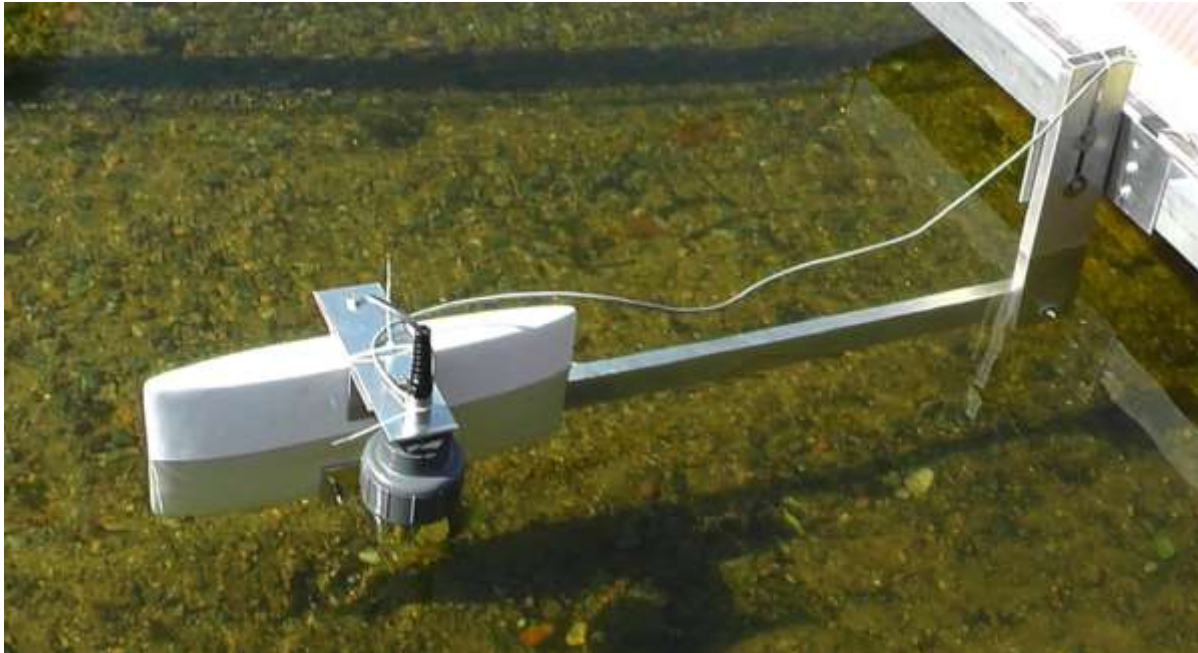


Figure 15: Redesigned sensor float assembly.

4.3. Autopilot System

The Garmin GHP™ Reactor Hydraulic Corepack with SmartPump™ system was selected as the autopilot for control of the boat's steering based on cost, performance, ease of integration, and availability. One of the reasons this unit was selected was the Garmin Helm Control Unit was supposed to provide a NMEA 0183/serial port-based autopilot interface, thus allowing for easy integration with the computer and control algorithm. Unfortunately, it was realized that this feature was not actually implemented by Garmin, so a decision was made to use an ActiSense NMEA 0183 to NMEA 2000 converter as well as a NMEA 2000 GPS to enable the system to receive heading commands from an external device.

An additional helm-mounted display (by Clipper Marine Instruments) was also needed because the Garmin helm display would not display information in route following mode. The Clipper display reads NMEA 0183 sentences and displays the heading information (desired and actual) on a small waterproof display. A complete block diagram of the autopilot system showing all of the various components is shown in Figure 16.

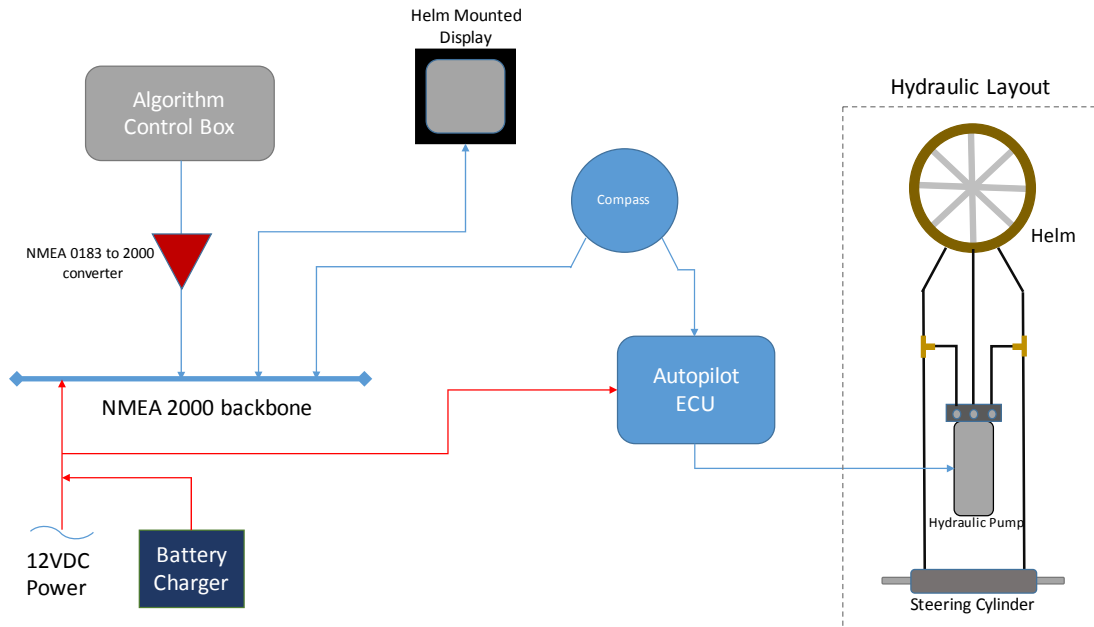


Figure 16: Autopilot system block diagram.

4.4. Computer Control System

The AOS monitoring and control software runs on a Twister 77E solid-state minicomputer. The software takes in position and heading data from the GPS, oil thickness/recovered oil readings from the DataQ A/D, and magnetic compass readings from the autopilot. The operator must specify the approximate shape and location of the oil spill. Based upon the location of the oil spill, the algorithm then calculates a waypoint, computes magnetic compass corrections and the heading to steer, and sends the desired heading to the autopilot.

The program keeps track of oil film thickness and builds up an oil patch map while performing skimming operations. The software uses oil film thickness readings to keep the skimmer in the oil patch. Additional data such as oil patch shape/profile and wind/current speed and direction can be entered manually to improve the program's performance. The skimmer control software can run oil recovery based on simulated or real oil sensor readings and simulated or real GPS position. While performing skimming operations, the software keeps track of oil being skimmed and displays recovered oil on a separate map. A flowchart of the software is shown Figure 17.

The flowchart shows the various steps to:

- input the estimated oil spill and wind,
- get initial position and heading,
- calculate a waypoint to recover oil based on a selected recovery algorithm,
- calculate desired course to way point,
- send course to autopilot,
- get new position and heading,
- get oil measurements,
- plot position on map, oil recovered on separate map, and display information,
- repeat until finished.

Most of the steps or processes in the software are straightforward except for the process to “calculate a waypoint to recover oil.” This process controls what pattern is generated to guide the vessel and recover oil in the most efficient way. Factors that affect this pattern include maximum skimmer speed and vessel turning radius. Several oil recovery algorithms were selected and tested to recover the oil. These algorithms are discussed in section 7.

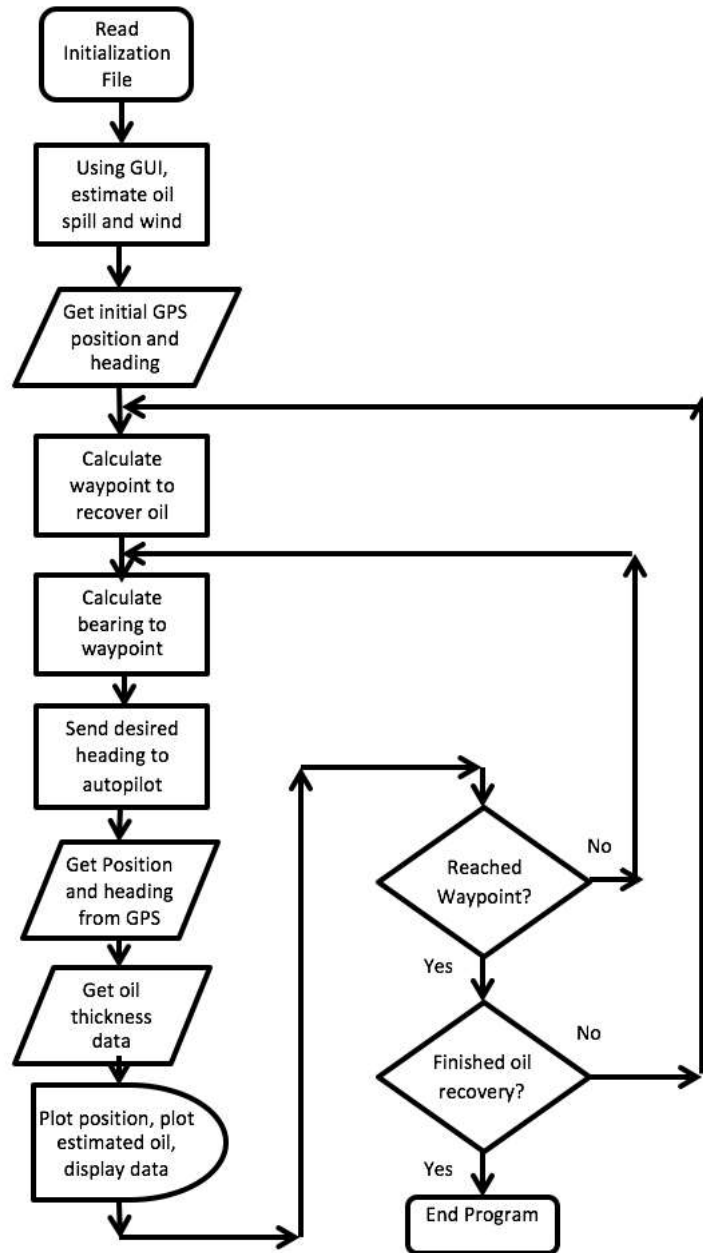


Figure 17: Oil skimmer control software flowchart.

The program reads position, heading, and speed information from the Novatel Flex6 GPS ALIGN system. It also reads oil thickness data from the oil thickness sensor and recovered oil

information from the inline percentage of oil in water sensor through the DataQ DI-245 data acquisition system.

The Oil Recovery program is written in MATLAB™ with a graphical user interface (GUI). The GUI is shown in Figure 18. After starting the program, the operator must specify the wind direction and the approximate shape and location of the oil spill. The shape and location is entered by specifying four points on a map that bounds the estimated oil spill. The operator may select one of two maps. These maps are generated in a separate program (MakeMap™) using Google Earth™ which allows the program to be used at various locations. The estimated oil spill is displayed in the left window of the GUI.

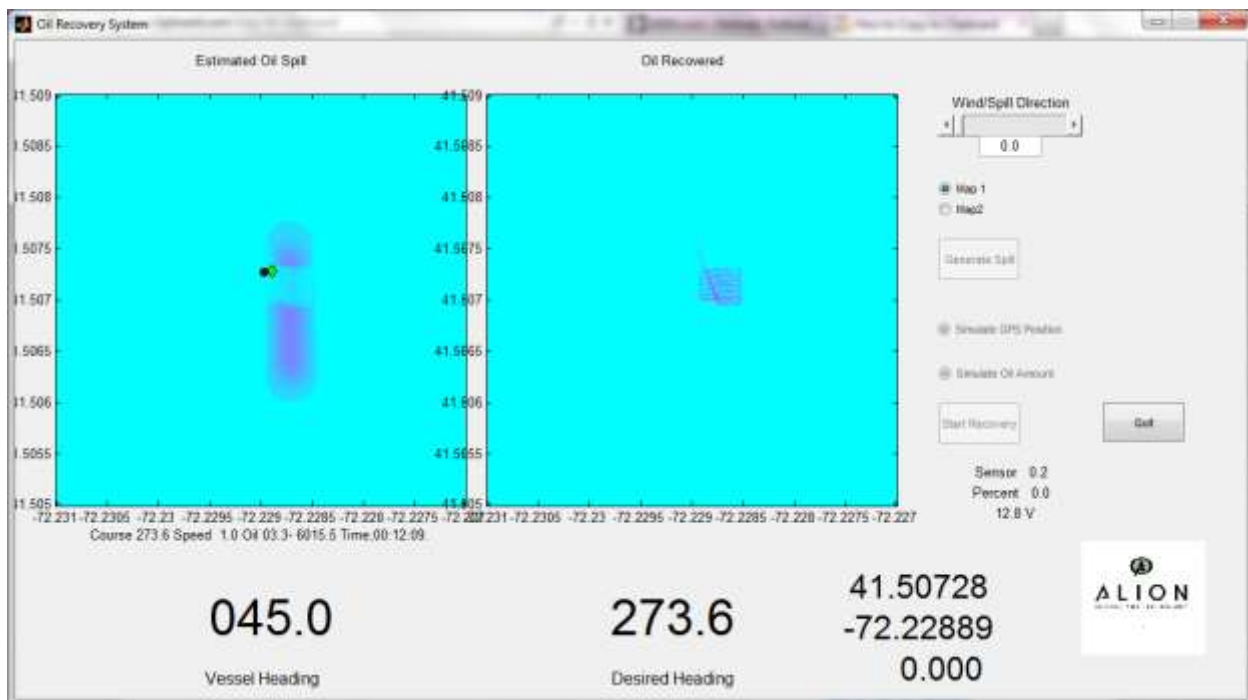


Figure 18: Oil Recovery Software Graphical User Interface

Once the estimated size and location of the oil spill is specified, the operator can begin the oil recovery. Based on the location of the oil spill, the program then calculates a series of waypoints and sends commands to the Garmin GHP autopilot. The autopilot requires waypoints rather than just a desired heading. To satisfy the autopilot, any time there was a change in the desired heading, a new waypoint is calculated and sent to the autopilot.

The Oil Recovery program keeps track of oil film thickness and builds up an oil recovered map while performing skimming operation. This map is displayed in the right window of the GUI. The program uses oil film thickness readings to keep the skimmer in the oil patch. Other information displayed on the GUI includes position (latitude and longitude), desired heading, current heading, speed, oil thickness, percentage of oil in water in recovered liquid, and estimated accumulated oil. The control software can be configured to run using simulated oil sensor readings and simulated GPS positions. This allows running various scenarios to test different oil recovery algorithms.

5. Open Water System Test

Gardner Lake in Salem, CT (a state park) was selected as the site for an open water test of the system without oil. Originally the Thames River was selected as the test site, but there were concerns about the river and tidal currents. Approval to use Gardner Lake as a test site was obtained from the Connecticut Department of Energy and Environmental Protection. Figure 19 shows an aerial view of Gardner Lake and the test site.

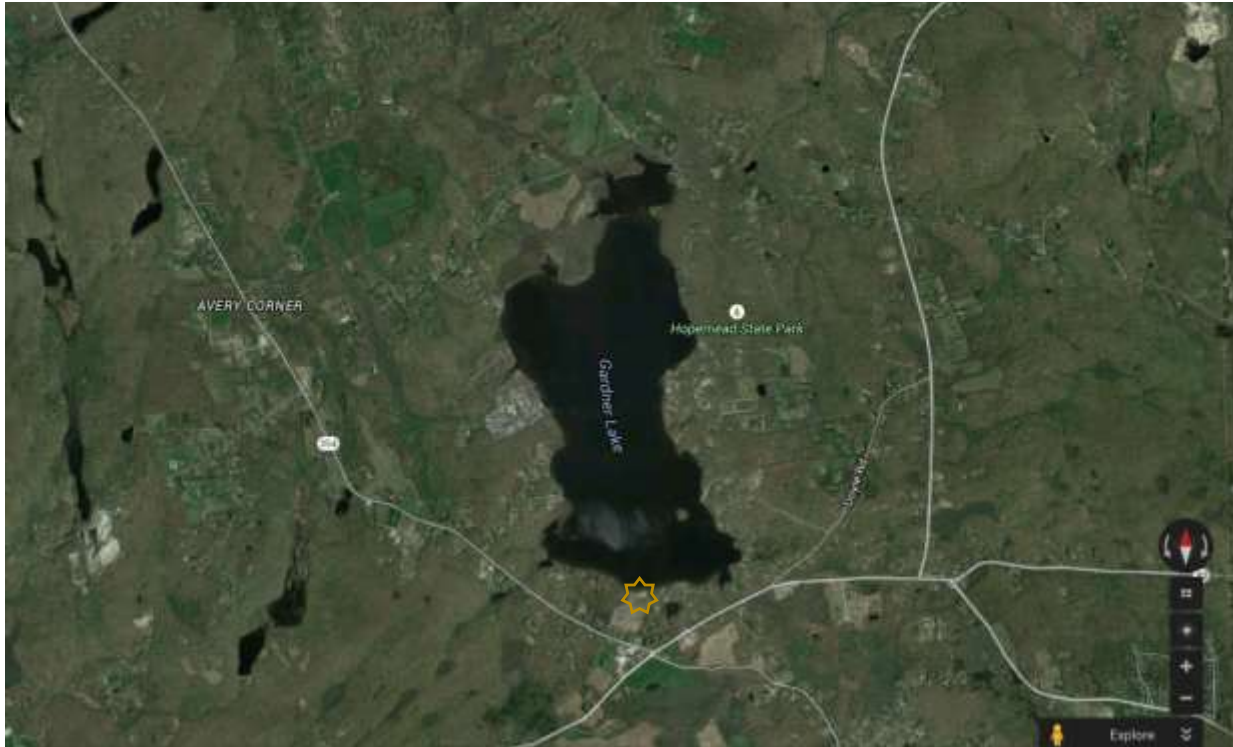


Figure 19: Test location at Gardner Lake; boat launch indicated by yellow star.

5.1. Vessel Installation

The following AOS equipment was installed on a 20-foot boat (leased from Clean Venture) as per the diagram shown in Figure 20.

1. GPS antennas
2. Autopilot controller, pump, and DC power
3. Generator
4. Autopilot display and Clipper GPS repeater
5. Control box
6. Suction pump
7. Oil in water inline sensor
8. Containment tank
9. Air compressor
10. Skimmer, booms
11. Oil Thickness Sensor
12. Pan, Tilt, and Zoom (PTZ) Internet Protocol (IP) video

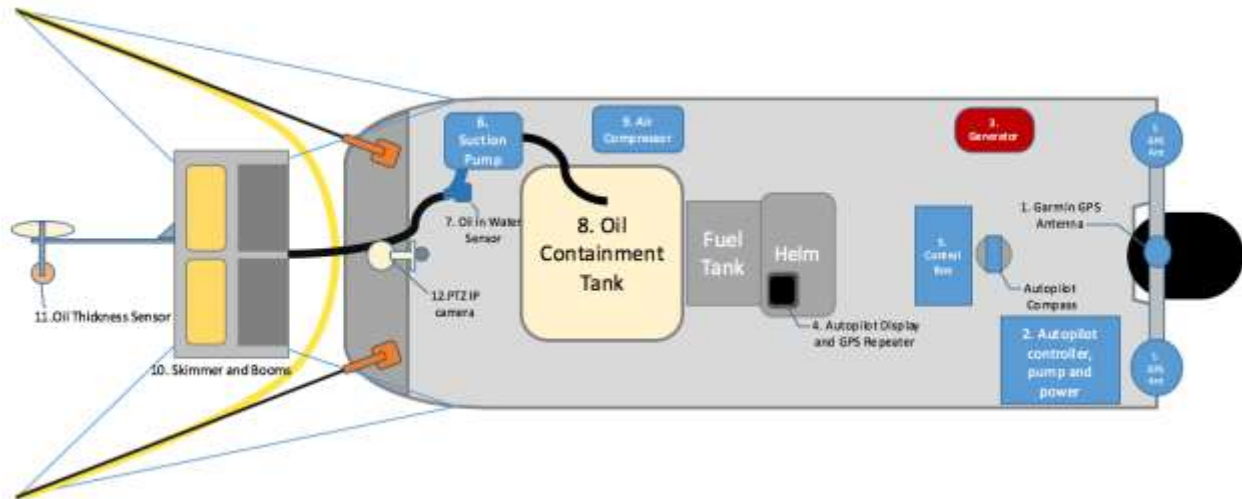


Figure 20: Equipment layout on vessel for Gardner Lake test.

The autopilot hydraulic pump was installed in the vessel by teeing short extension hoses into the existing hydraulic hoses attached between the steering ram and helm (this was done by a certified marine technician at Three Belles Maria, East Lyme CT). The system was then thoroughly bled of air to ensure smooth operation of the steering system. This was an important step because the autopilot did not use an additional rudder feedback sensor to determine rudder position. The smart pump and autopilot controller use time and pump revolutions per minute (RPM) to calculate the position of the ram, any air in the system causes erratic movement, which the system is unable to detect.

5.2. Gardner Lake Results

5.2.1. Initial Testing Results

On the first operational test of the boat it was apparent the vertical stanchion holding the oil thickness sensor to the skimmer was not sufficient. At even very slow speeds the thickness sensor arm bent to either side due to the water force. Upon a slightly higher speed test it became permanently twisted. A new adjustable stanchion with reinforced structure proved to track much better and remained true (see Figure 21). Once the vertical stanchion was replaced, the new sensor mount appeared to work very well hydrodynamically; keeping the sensor head on the surface of the water under most conditions.

The smart skimmer monitoring and control system ran the oil skimming operation by using a simulated oil spill and simulated oil sensor readings. The algorithm performed as expected, and was able to steer the boat based on position and heading, and provided a reasonable skimming path.



Figure 21: New skimmer float assembly in operation, note that the sensor and float remain perpendicular to front of skimmer.

The original control software used a simple “lawn mower” pattern to recover the oil. Once the user specifies the approximate shape of the oil spill, the algorithm first sends the vessel to the center of the spill. Next it moves perpendicular to the wind direction until it exits the oil spill. It then makes a U-turn and moves until it exits the spill on the other side. It continues back and forth – slowly moving up wind until it reached the end of the spill. Next it travels back to the center of the spill and repeats the pattern in a different direction.

Under ideal conditions, the vessel could make a U-turn within a short distance; however, during tests using the 20-foot open workboat, it was discovered that the boat could not make quick U-turns because of limitations in the autopilot and the need to limit the turn rate so as to not spill oil over the boom. Operational testing resulted in limiting the turn rate to one degree per second; this rate was judged by the vessel operator to be slow enough to not lose oil out of the booms and kept the autopilot from trying to drive the engine position beyond the stop. Figure 22 shows the results when the boat is limited to very slow turns. The turning radius of the turns is quite large and most of the turn is outside the area of the oil spill. After this test, it was apparent that the ‘lawn-mower’ pattern becomes difficult to maintain and a more efficient pattern, which incorporates the slow course changes, needed to be investigated.

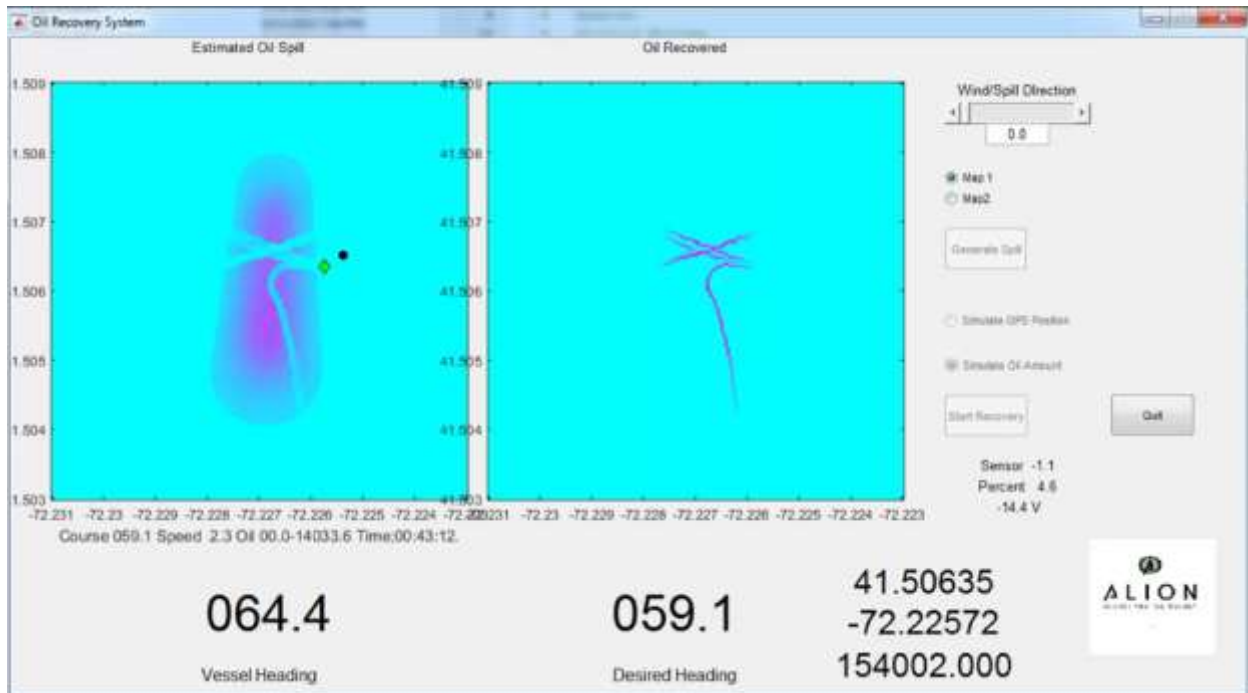


Figure 22: Oil Recovery with limited turns.

5.2.2. Navigation System Test Results

Two Novatel Flex6 GPS receivers are used in tandem to compute the boat's position, speed and direction (supplied by Novatel's dual-antenna/receiver Align® algorithm). They were very reliable and provided a highly stable heading and position solution during the test. To provide increased position accuracy in the confines of the tank at Ohmsett, a real-time-kinematic (RTK) solution using a fixed GPS base station was investigated and implemented for the Ohmsett test.

5.2.3. Autopilot Test Results

The autopilot system exhibited the ability to accept and track the algorithm's intended waypoint commands. One shortcoming of the system was the lack of feedback of the rudder angle. The Garmin autopilot system used a pump RPM sensor rather than a pressure sensor or a mechanically attached rudder angle indicator. When commanded to make large heading changes, the autopilot pump would continue to apply pressure to the hydraulic system after the stop was reached. This caused concern about excess wear on the steering system and the existing hydraulic hoses. Careful manual calibration of the autopilot system limited the added pressure applied when reaching the stop. The decision to slow the rate of turn after the vessel leaves the oil spill further decreased steering issues by limiting the steering angle needed to turn the vessel to about $\frac{3}{4}$ of the steering ram distance. The slower rate of turn should also limit the amount of oil spilled from the boom during actual oil spill recovery operations.

The two-battery setup and 20 ampere battery charger housed in the autopilot box provided ample power to both the autopilot system and control system. The display mount fabricated using a "ram mount" was easily attached to the windshield frame on the boat's center console and allowed for simple adjustment of the displays.

The issues encountered with this autopilot system should not pose a major problem if future operational installations are desired. Autopilot systems designed for outboard motors (which are not as robust as most of the inboard systems) are fairly uncommon, as is the use of an outboard driven vessel for skimming operations. In deployment it would not be advisable to attach a generic autopilot system to the vessel of opportunity because these systems must be tailored to the individual vessel based on the size of the steering rams and vessel, and fluid capacity of the system. Installation of the autopilot must also be performed by a competent marine technician. Improper installation of the system could cause complete loss of steering, which would prove to be a major safety concern. Integrating the control algorithm with an existing autopilot system would alleviate most of the pitfalls experienced during the lake testing.

Vessels with outboard engines or that would not support an autopilot system (without major re-engineering) would still benefit from the AOS's navigation schemes based on its algorithm. In these instances, the boat driver would read the navigation directions (like when driving a car with GPS). The boat driver would benefit in multiple ways. First, the computer would be calculating the best course for maximum oil recovery thus relieving the boat driver from deciding mentally where to go. Second, the system would still be able to track where oil was skimmed from and the effectiveness of skimming operations. And third, the oil recovery system would be still providing valuable historical data; the algorithm's effectiveness and efficiencies increase with more data. Every time the AOS is used, despite the use of an autopilot, the data can be used to improve the algorithm.

5.2.4. PTZ IP Camera Test Results

The camera mounting system easily attached with U-bolts to the vertical stanchion on the bow of the Clean Venture vessel. The camera controls were functional through the remote connection to the control computer. Some lag was experienced when viewing remotely due to the somewhat slow connection over the cellular data link but overall was able to be controlled and provided real-time feedback to shore on what the sensor and skimmer were doing. Figure 21 was captured from the PTZ camera.

5.2.5. Control Box issues identified in testing

The control box was mounted in an unprotected area of the boat. The method of routing wires did not allow the rear cover of the box to be attached so plastic sheeting was used to cover the opening to prevent any possible water splashing from reaching the electronics. The initial control box wiring was updated after the test to allow the rear and top cover of the box to remain closed during operation. A connection panel at located on the front of the box was designed to allow accessory components such as the GPS antennas and sensors to be routed as needed. A schematic of the final control box wiring is included in Appendix C and a picture of the box on the Clean Venture boat is shown in Figure 23.

The cell modem/router supporting the remote connection did not suffer from connectivity issues but needed approximately 3 minutes to acquire the cell signal and connect to the Internet. Once connected, full remote operation, including viewing the real-time camera feed was possible.



Figure 23: Navigation/Control box on vessel.

6. Sensor Performance during Second Ohmsett Test

The March 2016 testing performed at Ohmsett provided for the evaluation of some of the improved prototype system components including the two oil slick thickness sensors, the percentage-oil-in-water discharge hose sensor, and a RTK GPS system. Testing was divided into two segments: on-water oil thickness sensor performance and discharge line water-in-oil testing.

Testing for each oil slick thickness sensor was performed with the sensor integrated into the same advancing skimming system tested on Gardner Lake, which was towed through patches of oil. Ohmsett produced controlled thickness oil slicks and wave conditions for evaluation at varying tow speeds. The RTK GPS system recorded position data during testing.

RTK satellite navigation is a technique used to enhance the precision of position data derived from the GPS system. It uses measurements of the phase of the signal's carrier wave, rather than the information content of the signal, and relies on a single reference station or interpolated virtual station to provide phase measurements from a known location. Centimeter-level accuracy is possible in real time using a double-differencing technique. Alion test engineers installed the single reference station on the side of the tank prior to testing. It is suggested that BSEE invest in a permanent single reference station that could be used for all further testing. This will save time for test engineers who desire the extremely accurate position data (they would not have to install it prior to testing and break it down after testing) and would also offer the precision position data for all testing performed at Ohmsett. For reference this would cost around \$15k based on current prices of RTK equipment.

The second test segment evaluated performance of the percentage water-in-oil sensor using actual oil recovery conditions. A stationary skimmer was placed into an oil slick in a boomed area and was controlled with respect to skimmer recovery rate and efficiency. Fluid recovered (oil/water mix) was offloaded through a typical discharge hose in which the oil/water sensor was installed. Percentage water-in-oil sensor data was collected as the skimmer operated through a broad range of efficiencies in order to correlate raw sensor output with actual water content in the fluid stream. To facilitate sensor calibration and performance evaluation, fluid samples were taken from the discharge hose directly after the sensor during operation and analyzed for bottom solids and water (BS&W).

6.1. Oil Thickness Sensor Tests

6.1.1. Oil Slick Thickness Sensor - Setup

The AOS system relies on input from an oil slick thickness sensor in order to detect and identify areas of the thickest oil concentration. For this prototype testing, the sensor being evaluated was deployed approximately 4 feet in front of an advancing commercial skimmer system and was subjected to multiple oil slicks, different travel speeds, and different surface conditions. The sensors were mounted to a buoyant hydrofoil attached to the end of a hinged outrigger beam allowing vertical movement for wave-following capabilities.

The operational position of the sensor relative to the water surface was predetermined and performance was dependent on the ability of the hydrofoil to conform and respond to wave conditions. The Clean Venture skimming system platform was comprised of a 20 foot flat-

bottomed boat equipped with two outriggers and guide ropes for control of a bow-mounted sweeping boom. An Elastec TDS118G grooved drum skimmer was fitted within the boom and was operated using compressed air from the main bridge to power the drum motor and remote offload pump (see Figure 24). The setup of the oil sensor and skimmer on the Clean Venture boat was similar to the setup during the Gardner Lake tests.



Figure 24: AOS vessel.

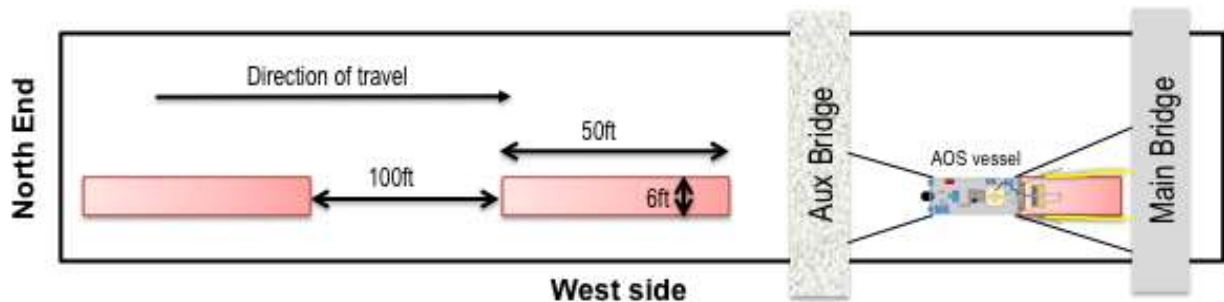


Figure 25: Test diagram.

The AOS was a stand-alone system on the vessel. The vessel was tethered between the main and auxiliary bridges such that controlled oil slicks were encountered while traveling south (see Figure 25). To create slicks of targeted thicknesses, the slick width and oil dispensing rate were controlled. The pump rates were predetermined to dispense the appropriate volume per unit area at the defined advancing speeds. A nominal slick width of 36 inches was created using two 35 foot long, 10 inch diameter booms positioned ahead of the skimmer forming a channel. While advancing, the test oil (Hydrocal 300) was dispensed from a wide spread T-manifold at the water's surface into the boom channel opening. The slick length was controlled by an operator

located on the main bridge at the pump who started and stopped flows using the facility’s built-in distribute/recirculation loop. A pneumatic actuator near the distribution T-manifold provided for concise on and off flow control. The channel length provided ample time for the dispensed oil to equalize and form a relatively uniform slick prior to reaching the sensor (see Figure 26).



Figure 26: Example oil slick.

6.1.2. Oil Slick Thickness Sensor – Test Performed

Alion prepared two oil slick thickness sensors for testing: an Arjay 2852-HCF and a GE Leakwise ID-227. One day of testing was allotted for each of the two sensors. Using new Hydrocal 300 test oil, the bridges traveled in the southerly direction at speeds ranging from 0.75 to 1.5 knots. As the system traveled along the length of the basin (800 ft), multiple oil slicks of controlled thicknesses ranging from 5 mm to 15 mm were produced. Each test run consisted of two or three individual oil slicks approximately 50 feet in length with approximately 75 feet of open water separating each. At the conclusion of each run, the remaining oil was cleared to the North of the test area with high pressure water jets in order to minimize any residual surface oil that might interfere with subsequent readings. Testing was performed in calm surface conditions and waves with amplitudes ranging from 4 to 10 inches and wavelengths of 25 to 40 feet. A series of 12 tests using defined parameters were repeated for each sensor. The Arjay test matrix is shown in Table 1 and the GE matrix is shown in Table 2.

Table 1: Arjay Oil Thickness Sensors Test Matrix.

Test	Target Oil Thickness (mm)	Oil dispensed at (gpm)	Spd (kt)	Wave Height (in)	Wave length (ft)	Est. Oil Thickness (mm)	Avg Sensor Reading (mA)	Std Dev Sensor Reading
1A	5	28	0.75	none	none	4.8, 5.3, 4.5	15.8, 15.5, 15.6	0.41, 0.20, 0.17
1B	5	46.6	1.25	none	none	4.9, 5.1, 5.0	13.9, 13.3, 13.9	1.06, 0.96, 0.54
1C	15	83.9	0.75	none	none	15.7, 15.6, 15.3	16.8, 16.9, 16.8	0.29, 0.29, 0.30
1D	15	139.8	1.25	none	none	14.4, 18.3, 18.2	16.4, 16.5, 16.4	0.39, 0.41, 0.18
1E	15	139.8	1.25	5.38	25.69	15.1, 17.1, 16.5	15.7, 15.9, 16.1	1.17, 0.85, 0.80
1F	15	139.8	1.25	6.46	41	16.6, 17.3, 16.2	15.7, 15.9, 15.9	1.32, 0.81, 0.73
1G	5	28	0.75	6.46	41	5.6, 5.7, 5.8	13.8, 14.5, 15.0	1.70, 1.16, 1.16
1H	5	28	0.75	9.9	36	5.3, 5.0, 6.4	12.9, 13.0, 13.9	2.04, 1.67, 1.50
1I	15	112	1	5.38	25.69	18.9, 17.2, 17.8	16.5, 15.2, 15.2	0.78, 1.71, 1.81
1J	10	112	1.5	5.38	25.69	14.1, 11.5, 12.8	15.3, 14.3, 14.1	2.03, 2.43, 2.58
1K	10	112	1.5	none	none	10.77, 11.1	15.6, 16.0	0.46, 0.50
1L	10	75	1	none	none	10.8, 10.2	16.0, 16.0	0.36, 0.38

Table 2: GE Oil Thickness Sensors Test Matrix.

Test	Target Oil Thickness (mm)	Oil dispensed at (gpm)	Spd (kt)	Wave Height (in)	Wave length (ft)	Est. Oil Thickness (mm)	Avg Sensor Reading (mA)	Std Dev Sensor Reading
2A	5	28	0.75	none	none	5.6, 3.9, 6.2	15.8, 16.4, 16.4	0.64, 0.14, 0.19
2B	5	46.6	1.25	none	none	4.8, 6.2, 5.9	16.0, 16.2, 16.2	0.44, 0.55, 0.73
2C	15	83.9	0.75	none	none	17.5, 15.6, 15.0	16.5, 16.7, 16.7	0.33, 0.17, 0.20
2D	15	139.8	1.25	none	none	20.6, 20.4, 20	16.5, 16.6, 16.5	0.44, 0.10, 0.49
2E	5	46.6	1.25	5.38	25.69	5.9, 4.7, 4.7	12.2, 11.9, 12.3	1.82, 1.15, 1.76
2F	5	46.6	1.25	6.46	41	5.1, 4.6, 4.7	14.3, 14.4, 14.9	1.32, 1.47, 0.84
2G	5	28	0.75	6.46	41	5.6, 5.5, 4.8	15.0, 15.7, 15.8	0.88, 0.51, 0.51
2H	5	28	0.75	9.9	36	5.8, 5.3, 5.0	14.4, 15.2, 15.8	0.91, 0.87, 0.69
2I	10	75	1	none	none	12.1, 11.5, 9.3	16.3, 16.4, 16.4	0.22, 0.14, 0.11
2J	10	112	1.5	none	none	10.2, 11.8	15.7, 16.1	0.30, 0.46
2K	10	75	1	6.46	41	12.3, 9.4, 10.4	15.5, 16.2, 16.1	1.20, 0.33, 0.36
2L	10	112	1.5	6.46	41	10.0, 10.5, 10.4	13.6, 14.1, 14.0	1.26, 1.34, 1.71

For each test run, oil storage tank level, wave height, weather data, tank water temperature, bridge position, and bridge speed data were recorded. Actual slick thicknesses were estimated from the amount of oil dispensed and the distance traveled while dispensing the oil (amount of oil verses surface area). Note that the values estimated in the table are a little bit high as video analysis indicated that there was some lag in the valve shut-offs leading to the oil being dispensed over a longer distance than recorded. Sensor readings were recorded at 10 Hz the entire run; markers were inserted into the data files to indicate entry to and exit from each oil patch. The times of entry/exit were then fine-tuned by viewing the video recordings. Average sensor values for the time periods in the oil patch were then computed. Complete data tables and graphs for each test are contained in Appendices D and E.

For tests with wave conditions the stroke (inches) and cycles per minute (cpm) for the wave machine were set to certain values and logged. These values were converted to significant wave height ($H_{1/3}$) and wavelength using calibration curves provided by Ohmsett. The calibration curves had been computed during a previous project Ohmsett project.

6.1.3. Oil Slick Thickness Sensor Results

The thickness sensor float assembly performed well during both the lake and Ohmsett testing. In calm water the float tracks well and allows constant sensor contact to the water surface. In rougher water the float did have the tendency to leave the surface but given the small footprint of each sensor this would be very difficult to avoid. During the tests with larger waves the vessel's flexible boom supports would lift and pull the actual skimmer frame, which would translate into the float arm at times. Mounting the skimmer floating in front of the vessel is not traditionally used for underway skimming so this issue may be localized to this particular setup.

6.1.3.1. Arjay Sensor

The results from the first run of the Arjay sensor can be seen in Figure 27 (5 mm, 0.75 knots, calm). This is representative of calm water results. All of the Arjay graphs can be found in Appendix D. The green lines in the figure show the times at which the sensor first encountered the oil patch and the red lines show the times at which the sensor left the patch. These times are based on the video recordings (with time overlay) taken from the skimmer boat.

Although the intent was for the patches of oil to be uniform thickness, with patches of no oil in between, in actuality the patches were not uniform and the water between the patches was not free of oil. This can be seen very clearly in the videos that were taken of the tests. The Arjay sensor actually gives a reasonably accurate reading of whether oil is present or not. For example, Figure 28 is a screen capture of the video from the first Arjay test at time 13:52:36, which should be a place clear of oil between patches one and two. However, the video shows a small patch of oil in this location, which was recorded as a spike of the sensor reading at that time (see arrow in Figure 27). It is also clear from the videos that in general the space between the patches has small amounts of oil, which is reflected by the sensor readings not going back to zero between patches.

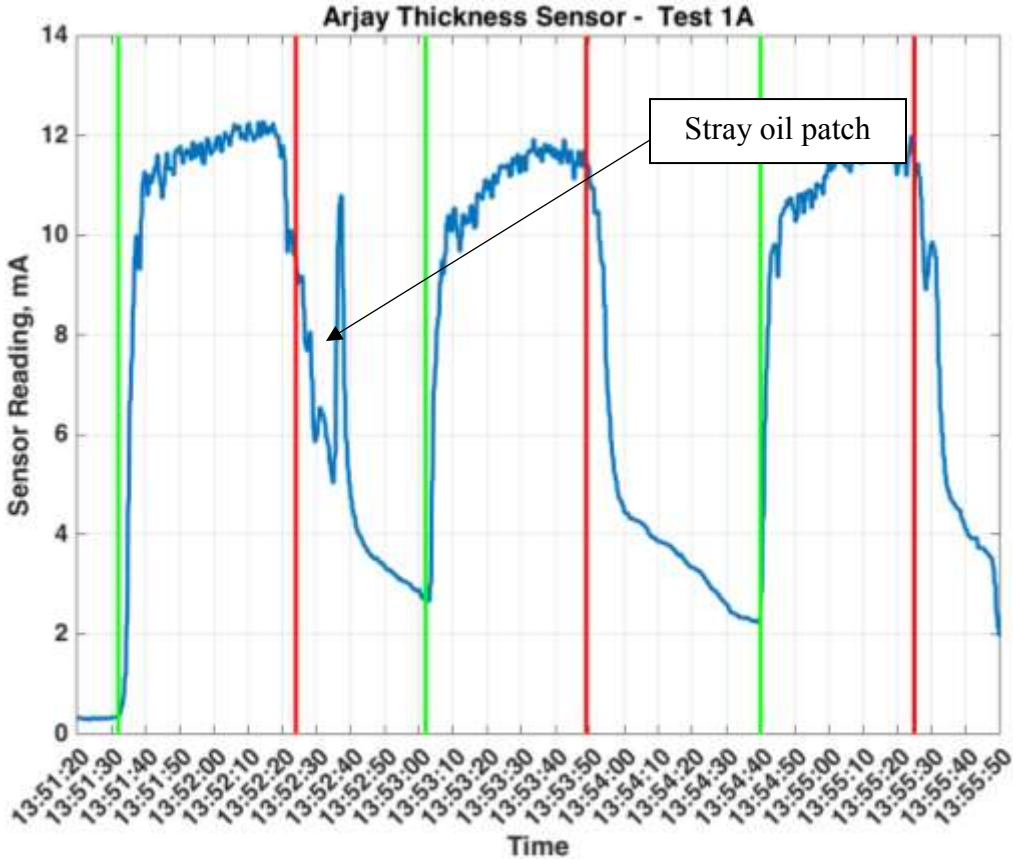


Figure 27: Arjay Sensor first run.



Figure 28: Screen capture of stray oil patch from Figure 27.

We can make the following general conclusions from the Arjay sensor tests:

- The sensor tracks the oil very well in calm water.
- The sensor also tracks fairly well in wave conditions, although the response is noisier and the sensor would occasionally leave the water surface.
- There is no measurable delay in the sensor reading compared to when the sensor actually encounters the oil.
- While the sensor gives an accurate indication of whether or not oil is present, there is not much difference in the sensor readings for the different thicknesses of oil. For example, readings (in calm water) for (target) 5 mm thickness were typically ~15.5 mA, ~16 mA for 10 mm, and 16.5-16.8 mA for 15 mm.
- When in wave conditions the sensor readings were quite a bit lower and more variable: ~12.9-15 mA for (target) 5 mm oil thickness, 11.5 – 14.1 mA for 10 mm, and 15.7 – 16.1 mA for 15 mm.
- The results were not 100% consistent as the average values for nominal 5 mm patches ranged from 13.3 mm to 15.8 mm. Due to the patchiness of the oil in the slicks, especially at the 5 mm nominal thickness, it is impossible to determine if this is sensor errors or just a result of the variable thickness experienced.
- All of the sensor readings were higher than what would have been expected based upon the calibration curves (Figure 5); whether this is inconsistent sensor performance or an indication of extra oil build-up under the sensor head is undetermined.
- There is an obvious slope at the end of the patch showing the sensor is leaving the oil.

6.1.3.2. GE Sensor Results

There appears to be a consistent delay between the time the GE sensor is immersed in oil and when the sensor data shows a response. This delay was determined by analyzing the forward boat video and comparing it to the recorded data. Figure 29 shows an example of a GE sensor results. Figure 30 shows a screen shot from the boat bow video of the first patch as the sensor enters the oil. For example, in Figure 29 the data began to indicate the presence of oil at approximately 14:14:33; however, the oil is clearly at the sensor at about 14:14:27 (Figure 30). This delay is about 5 seconds and is believed to be due to averaging in the sensor interface.

There also appears to be a delay when the oil dissipates from around the sensor although this is harder to determine since the oil dissipates slowly and unevenly. Also it is unknown what is happening under the sensor, i.e. the oil that is pooled around it and “stuck” to it before the moving water forces all the oils away from the sensor.). All of the GE graphs can be found in Appendix E.

Figure 31 and Figure 32 show that while the oil has clearly passed the sensor, the sensor continues to report a (lesser) presence of oil. This may be due to oil under the sensor taking longer to be “cleansed” from the sensor by the moving water. The sensor reported no oil only during the very first test in each subset. This may be due to the fact that high pressure water cannons were used to move all the residual oil back and the sensor had longer to dissipate all residual oil under and around the sensor.

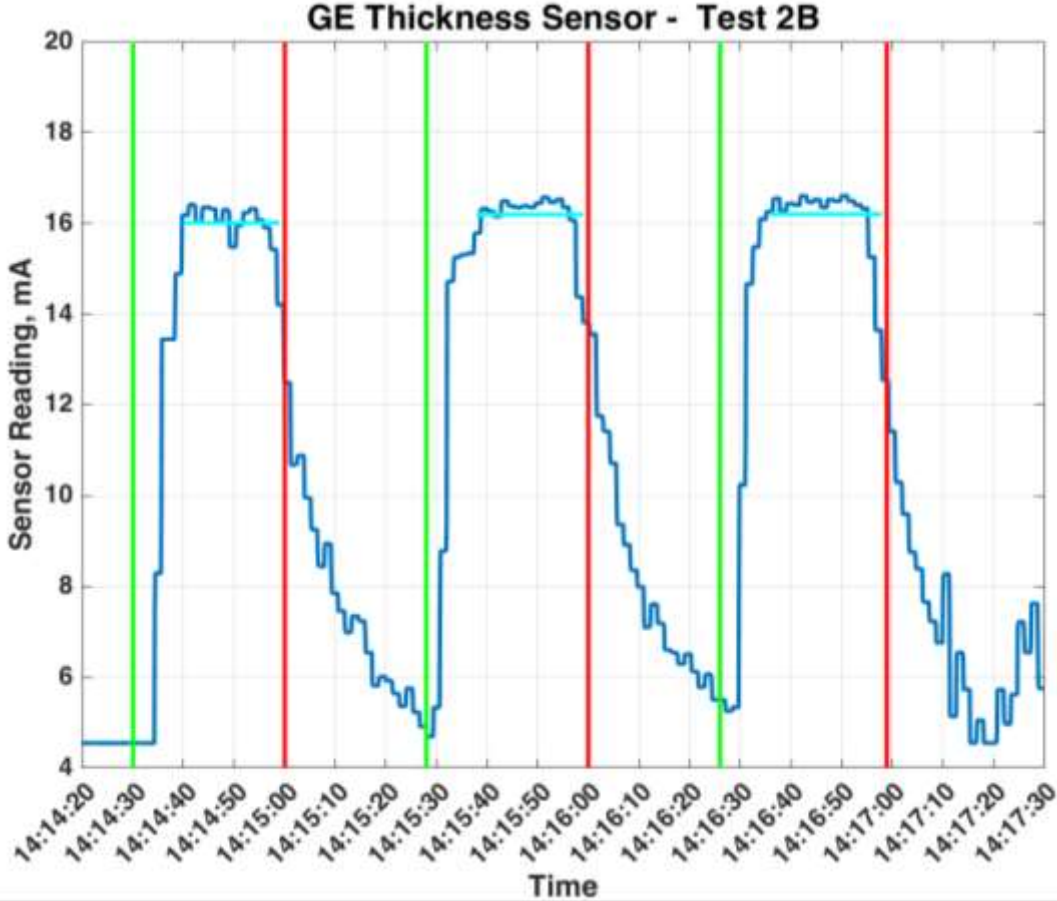


Figure 29: GE sensor example run.

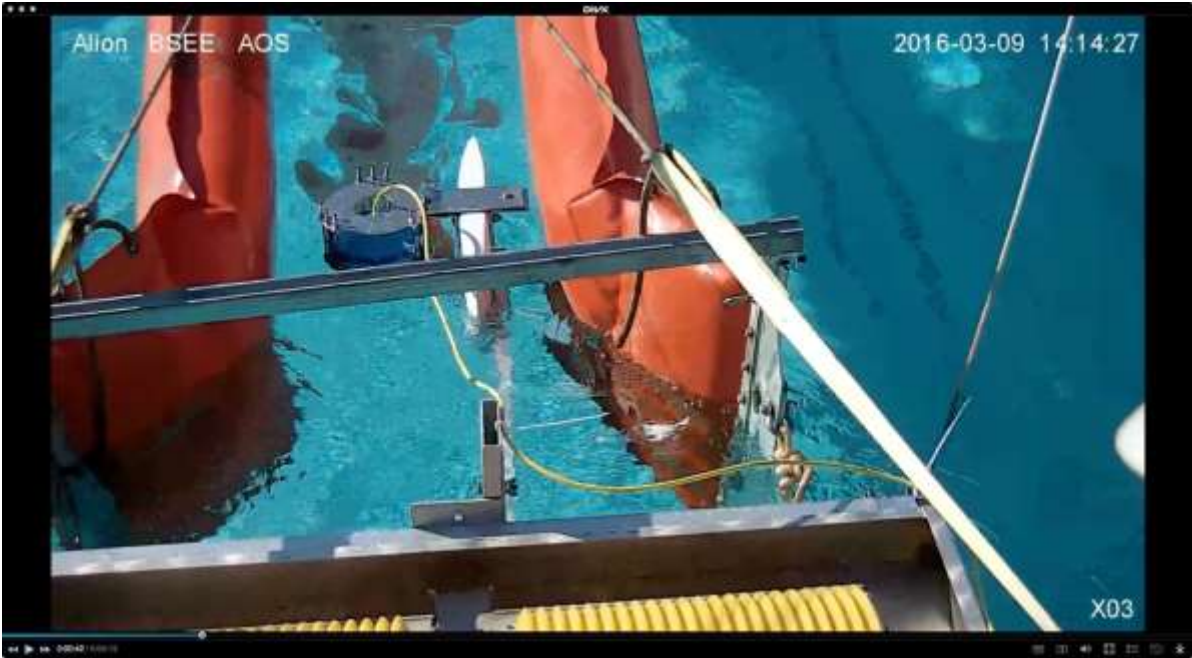


Figure 30: Screen capture of GE sensor entering oil patch.

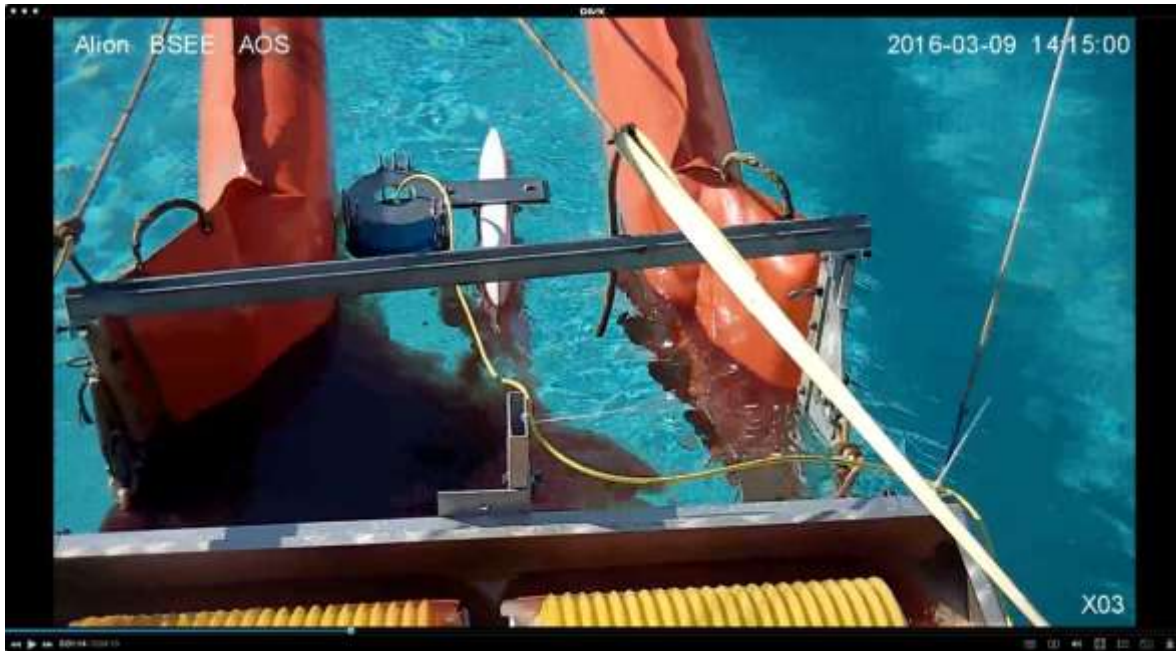


Figure 31: Screen capture of GE sensor leaving oil patch.

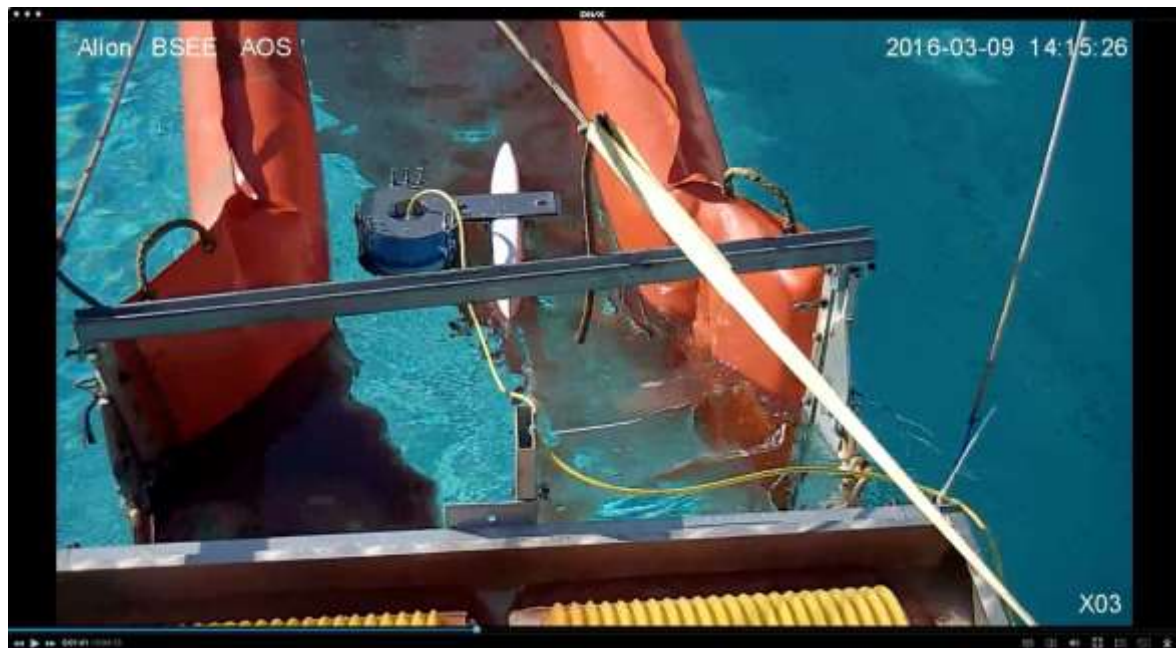


Figure 32: Screen capture of GE sensor prior to entering oil patch.

We can make the following general conclusions from the GE sensor tests:

- The sensor tracks the surface well in calm water and long period waves.
- The GE sensor did not track as well as the Arjay sensor in long period waves. It was “bouncier,” which may have been due partially to its heavier weight.

- There was a ~5 second delay in the sensor reading compared to when the sensor actually encounters the oil. This is most likely due to the sensor electronics. There is no way to configure the electronics to remove the delay.
- The sensor did not give continuous readings. It uses a sample and hold technique, which results in a step response output (actually, it is undetermined whether the sensor unit averages sensor readings for a second and then holds this average value as the output for the next second or whether it holds the instantaneous sampled value for the next second).
- In waves, the results are hindered by the sampling time. The sensor could be off the surface when capturing the data point.
- While the sensor gives an accurate indication of whether or not oil is present, there is not much difference in the sensor readings for the different thicknesses of oil. For example, readings (in calm water) for (target) 5 mm thickness were typically ~16.2 mA, ~16.3 mA for 10 mm, and 16.6 mA for 15 mm.
- When in wave conditions the sensor readings were quite a bit lower and more variable (similar to the Arjay results): ~11.9-15.8 mA for (target) 5 mm oil thickness and 13.6 – 16.4 mA for 10 mm.
- The results were not 100% consistent (although not as bad as on the Arjay sensor, maybe due to the sensor interface averaging) as the average values for nominal 5 mm patches ranged from 15.8 – 16.2 mA. Due to the patchiness of the oil in the slicks, especially at the 5 mm nominal thickness, it is impossible to determine if this is sensor errors or just a result of the variable thickness experienced.
- The sensor readings were higher than what would have been expected based upon the calibration curves (Figure 5) for the low oil thickness, and less than expected for the high oil thickness; whether this is inconsistent sensor performance or an indication of extra oil build-up under the sensor head is undetermined.
- As with the Arjay sensor, there is an obvious slope at the end of the patch showing the sensor is leaving the oil.

6.2. Discharge Line Oil Sensor Tests

6.2.1. Oil-in-Water Sensor – Setup

In order to evaluate the performance of the oil-in-water sensor, the objective was to provide conditions of varying oil/water concentration in a flow stream for measurement purposes. To accomplish this, a stationary skimmer was set up in a test area of approximately 15 by 15 feet square that provided a controlled environment to recover the oil and water to be sent through the discharge hose. An Elastec TDS118G grooved drum skimmer was used as the collection device with one wiper removed in order to reduce the recovery rate of the skimmer, achieve longer steady state conditions, and reduce oil consumption during each test. A cargo hose was routed from the skimmer's recovery pump to the Arjay 2852-OWI sensor, which was installed in a hard pipe and rigidly mounted to a forklift mast for stability. Immediately after the sensor location, a three-way valve was installed, which allowed for flow to be directed into a collection tank or to a second exit port for sampling (Figure 34).



Figure 33: Actual discharge sensor test setup.

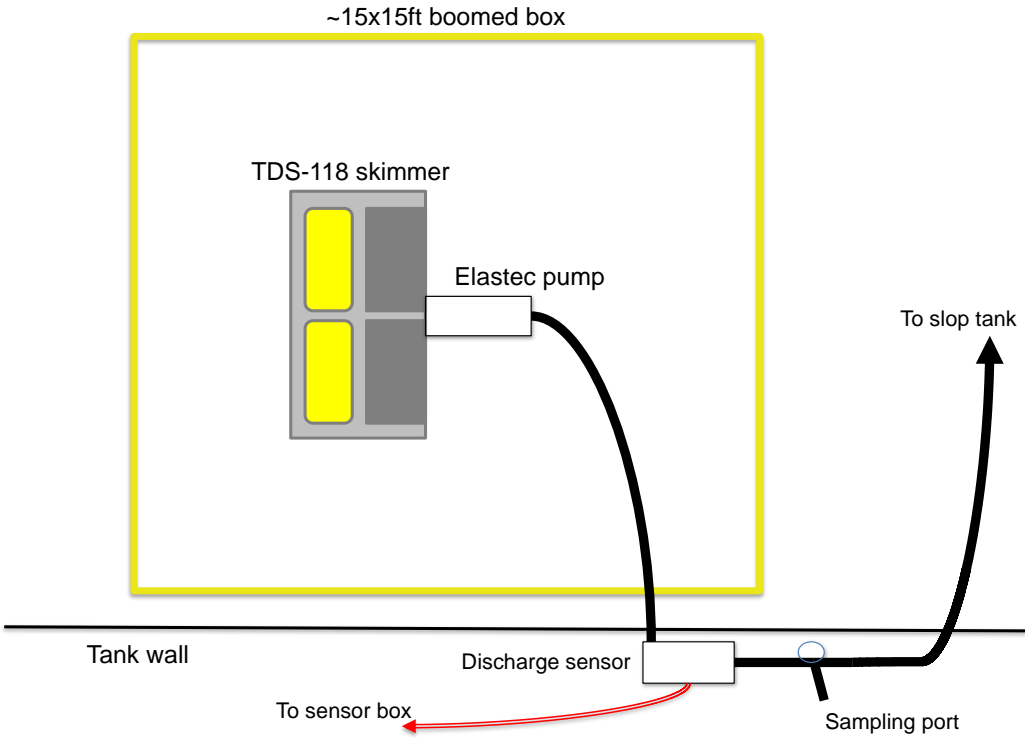


Figure 34: Configuration for Discharge Line Sensor test (hydraulic lines not shown).

6.2.2. Oil-in-Water Sensor – Test Performed

Prior to test start, the area was preloaded with used Hydrocal test oil to create a ~3-inch slick. Testing began by operating the skimmer at a slow drum speed to achieve a high oil-to-water ratio for the sensor measurement. Operational speeds of the skimmer were varied until the desired sensor output reading was achieved and reasonably steady. Flow was then quickly diverted from the discharge hose to sample containers (5 gallon bucket or 1 quart jar). Two samples were collected in sequence for each of the oil/water concentrations. Skimmer efficiency was intentionally increased or decreased in small increments in order to cover the full signal range of the sensor, which spanned 7 mA to 20 mA based on oil/water concentration. Eight tests were performed (labeled tests 25-32).

The sensor data was recorded continuously. Time markers were inserted into the data stream at the start and stop of each sample in order to compare fluid samples representative of the fluid stream passing the sensor as data was recorded. The point for each sample collection plotted in Figure 36 is the averaged sensor readings with standard deviation between the recorded start and stop marker. An example graph of the recorded sensor data is included in Figure 35. It was found to be difficult to keep a constant oil/water concentration, which led to constantly varying sensor output that can be observed in this graph. The negative slope of sample 3 results in a larger standard deviation than sample 4. Samples collected were later analyzed in the lab for BS&W.

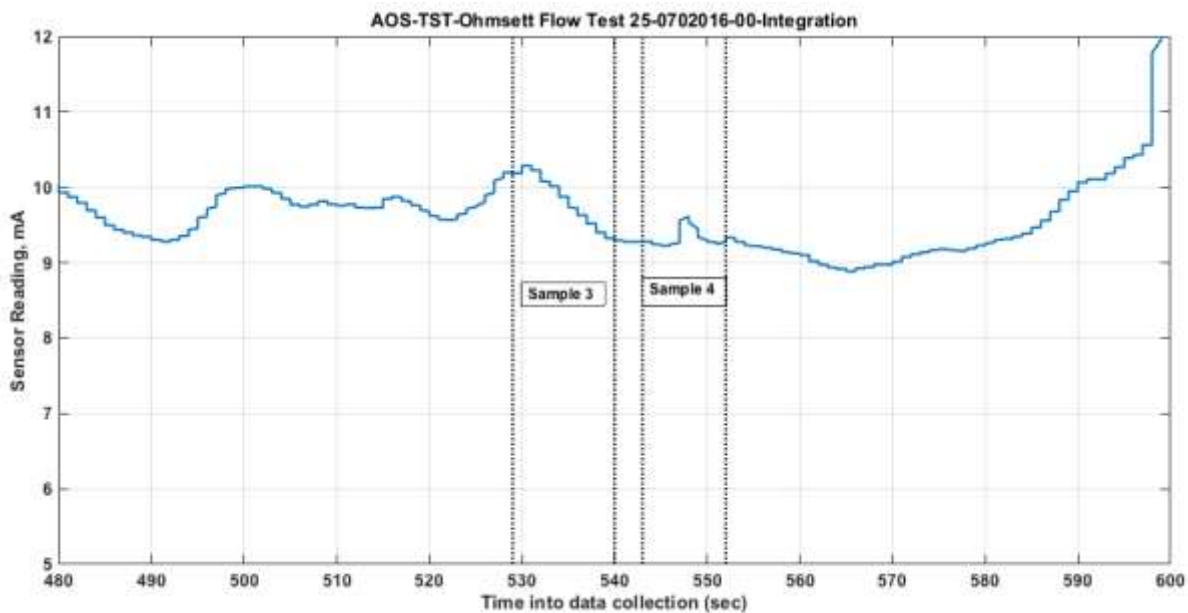


Figure 35: Example Oil-In-Water sensor output.

In an effort to cover the entire sensor range and conserve oil, the discharge hose was routed back to the test area for several tests. During these tests (labeled tests 33-36), increasing emulsification of the test oil was observed. The test area was skimmed and cleared before adding one inch of Hydrocal prior to the start of test 37. Four tests were performed in this configuration with samples retrieved for analysis. The listing of tests, sample numbers, drum speeds, and resulting oil concentration and average sensor readings are listed in Table 3.

Table 3: Discharge Line Sensor Tests and Results.

Sample Container Number	Test	Drum Speed (rpm)	Sensor Reading (mA)	Percent Oil in Fluid Stream (%)
1	25	27.0	6.8749	97.5
2	25	27.0	6.8672	97.5
3	26	50.0	9.859	78.5
4	26	50.0	9.3256	78.9
5	27	49.0	18.4498	78.4
6	27	49.0	18.1484	76.6
7	28	44.0	10.7319	73.8
8	28	44.0	10.8476	73.8
9	29	61.0	17.034	67.7
10	29	61.0	16.9418	59.9
11	30	47.0	15.4641	71.1
12	30	47.0	15.4213	62.2
13	31	27.0	12.2167	72.5
14	31	27.0	11.4318	72.5
15	32	31.0	7.7655	86.2
16	32	31.0	7.5953	87.5
17	33	49.0	19.9229	62.0
18	33	49.0	19.9911	64.0
19	34	40.0	10.7582	69.0
20	34	40.0	10.8879	68.0
21	35	35.0	15.4878	40.0
22	35	35.0	14.567	50.0
23	36	35.0	14.1055	47.0
24	36	35.0	14.212	43.0
25	37	16.0	12.6035	72.0
26	37	16.0	12.3274	72.0
27	38	16.0	13.5831	65.0
28	38	16.0	12.8232	62.0
29	39	16.0	15.392	57.0
30	39	16.0	15.2107	57.0
31	40	37.0	16.3574	52.0
32	40	37.0	15.589	50.0
Samples obtained in 5 gallon buckets				
Samples obtained in 1 Qt. mason jars				

6.2.3. Oil-in-Water Sensor – Results

The results of the Oil-In-Water sensor test are shown in Figure 36. The sensor appears to do a fairly good job of tracking instances of high oil concentration. There were four anomalous data points (circled); it is not clear why the sensor reading was so high for those particular points. As the sensor readings drop below 70% the readings become fairly erratic. There are two possible causes for this. First, the sensor is primarily intended for detecting low concentrations of water in oil and the manufacturer only claims good performance at higher oil concentrations. Second, it was difficult to use the skimmer to get higher water concentrations as it is an oleophilic skimmer that is designed to pick up oil and not water. To increase the water content a hose was run into the skimmer sump and water added; this water may not have been well mixed with the oil prior to being pumped out of the sump and past the sensor.

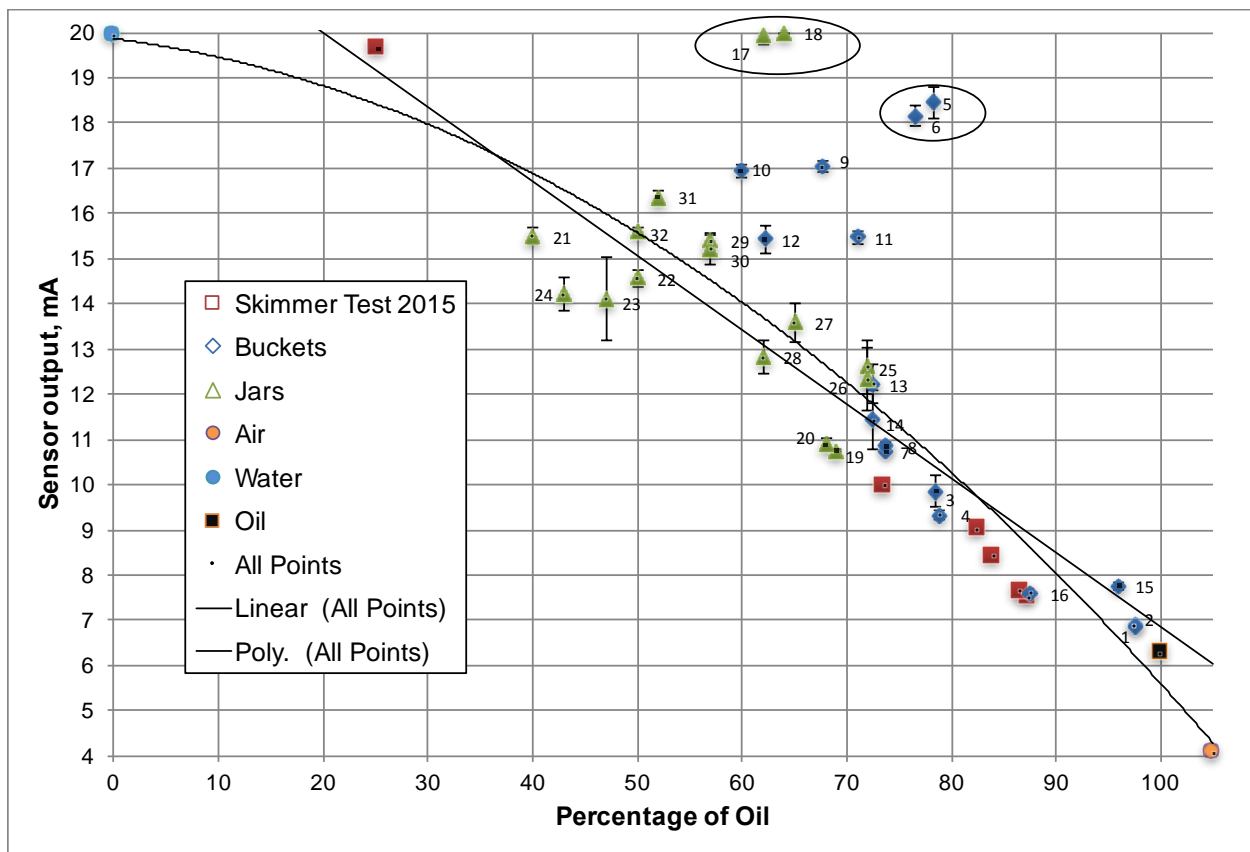


Figure 36: Oil-In-Water sensor results.

7. Algorithm Performance

During the Gardner Lake test, it was determined that the original “lawn mower” skimming pattern is not ideal for oil skimming due to the limited turn rate of the skimming vessel. Using a modification of the original MATLAB program and algorithm, several new potential oil skimming algorithms were implemented taking this slower turn rate into account. These algorithms were implemented and tested on several different spill shapes of approximately the same area in order to compare their performance relative to each other. The three oil spill patterns used were: oblong, round, and narrow (see Figure 37).

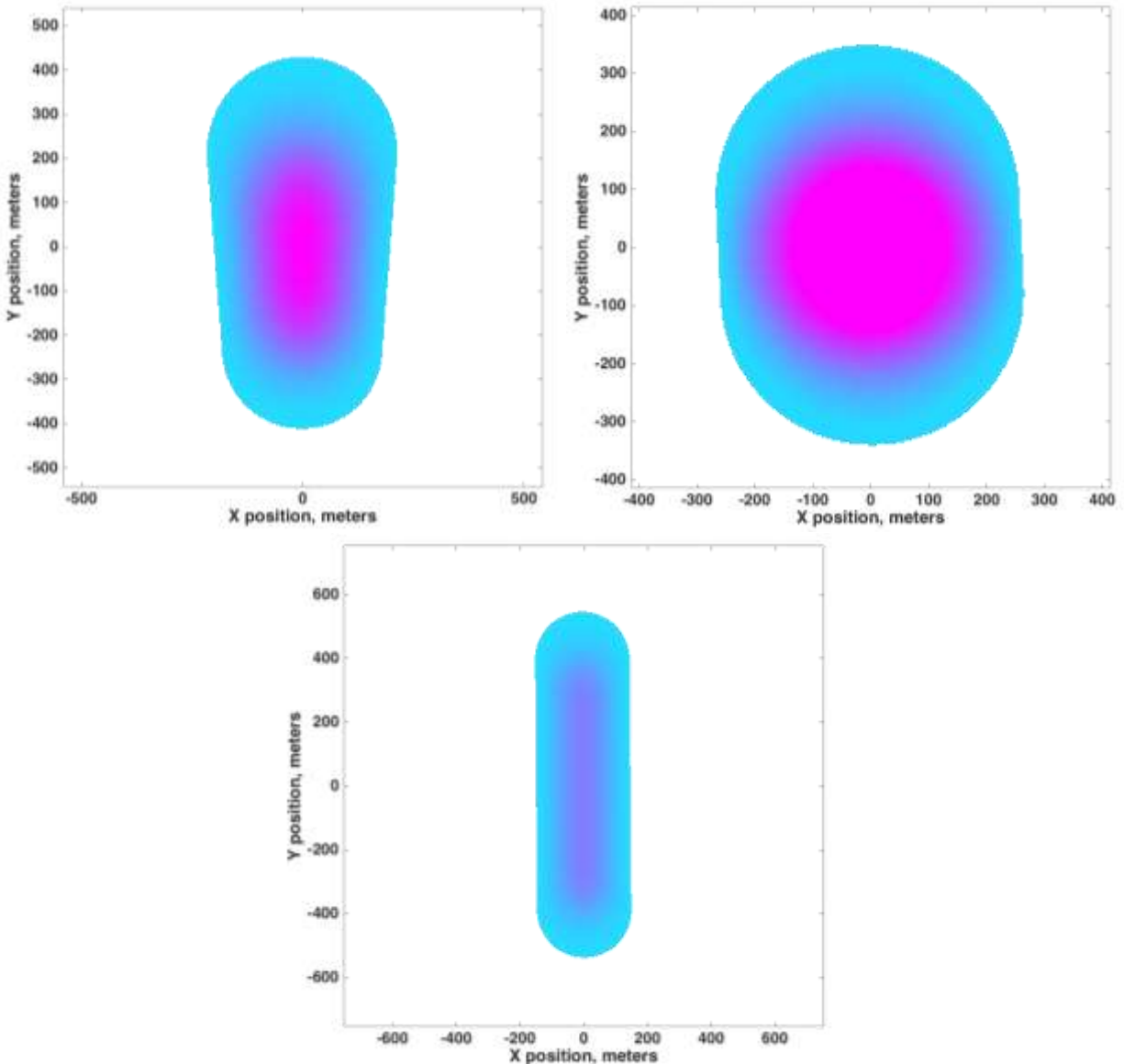


Figure 37: Oil spill patterns; oblong (top left), round (top right), and narrow (bottom).

The original MATLAB program was restructured and simplified to make the implementation of new algorithms easier. Simple vessel movements were placed into functions to create a cleaner and simpler implementation interface. The new program was also modified to allow for standard

spill shapes to be selected for consistency between algorithm simulations. Geographic coordinates were replaced with Cartesian coordinates for simplicity and clarity.

Several features were also added to the simulation program to make the simulations more realistic and the algorithms more efficient. The simple averaging spill-smoothing function was replaced with a gradual multi-step vessel path smoothing function in addition to periodic global Gaussian spill smoothing to more accurately represent oil slick diffusion. To increase skimming efficiency, an optional geometric virtual boundary was added that can restrict the vessel's movement to the more concentrated areas within the spill. Also, the oil pickup method itself was changed to more realistically model oil skimming, which is largely dependent on the maximum pickup rate of the skimmer.

7.1. Algorithm Descriptions

The following algorithms were tested (note: the algorithm figures show exaggerated movements to more clearly show algorithm progression):

7.1.1. Semi-random (Figure 38)

1. Pass through the spill.
2. When the edge is reached, turn a semi-random amount.
3. Repeat steps 1-2 as long as desired.

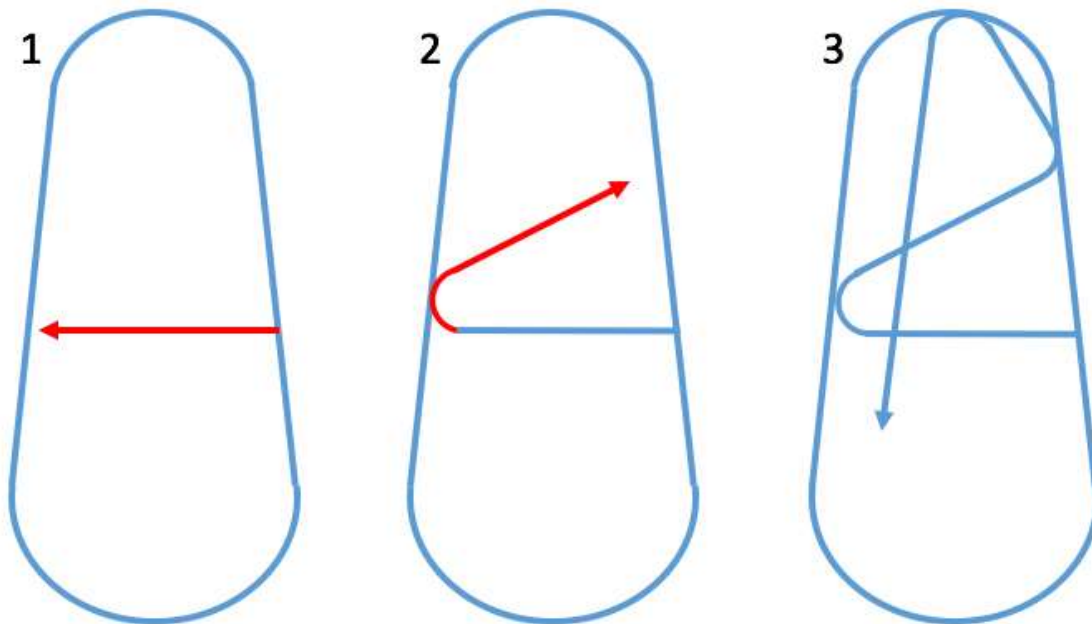


Figure 38: Semi-random algorithm pattern.

7.1.2. Star (Figure 39)

1. Pass through the spill, recording the amount of oil at each point.
2. Turn at the edge and return to the point with the most recorded oil.
3. Turn to a random direction and travel to the edge.
4. Turn around and travel straight through the spill, passing through the previous maximum oil point and again recording the amount of oil at each point.
5. Repeat steps 2-4 as long as desired.

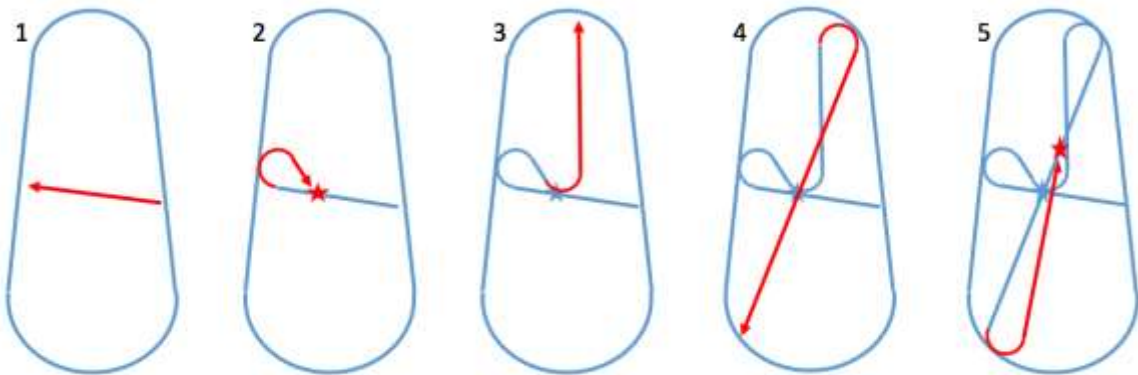


Figure 39: Star algorithm pattern.

7.1.3. Figure-8 (Figure 40)

1. Starting at a specified position, travel toward the edge at a slight angle relative to spill-oriented cardinal axes.
2. Turn around at the edge and travel through the spill, traveling toward a slightly lower point at the opposite edge.
3. Repeat step 2 until the spill has been traversed to the far edge.
4. When the edge is reached, return to specified starting position and repeat steps 1-3 in another orientation relative to the spill.

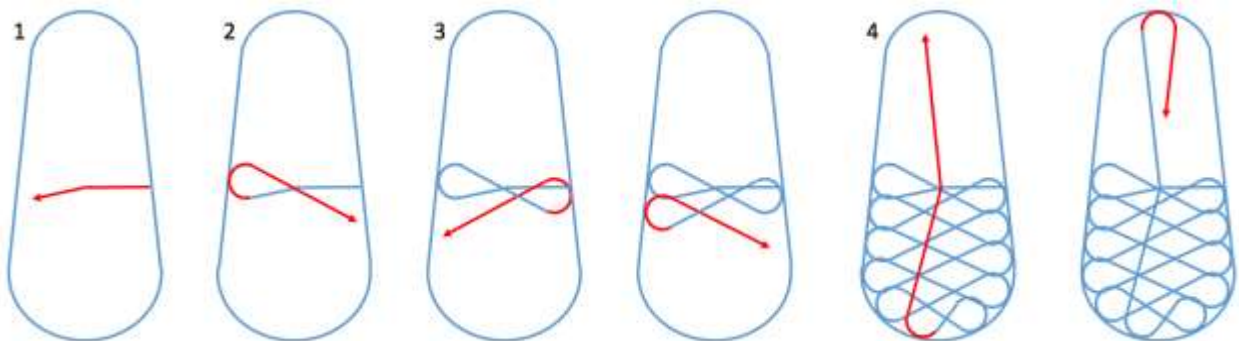


Figure 40: Figure-8 algorithm pattern.

7.1.4. Spiral (Figure 41)

1. Starting at the edge, follow the edge within a certain threshold and travel inward in a spiral shape.

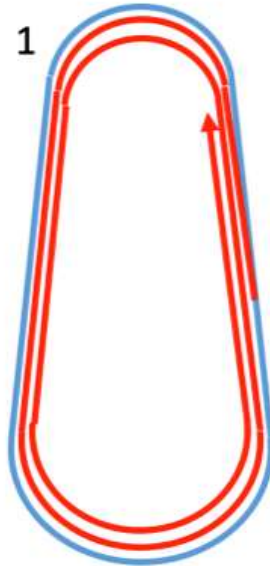


Figure 41: Spiral algorithm pattern.

7.1.5. Flower (Figure 42)

1. Pass through spill until edge is reached.
2. At edge, turn a specified angle (~180 degrees) and pass straight through spill again.
3. Repeat step 2 as long as desired to form a rotating oval pattern.

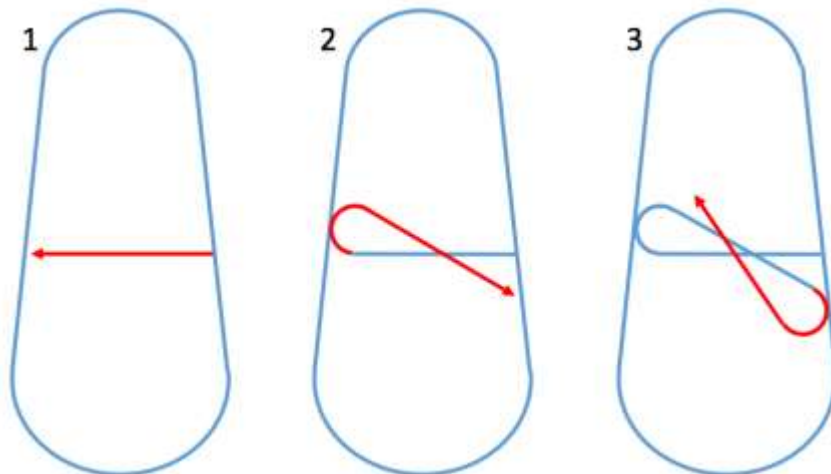


Figure 42: Flower algorithm pattern.

7.1.6. Looping (Figure 43)

1. Starting at a specified position, travel perpendicular to spill direction until edge is reached
2. Turn around 180 degrees at edge and travel through spill, parallel to original path.
3. Turn at the next edge, the same direction as before and slightly more than 180 degrees, to increment the looping along the length of the spill.
4. Repeat steps 2-3 until the conditions for step 5 or 6 have been met.
5. (optional) When the pattern begins to overlap the previously-covered area, change the turn direction to “jump” to the next pattern segment and again repeat steps 2-3.
6. When the edge is reached, return to specified starting position and repeat steps 1-4 in another orientation relative to the spill.

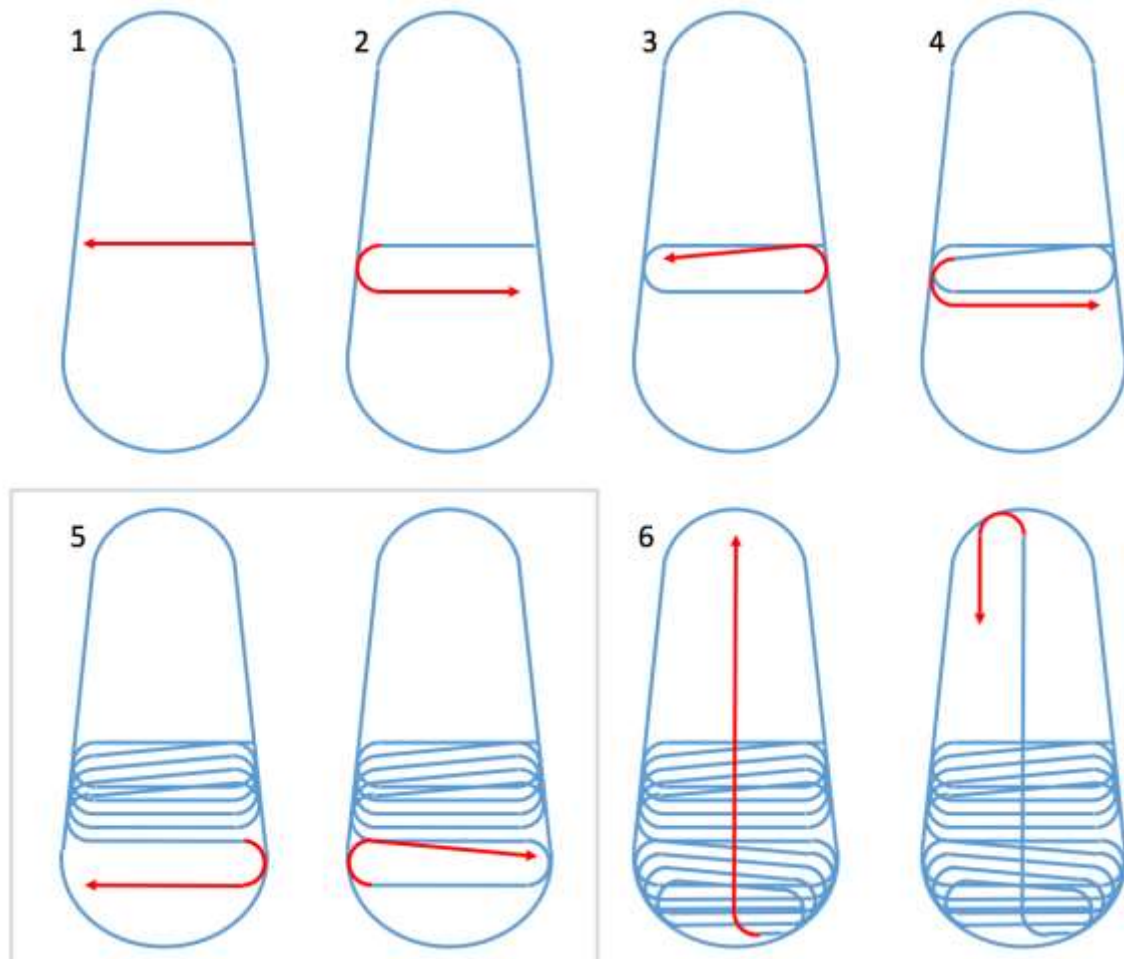


Figure 43: Looping algorithm pattern.

7.2. Algorithm Simulation Methodology

Each algorithm was simulated with a range of variable parameters in order to find the parameters that resulted in the optimal performance for each spill. First, several batches of simulations were run to determine the effects of skimming speed on skimming performance for each algorithm. It was found that the ideal skimming speed for most algorithms was 0.75 knots while going straight and 1.0 knot while turning. This speed distribution is not practical; however, since speeding up

during turns would likely result in oil spilling over the side of the booms near the edges of the spill. Because of this, further simulations were run at a constant speed of 1.0 knot during the entirety of skimming, which was the next most effective skimming speed for most algorithms.

Then a series of simulations was run for each algorithm and spill shape combination to determine the optimal parameters for each run. These simulation batches consisted of individual simulation iterations in every combination of the determined variable parameters. The primary variable parameters for each algorithm were:

- Figure-8: crawl distance along the length of the spill.
- Looping: crawl distance along the length of the spill, and optional “jump” or not.
- Flower: crawl distance along the circumference of the spill.
- Semi-Random and Star: range of angles for random direction choice.
- Spiral: oil concentration tolerance for inward spiral progression.

The optimal parameters for each algorithm were determined by running a separate simulation with each combination of algorithm parameters, then comparing the results to determine which set of parameters was most effective overall in skimming oil. This effectiveness was determined by observing the percentage of the spill’s total oil is picked up over time.

7.3. Algorithm Simulation Results

It can be seen in the results below that for each oil slick shape, each algorithm exhibits a very similar effectiveness over the (expedited) 60-hour simulation period. Starting as early as 12-hours into the simulation, though, a slight divide begins to emerge between two groups of algorithms and one outlier. The Figure-8 and both Looping algorithm variations, all of which gradually crawl along the length of the spill, perform marginally better than the other algorithms later in the simulation. The Flower, Semi-Random, and Star algorithms, which continually rotate to different orientations with respect to the spill, are less effective. The Spiral algorithm falls into a class of its own because of its unique performance behavior.

The difference between the “crawling” and the “rotating” algorithms is caused by the “crawling” algorithms being more consistent in their progression; they focus on one half of the spill at a time, moving onto another half of the spill once finished. The “rotating” algorithms, by comparison, are more likely to not exhibit as much coverage later during simulation. Because they do not follow a set progression between sections of the spill but instead repeat a pattern over the spill as a whole, they are more likely to not encounter any small, stray concentrations of oil that may occur within the spill. This inconsistency is even more apparent as the slick becomes longer and more stretched out, as in Spill 3, Figure 46 and Table 6.

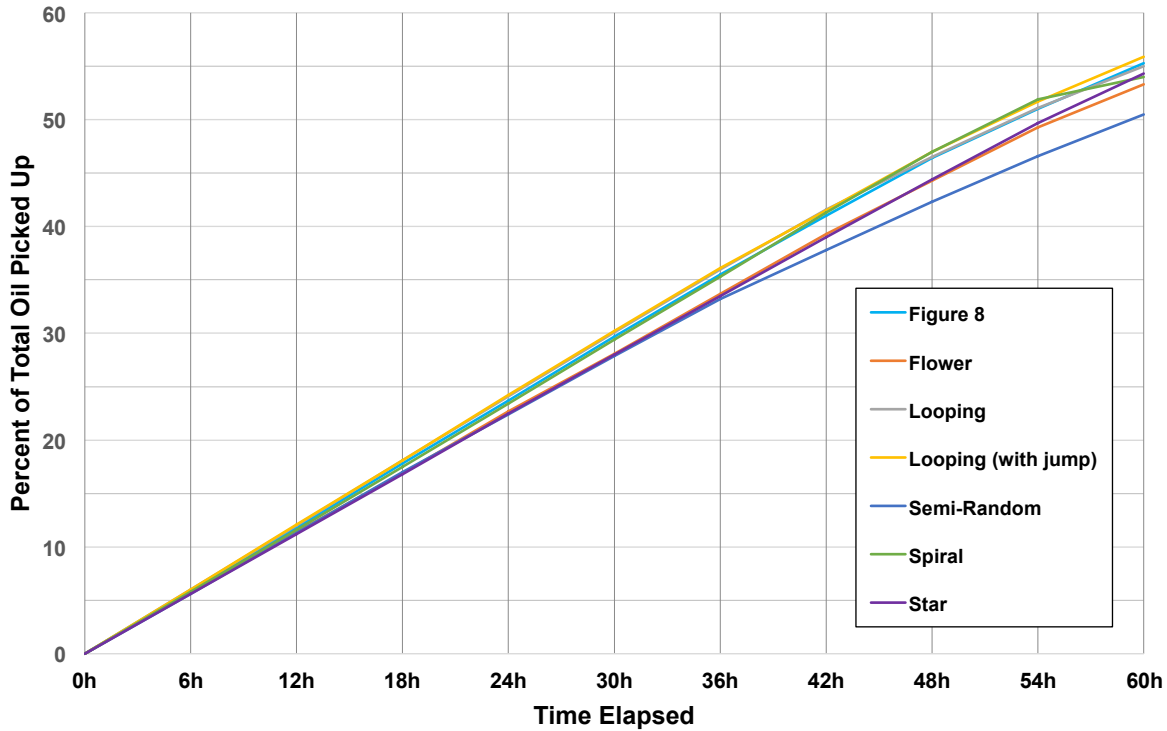


Figure 44: Spill 1, oblong pattern.

The Spiral algorithm begins simulation below the “crawling” group in effectiveness, but partway through simulation increases in effectiveness relative to the other algorithms before plateauing at the end of its run. This performance results from the unique behavior of the Spiral algorithm, which is thorough but in theory covers each point of the spill only once. For this algorithm to be practically implemented, it would need to be tuned to each specific oil slick so that it would be able to be as thorough as possible yet still reach the center of the spill within a given time frame.

Table 4: Spill 1, Oblong Pattern, Percent Oil Recovered after N Hours for Each Algorithm.

Spill 1	0h	6h	12h	18h	24h	30h	36h	42h	48h	54h	60h
Figure 8	0.0	5.9	11.8	17.8	23.7	29.7	35.5	41.0	46.4	51.0	55.3
Flower	0.0	5.8	11.4	16.9	22.7	28.1	33.7	39.3	44.3	49.3	53.3
Looping	0.0	6.0	12.0	18.1	24.1	30.1	36.0	41.6	46.5	51.1	55.0
Looping (with flip)	0.0	6.0	12.1	18.1	24.2	30.2	36.1	41.5	47.0	51.7	55.9
Semi-Random	0.0	5.6	11.3	17.0	22.4	27.9	33.2	37.8	42.3	46.6	50.5
Spiral	0.0	5.8	11.6	17.5	23.4	29.4	35.3	41.3	47.0	51.9	54.0
Star	0.0	5.6	11.2	16.8	22.5	28.0	33.5	39.0	44.4	49.7	54.3

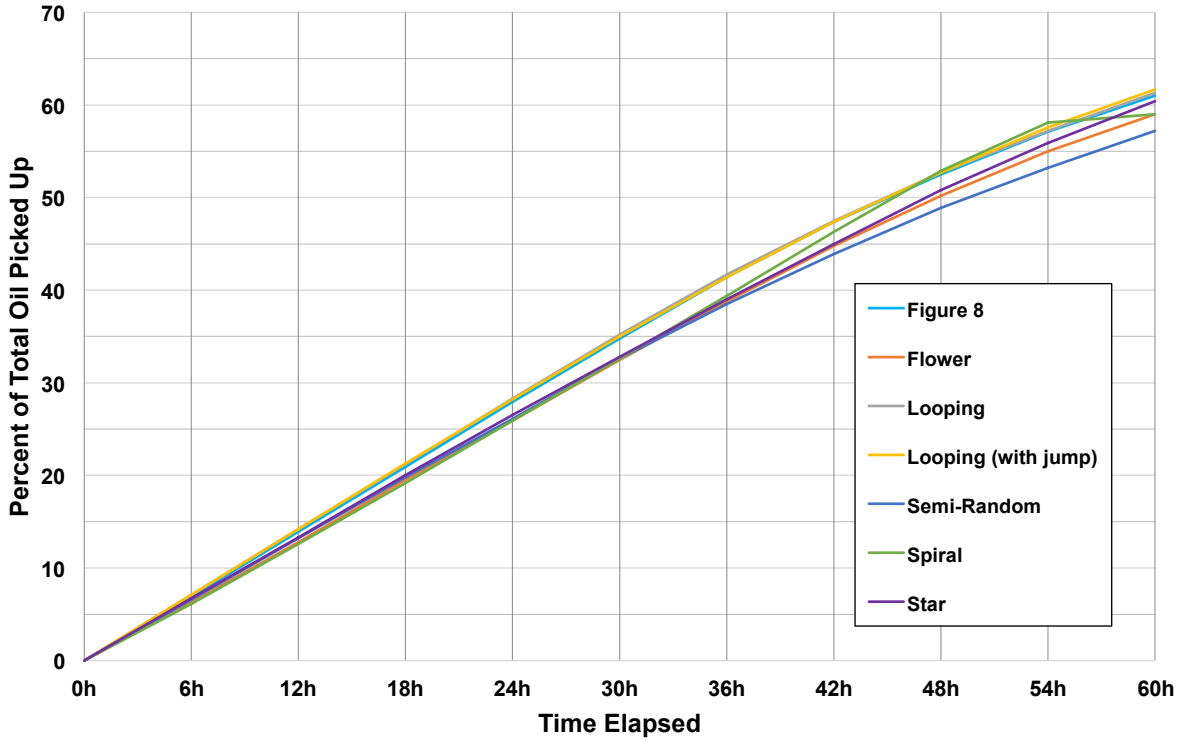


Figure 45: Spill 2, Round Pattern.

Table 5: Spill 2, Round Pattern, Percent Oil Recovered after N Hours for Each Algorithm.

Spill 2	0h	6h	12h	18h	24h	30h	36h	42h	48h	54h	60h
Figure 8	0.0	6.9	13.9	20.9	27.9	34.8	41.4	47.4	52.5	57.1	61.0
Flower	0.0	6.3	12.8	19.5	25.9	32.5	38.8	44.8	50.2	55.0	59.0
Looping	0.0	7.1	14.2	21.2	28.3	35.2	41.7	47.5	52.7	57.2	61.3
Looping (with flip)	0.0	7.1	14.2	21.3	28.2	35.0	41.4	47.4	52.7	57.6	61.7
Semi-Random	0.0	6.6	13.2	19.8	26.1	32.6	38.5	43.9	48.9	53.2	57.2
Spiral	0.0	6.1	12.6	19.2	25.9	32.6	39.4	46.3	52.9	58.1	59.0
Star	0.0	6.7	13.3	20.0	26.5	32.8	39.0	45.0	50.8	55.9	60.4

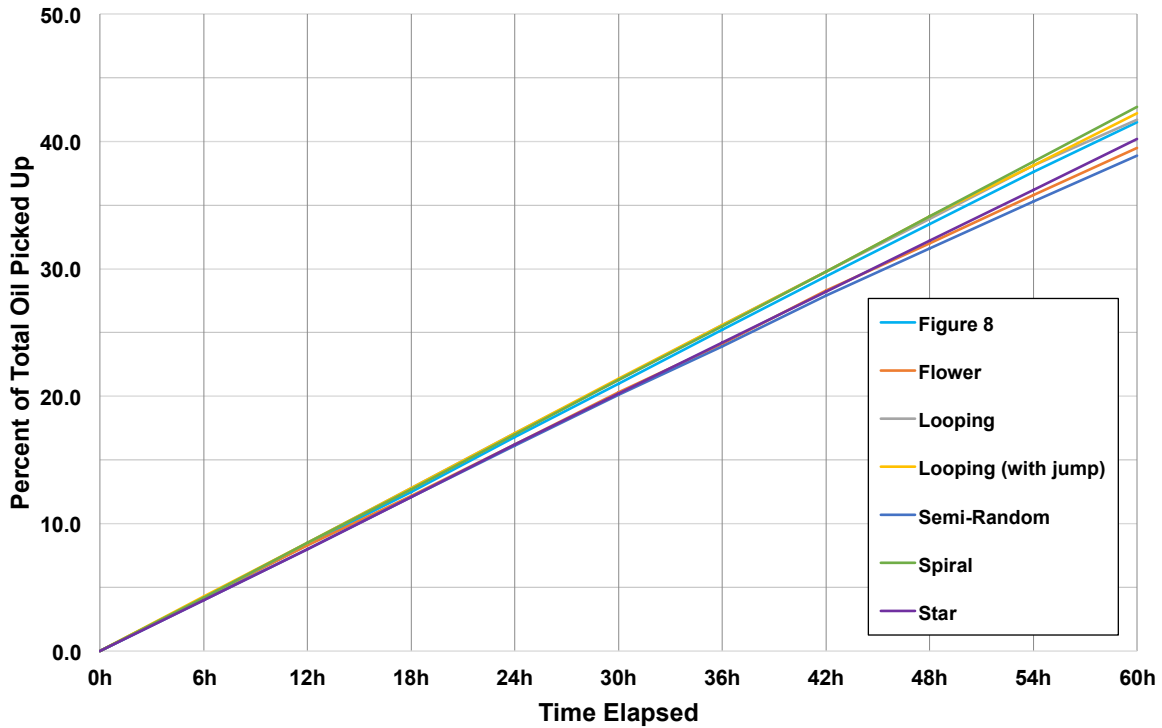


Figure 46: Spill 3, Long and Narrow Pattern.

Table 6: Spill 3, Long and Narrow Pattern, Percent Oil Recovered after N Hours for Each Algorithm.

Spill 3	0h	6h	12h	18h	24h	30h	36h	42h	48h	54h	60h
Figure 8	0.0	4.1	8.4	12.5	16.8	21.0	25.2	29.4	33.5	37.6	41.5
Flower	0.0	4.2	8.3	12.2	16.2	20.3	24.1	28.3	32.0	35.8	39.5
Looping	0.0	4.2	8.5	12.8	17.1	21.3	25.6	29.8	33.9	38.1	41.7
Looping (with flip)	0.0	4.3	8.5	12.8	17.1	21.4	25.6	29.8	34.1	38.1	42.2
Semi-Random	0.0	4.0	8.0	12.1	16.1	20.1	23.9	27.9	31.6	35.3	38.9
Spiral	0.0	4.2	8.5	12.7	17.0	21.3	25.5	29.8	34.1	38.4	42.7
Star	0.0	4.0	8.0	12.1	16.2	20.2	24.2	28.2	32.2	36.2	40.2

The looping (with flip) pattern seemed to perform the best of the seven across all times and patterns; although the absolute differences were not that great.

8. Recommendations

8.1. Thickness Sensors

Neither of the two thickness sensors worked as well as desired. Although both easily detect the transitions from oil to water and vice versa, there is no solid thickness assessment. The sensors appear to be able to give some relative indication of thickness, but only in a gross sense, not small differences in thickness. It is not clear whether this is a fundamental limitation of the sensor technology or the hydrodynamic packaging. One flaw with any sensor that must be in contact with the oil surface is that the act of making the measurement disturbs the surface being measured. Also, if it does not remain exactly on the surface, then the measurement is also inaccurate. It is difficult to ensure a contact sensor remains exactly on the surface given the interactions of the waves (swell and chop) with the movement of the sensor float and supporting structure (skimmer and vessel). Attempts to improve the performance will just make the entire structure more complex and thus less supportable in the field (both installation and maintenance as well as use by non-technical vessel operators).

8.2. Inline Sensor

The inline sensor worked reasonably well for high oil concentrations. Although the sensor was erratic below about 70% oil, this should not be a problem for typical oil spill recovery operations as most skimmers have efficiency much better than this. Coupled with a flow sensor, this could be used to provide real-time estimates of recovery rate and efficiency.

8.3. Autopilot/vessel Integration

The Alion AOS concept is for the system to be mounted onto a vessel of opportunity, mainly (but not exclusively) vessels belonging to Oil Spill Response Organizations (OSROs). To this end, partnering with an OSRO would be extremely beneficial for further open water vessel testing. Many of the OSRO's have vessels outfitted with commercial autopilot systems, the latest in underway skimming technologies, and advanced sensor packages. This partnership would aid in the integration of the system to existing platforms as well as gain access to a wealth of knowledge from professional oil spill management personnel.

If a standardized system is developed and implemented, an Oil Recovery Workboat such as LAMOR's 15000 (Figure 47) could have the modifications already installed to ease the installation of the AOS. Instead of the field technicians "tapping" into the autopilot a pre-installed access port would allow a quick installation of the AOS. This would be analogous to a harbor pilot boarding a vessel for pilotage and plugging his navigation computer into the existing "pilot port" all large vessels are required to have.

A further consideration for vessels that do not have an existing autopilot system or where safety concerns necessitate manual steering, the system may still be used to direct the operations by providing heading commands to an operator using the display. This is analogous to the way people receive directions from the GPS map system in their car, which provides turn-by-turn driving instructions, but does not actually steer the car.

For both applications, a monitor for the crew should be designed to aid in improving efficiency of the skimming operations. Information such as current heading and position may be showed as

well as the estimated time of arrival to the next waypoint and the intended new course. A portion of the screen may also be dedicated to the oil collection statistics like estimated quantity of oil collected to aid with scheduling tank offloads. For manual steering operations this information can be augmented with audible cues much like current automotive navigation systems.



Figure 47: LAMOR Oil Recovery Workboat.

Many of the larger OSRO vessels are currently using thermal infrared and X-band radar to aid in detecting oil concentrations. The current method of determining the oil concentration is through a human observer's perception rather than advanced image processing. A possibility would be to also integrate with these systems for automatic noncontact thickness detection much like is discussed in Section 8.4.

8.4. IR Sensor

As another potential oil sensor, Alion test engineers considered how an infrared (IR) camera could be used to identify the location and, perhaps, relative thickness of floating oil. Relevant literature discussing the potential of this approach include [Brekke2005], [Jha2008], [Shih2008], and [Fingas2014]. The basic principle is that oil and water have different thermal characteristics; hence, when viewed using thermal imaging, would appear to be at different temperatures. Further, that this difference would (at least in a relative sense) depend upon the oil layer's thickness. Below are examples to suggest that such an approach could be useful in oil recovery efforts.

The thermal IR camera used for capturing IR data was the Forward Looking Infrared (FLIR) Vue Pro (Figure 48). The camera is designed to be mounted on small Unmanned Aerial Vehicle (UAV)'s and features a small form factor and all-in-one design. 14-bit still Tagged Image File Format (TIFF) images were recorded to an internal Secure Digital (SD) memory card at a rate of

1 frame per second. The test setup was accompanied by a visual camera collecting the same image area to aid in referencing the captured IR images.



Figure 48: FLIR Vue Pro Thermal Infrared Camera.

The first set of examples piggybacked on oil skimming activities at Ohmsett in which deposits of oil traveled down a boom chute toward a skimmer. The data collection included both visual and IR images of the alternating regions of oil and water in the chute. The primary conclusion is that the oil and water are clearly distinguishable in the IR data.

To better assess the ability of the IR data to show relative thickness of the floating oil a simple, in-lab test was constructed. In this simple test four thin-walled plastic cylindrical containers were suspended in a tub of water. The containers were open at both top and bottom so as to allow normal heating and cooling of the oil. Different amounts of oil were placed within the containers and profiles were taken across the containers. See Appendix F for details of the tests.

In summary:

1. The experimental results suggest that the IR sensor is effective at locating floating oil and that relative thickness can be sensed.
2. In comparison to the floating sensors, the IR sensor provides additional spatial information; not just the thickness at the sensor location but also for an adjacent area.
3. When properly mounted above the water surface, image processing of the IR data can provide information for navigating the skimmer to stay within the thickest region of an oil spill.
4. Waves and chop did make the IR data noisier; however, this can probably be reduced/eliminated by averaging over multiple IR images.
5. While some variation with distance from the sensor is possible, it seems small. If this is due to lens distortion, it can be measured and corrected for.

These comments, especially numbers 3 and 4, suggest that an IR-based system would have significant performance advantages over the floating sensors – specifically, the ability to sense oil over a larger region and the (likely) insensitivity of the IR process to waves – hence, the use of IR sensors merits additional exploration.

One specific area of IR sensing that warrants further research is the environmental effects that alter the heat signature of the oil slick. When the oil present in the image is not absorbing solar energy (evening or heavy cloud cover) the oil may actually appear darker (cooler) than the surrounding water [Jha 2008]. Profiles of these IR effects must be developed that take environmental conditions into account allowing the effective detection of the relative thickness of the oil and location in the image.

8.5. Algorithm Development

Because the skimming algorithm simulations were unable to accurately model many of the intricacies present in real world oil skimming, it would be valuable to perform tests of algorithms using an actual oil skimming vessel. Different factors such as the safe turning radius, optimal speed, and actual skimming efficiency can be tested by running several algorithms using different sizes of vessels and different types of oil skimmers.

8.6. Aerial Surveillance

Another idea for improving operations would be to include near real-time aerial surveillance. One possible method would be to use a low-cost drone or aerostat to provide geo-referenced images of the oil spill area. A few of the OSRO's have these systems readily deployable in their fleet. These images could then be used to allow the AOS algorithm to maximize the time spent in the thickest oil concentrations and aid in tracking the actual movement of the spill due to current and wind.

Aerostats have many inherent issues and limitations; however, drones have many capabilities and drones are becoming less expensive and more capable every year. The Federal Aviation Administration (FAA) recently started requiring drone owners to register their drones and also began stricter regulations. However, recent decisions by the FAA have made it easier for corporations to be exempt from these restrictions. Tethered drones can also be made exempt under Section 333 of the FAA Modernization and Reform Act of 2012 (FMRA).

Tethered drones have many advantages over untethered drones: they do not need onboard power, they can fly almost indefinitely since the power comes from the ground, and they can send high definition video and data down the tether instead of relying on a wireless solution. Being tethered, they can only go so far and so high; these parameters could be set by the onscene commander. Also the skill level of the "pilot" is much lower than for an untethered drone for obvious reasons. Many manufacturers are now designing and building tethered drones for news stations, fire departments, and law enforcement. Drone Aviation Corporation is one of those companies. Figure 49 is an example of their WATT200.

A tethered drone with video and an IR sensor would make it possible to provide the recovery team surveillance and map the initial spill area. It would also help develop IR technology as a viable means of finding and quantifying oil floating on water. Ideally, real-time imagery could be uploaded to federal and state shore commands and OSROs (providing there is a data pipe available).

MISR - MOBILE ISR

MOBILE INTELLIGENCE, SURVEILLANCE, AND RECONNAISSANCE



Figure 49: Drone Aviation Corporation WATT200 tethered drone.

8.7. Group Coordination / tracking

Finally, the current monitoring of the individual AOS could be extended to monitoring (and coordinating) a group of AOS systems. The monitoring would provide a real-time view of oil spill recovery operations and effectiveness both to guide further recovery operations and as a public relations tool.

A “subset” of this could be “Group Control” where individual AOS equipped vessels could be controlled simultaneously to move booms. Figure 50 shows a classic example of two vessels controlling booms with a “master” vessel skimming.

In this scenario, the three vessels’ AOS computers would communicate with each other, updating the positions of the vessels. The master AOS computer would then give the navigation information to the secondary vessels so the booms would be at their optimal locations. Of course this would not replace the vessels operators, no autopilot system should; however, the pilots of the vessels would not be taxed with constantly trying to keep all the vessels in the proper and most efficient formation.



Figure 50: Two vessels towing booms could be controlled autonomously by the master vessel.

9. References

- [Brekke2005] “Oil spill detection by satellite remote sensing,” C. Brekke and A. H. S. Solberg, *Remote Sensing of Envir.*, vol. 95, 2005, pp. 1-13.
- [Jha2008] “Advances in remote sensing for oil spill disaster management: state-of-the-art sensors technology for oil spill surveillance,” M. N. Jha, J. Levy, and Y. Gao, *Sensors*, vol. 8, 2008, pp. 236-255.
- [Shih2008] “Modeling of thickness dependent infrared radiance contrast of native and crude oil covered water surfaces,” W.C. Shih and A. B. Andrews, *Optics Express*, vol. 16, July 2008, pp. 10535-10542.
- [Fingas2014] “Review of oil spill remote sensing,” M. Fingas and C. Brown, *Marine Pollution Bull.*, vol. 83, 2014, pp. 9-23.

Appendix A. Initial Sensor Test Results

A.1 GE Sensors

Table 7: GE initial sensor results without flow diverter.

Test	Patch #	Est. Oil Thickness (mm)	Speed (kt)	Avg Measured Thickness (mm)	Notes
1A	1	14.3	0.5	16.56 mA = 9.5	Noticed that bubblers tended to wash the oil off.
	2	11.7		17.4 mA = >20mm	
1B	3	12.4	1	17.24 mA = >20mm	
	4	11.1		17.26 mA = >20mm	
1C	1	14.3	1.5	16.45 mA = 8.5mm	
	2	11.7		16.72 mA = 10.5mm	
1D	3	12.4	2	10.56 mA = <4mm	at 2 knots sensor was pitched down and the tow point was creating a v of clear water - noticeable in data
	4	11.1		11.43 mA = <4mm	
1E	1	14.3	2.5	12.41 mA = <4mm	bunch of oil dragged out of patches
	2	11.7		14.91 mA = 5.5mm	didn't get up to 2.5 knts until into patch 3
1F	3 / 4	12.4 / 11.1	3	No clear patch response	
2B	1	14	1	16.91 mA = 13mm	Thin slicks of oil between all patches due to oil dragged out
	2	11.5		16.83 mA = 12mm	
2C	3	11.1	1.5	17.04 mA = 14-17mm	Turned last bubble off to allow spreading
	4	8.4		17.04 mA = 14-17mm	

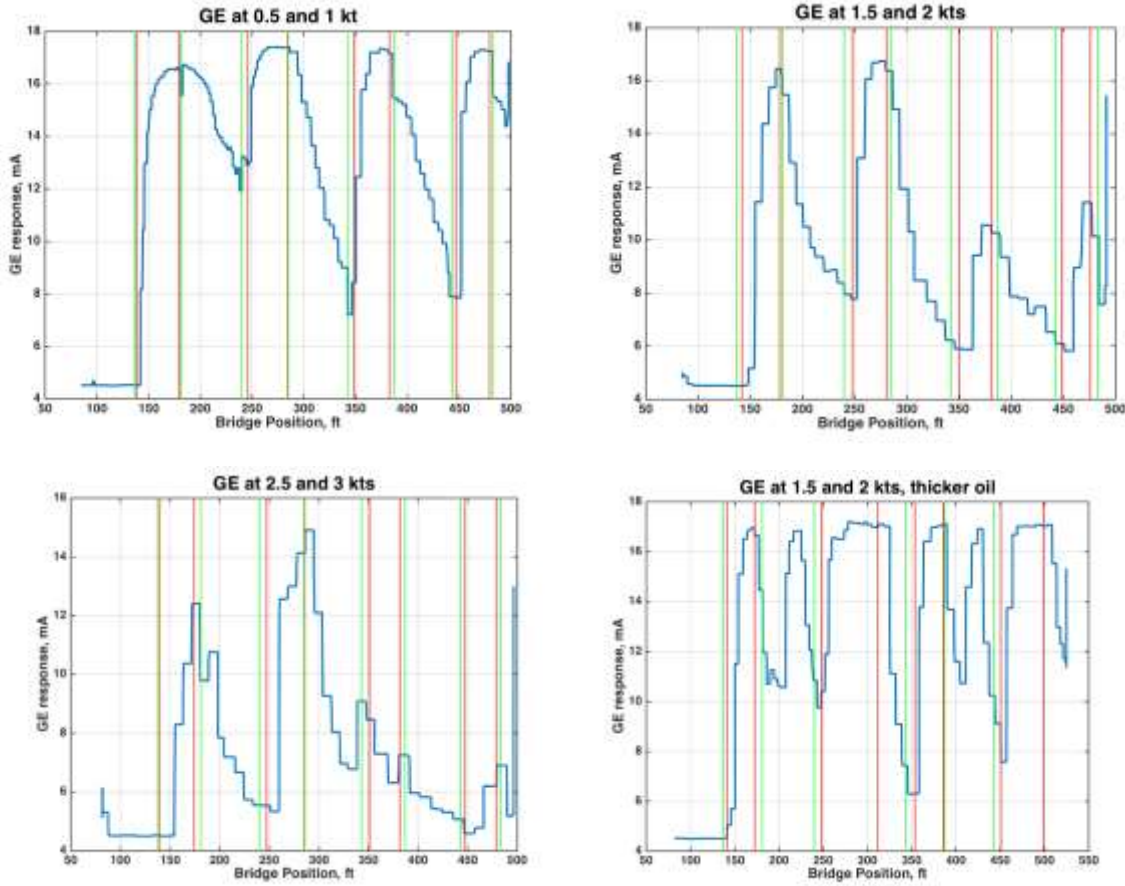


Figure 51: GE sensor results without flow diverter.

For all sensor plots, the green vertical lines indicate the approximate bubbler locations and the red vertical lines indicate when the sensor entered and left the oil patch. The first 2 patches are at the first speed in the title and the second 2 patches at the 2nd speed (acceleration starts right after leaving the 2nd patch). The blue line is the sensor response; higher values indicate thicker oil.

Table 8: GE initial results with flow diverter.

Test	Patch #	Est. Oil Thickness (mm)	Speed (kt)	Avg Measured Thickness (mm)	Notes
2A	1	14	0.5	No patch response	missing a big chunk of oil in patch 1, put oil back in patch 2 with bubbler prior to start
	2	10.8		12.85 mA = <4mm	
2B	3	11.1	1	15.88 mA = 6.5mm	missing chunk of oil in patch 3, not missing any oil in 4
	4	13.2		16.38 mA = 8.5mm	

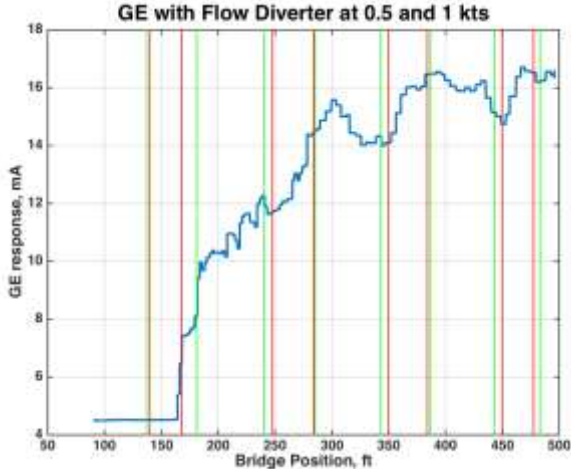
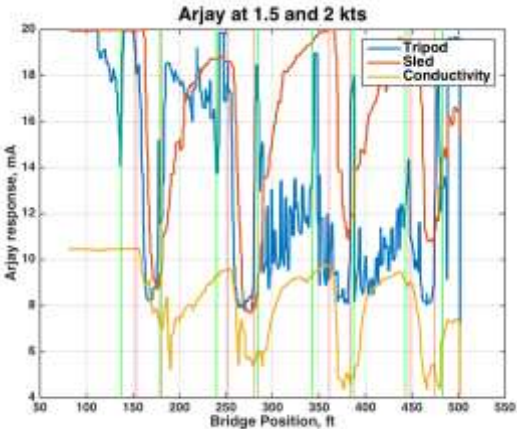
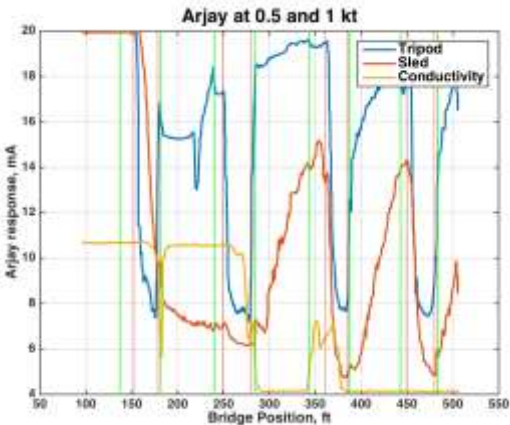


Figure 52: GE sensor results with flow diverter.

A.2 Arjay Floating Sensor

For all sensor plots, the green vertical lines indicate the approximate bubbler locations and the red vertical lines indicate when the sensor entered and left the oil patch. The first 2 patches are at the first speed in the title and the second 2 patches at the 2nd speed (acceleration starts right after leaving the 2nd patch). The blue line is the tripod sensor response and the red line the sled sensor response; lower values indicate thicker oil. The gold line is a conductivity sensor, lower conductivity values indicate oil.



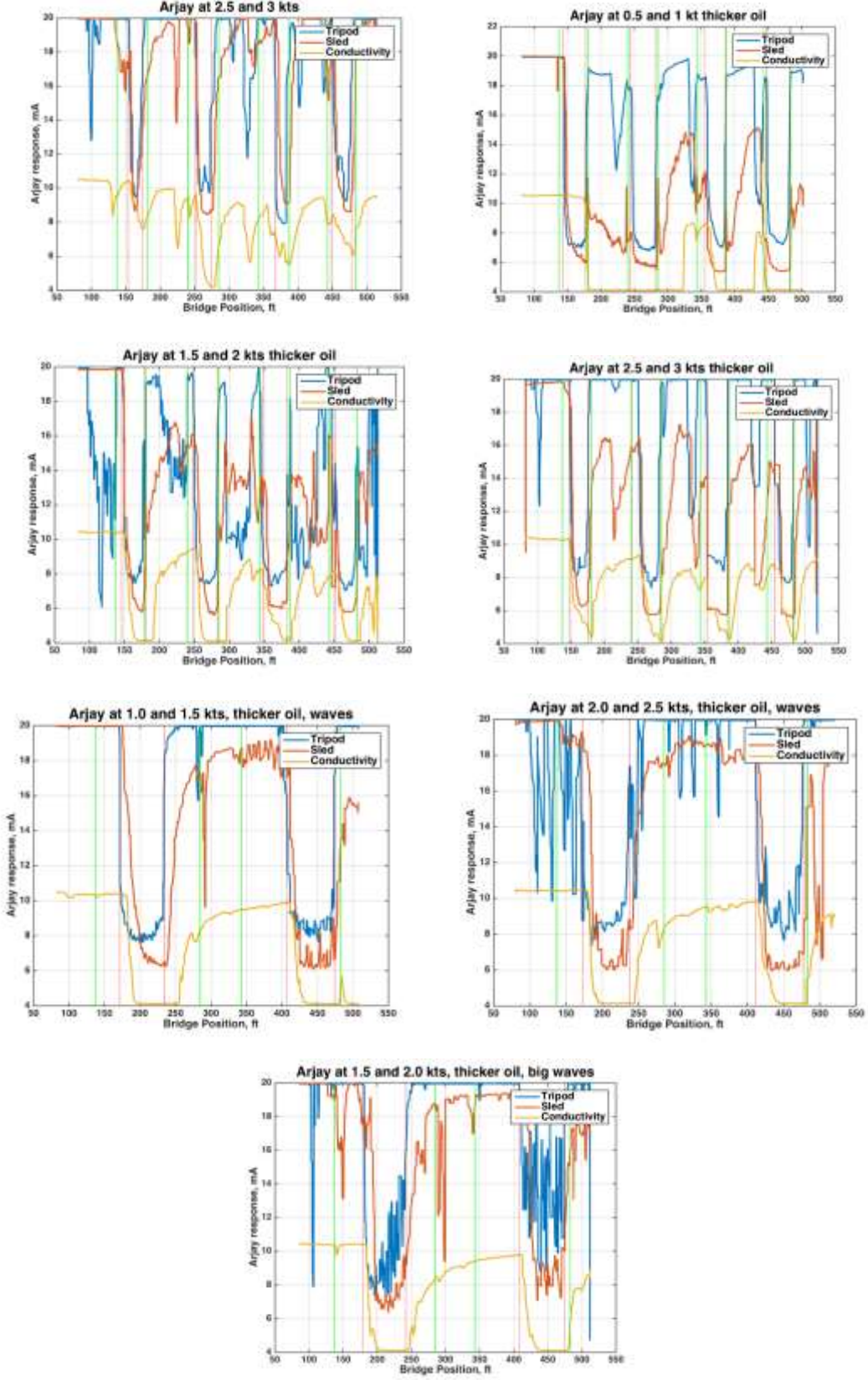


Figure 53: Arjay initial floating sensor results.

Table 9: Arjay initial sensor results.

Test	Patch #	Est. Oil Thickness (mm)	Speed (kt)	Waves	Avg Measured Thickness (mA)		Notes
					Tripod	Sled	
5A	1	9.4	0.5	no	7.67	No response	Sled was slow to get oil in and slow to release it -- was better as speed increased
	2	7.5			7.71	6.33	
5B	3	9.2	1	no	7.9	5.20	
	4	10.5			7.62	5.59	at 1 kt tripod started to dig in some
5C	1	9.4	1.5	no	8.44	9.51	Moved tow point for tripod
	2	7.5			8.16	8.17	
5D	3	9.2	2	no	8.26	11.66	tripod starting to bog down (needs skis instead of the ball), bow wave building up, sled behaving better
	4	10.5			8.18	11.00	
5E	1	9.4	2.5	no	9.93	9.94	adjusted tow rope on skiff higher. For first patch, shackle was dragging creating a clear spot in front of sled
	2	7.5			10.27	8.92	
5F	3	9.2	3	no	8.12	9.62	better results by manipulating rope to get tripod sensor up on plane and higher tow point on sled
	4	10.5			10.15	9.35	
6A	1	14.0	0.5	no	7.23	6.98	sled seemed to work better with bottom plate cut off but still lagging (oil flow is not as good as we liked) - looking at data - very little lag on the start, but never totally clears out
	2	10.8			7.07	5.94	
6B	3	13.6	1	no	7.85	5.71	
	4	12.8			7.66	5.73	
6C	1	14.0	1.5	no	7.95	7.04	tripod starting to bog down but doing OK - - readings may not be 100% accurate
	2	10.8			7.79	6.62	
6D	3	13.6	2	no	8.07	6.31	sled still not clearing out to zero but better -- conductivity sensor started to pick up now
	4	12.8			7.75	6.00	
6E	1	14.0	2.5	no	8.75	7.00	tripod having difficulty with speed - data may not be totally accurate
	2	10.8			8.26	5.95	
6F	3	13.6	3	no	8.96	6.00	sled did better - still doesn't clear all oil out
	4	12.8			8.23	5.72	
7A	1	12.4	1	Small	8.26	6.65	waves did not seem to have much impact on sensors -- speed was impacted as sled would lag and then surge. 3in stroke 22cycles per min (approx 6" peak to trough and 38ft wavelength)
7B	2	13.4	1.5	Small	8.75	6.83	
7C	1	14	2	Small	8.73	7.0	
7D	2	13.4	2.5	Small	9.38	6.35	
7E	1	13.4	1.5	Big	9.67	7.45	Increased waves to 3in stroke, 35 cycles per min, the max possible wave height these sensors could handle
7F	2	13.4	2	Big	13.7	8.61	

A.3 Arjay Flow Sensor

Table 10: Arjay percentage oil sensor – pump test results.

Test	Oil Flow (gpm)	Water Flow (gpm)	Total Flow Rate	% Oil based on flow	Flow into Tank (gals in 1min)	% Oil in Tank (meas.)	Notes
13A	20	0	20	100%	18.9	99.9	
13B	20	2	22	91%	21.9	93.2	
13C	20	4	24	83%	24.1	84.6	
13D	20	7	27	74%	23.3	87.3	Leaking tank valve so this data point is off
13E	20	12	32	63%	35	70.6	
13F	20	17	37	54%	49.6	52.9	
13G	20	20	40	50%	75.8	36.4	Much higher water flow and water % than planned
13H	0	20	20	0	n/a	0	

Table 11: Arjay percentage oil sensor - skimmer test results.

Test #	Skimmer Drum Speed	Flow Rate (gpm)	Avg. Sensor Reading (mA)	% Oil in Flow Stream Measured	Notes
14A	18	5.8	7.49	87.4	From observation, pretty much all oil
14B	33	8.7	8.42	84.0	
14C	60	30.6	19.63	25.2	From visual observation, a lot of water, emulsified
14D	18	10.2	7.64	86.6	took a while for the water to clear out and get down to the oil reading
14E	28	10.2	9.02	82.5	
14F	38	13.1	9.97	73.6	

For all figures, the green line indicates where data averaging starts and the red where it ends – these periods equate to one of the concentrations of oil. Blue line is the sensor response, large values indicate higher percentage water.

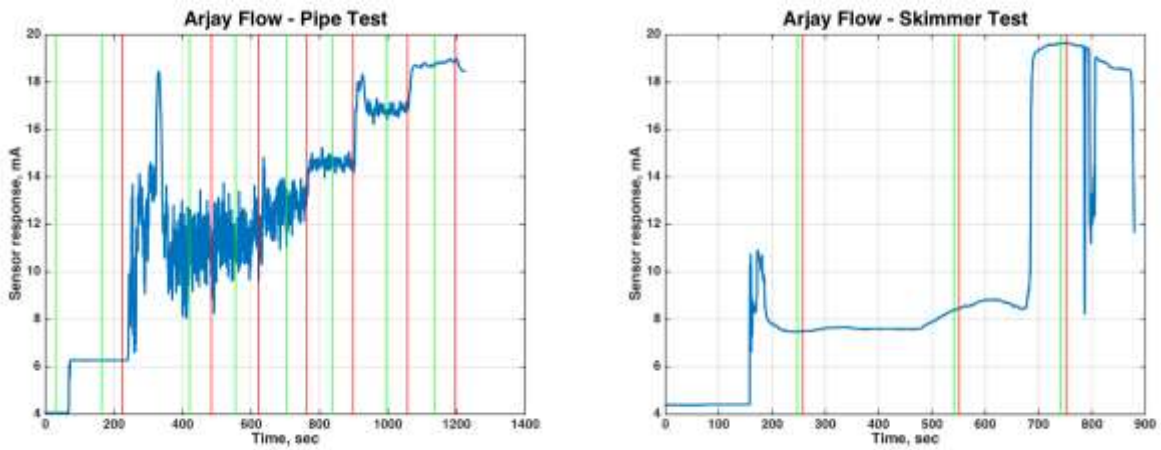


Figure 54: Inline sensor raw data.

Appendix B. Alion Floating Sensor Mount

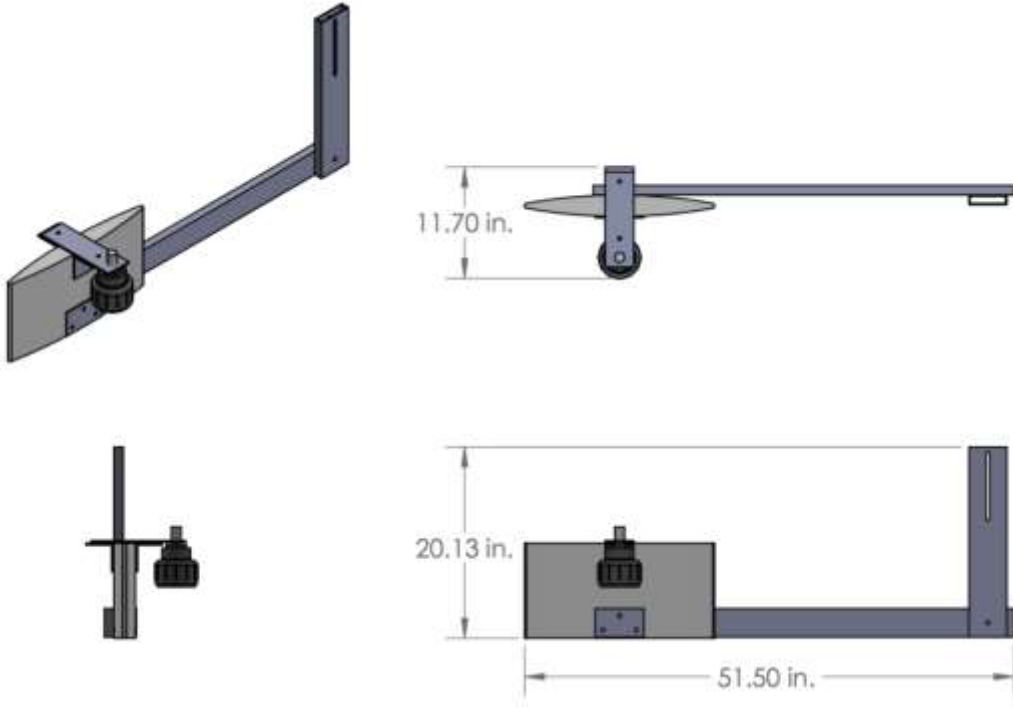


Figure 55: Sensor mount - Arjay sensor version.

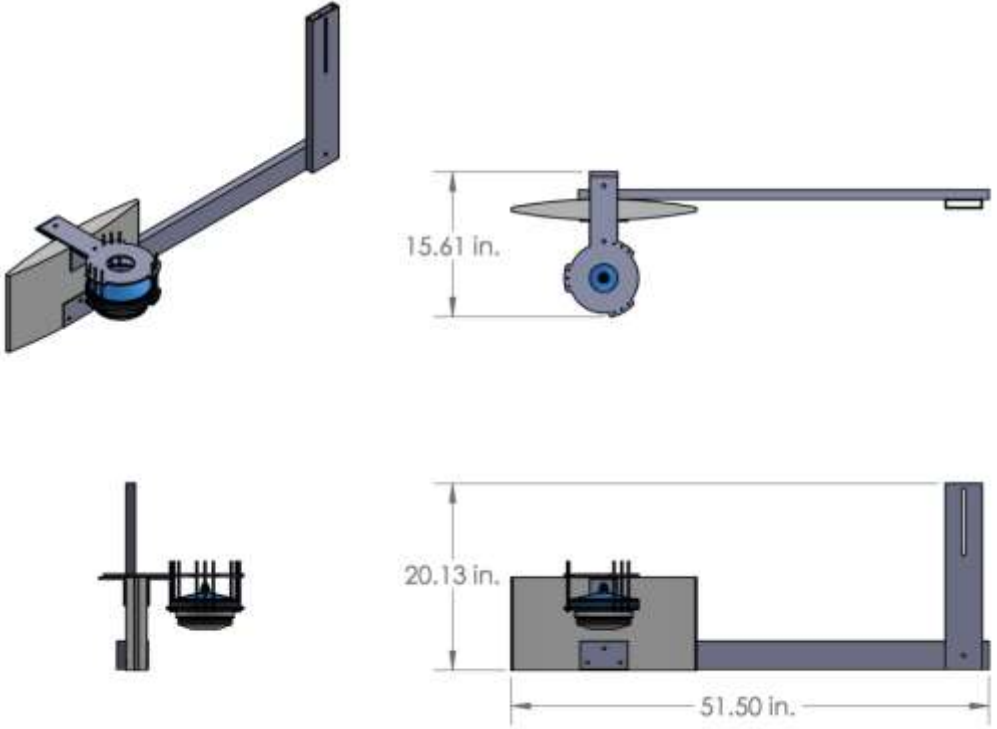


Figure 56: Sensor mount - GE sensor version.

Appendix C. Control Panel Schematic

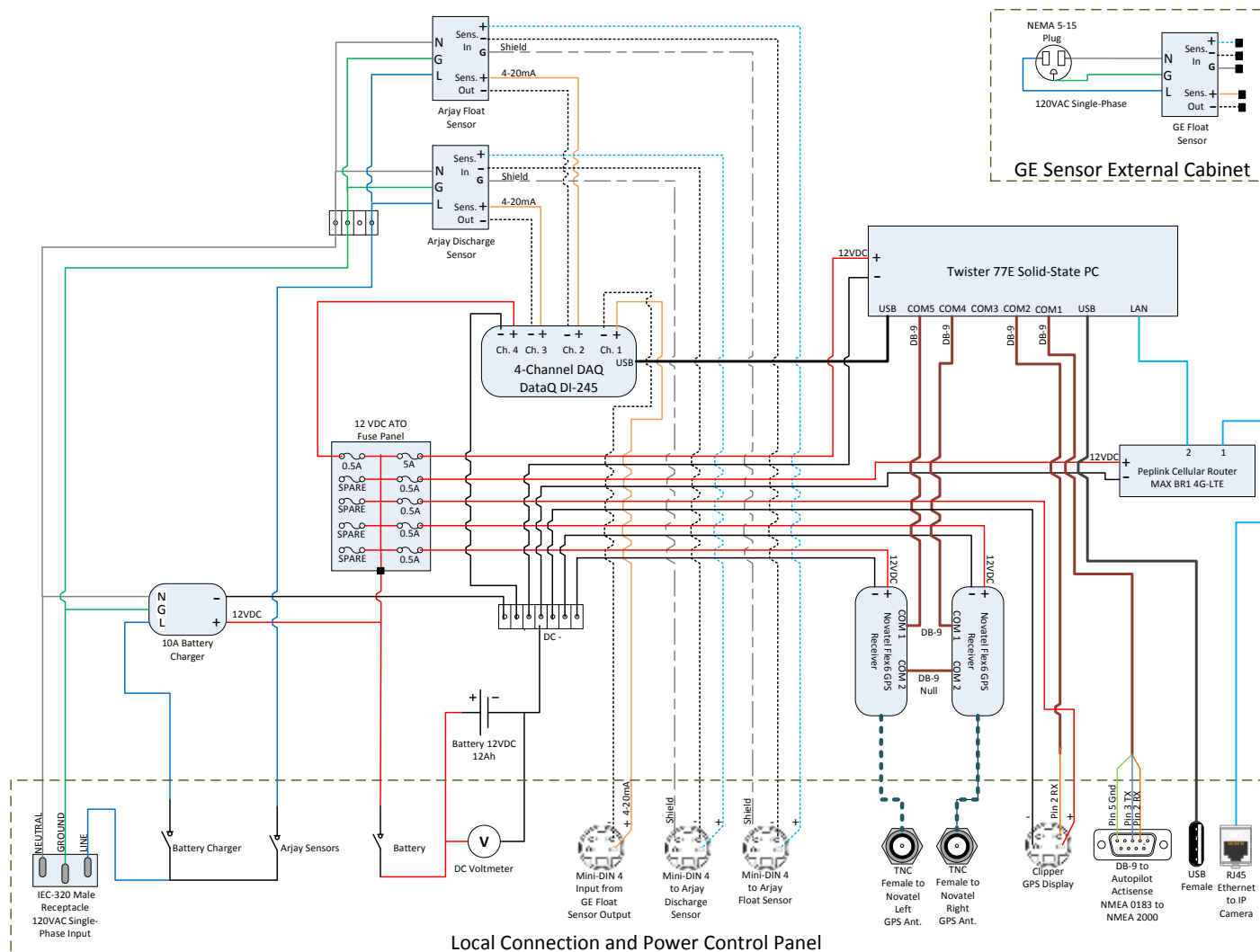


Figure 57: Control panel schematic.

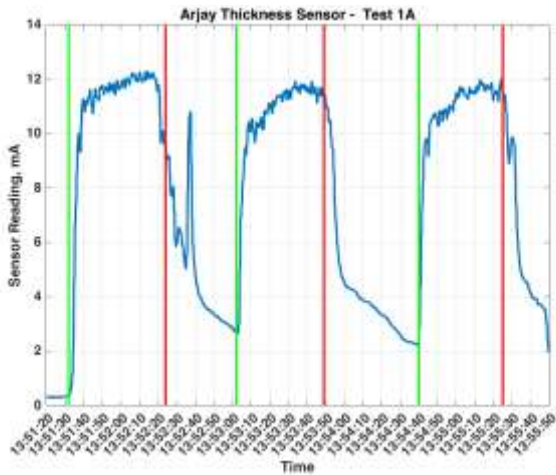
Appendix D. Arjay Sensor Results

Table 12: Arjay Sensor Results.

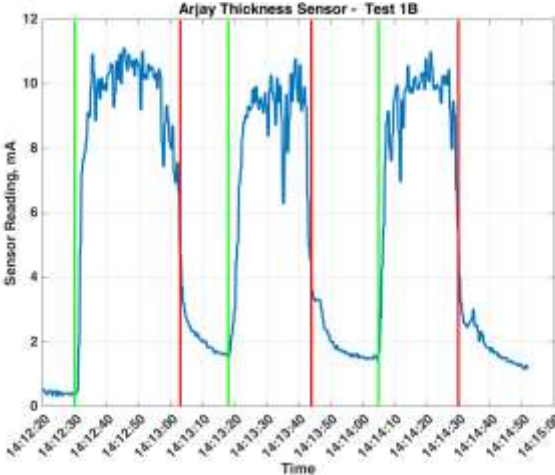
Test	Ohmsett Test #	Target Oil Thickness (mm)	Oil dispensed at (gpm)	Spd (kt)	Wave settings	Wave Height (in)	Wave length (ft)	Oil Dispensed (gal)	Est. Oil Thickness (mm)	Avg Sensor Reading (mA)	Std Dev Sensor Reading
1A	1	5	28	0.75	none	none	none	15.8, 17.5, 17.5	4.8, 5.3, 4.5	15.8, 15.5, 15.6	0.41, 0.20, 0.17
1B	2	5	46.6	1.25	none	none	none	15.8, 15.8, 17.5	4.9, 5.1, 5.0	13.9, 13.3, 13.9	1.06, 0.96, 0.54
1C	3	15	83.9	0.75	none	none	none	49.1, 50.9, 52.6	15.7, 15.6, 15.3	16.8, 16.9, 16.8	0.29, 0.29, 0.30
1D	4	15	139.8	1.25	none	none	none	50.9, 52.6, 47.4	14.4, 18.3, 18.2	16.4, 16.5, 16.4	0.39, 0.41, 0.18
1E	5	15	139.8	1.25	3" 25 cpm	5.38	25.69	42.1, 51.4, 50.9	15.1, 17.1, 16.5	15.7, 15.9, 16.1	1.17, 0.85, 0.80
1F	6	15	139.8	1.25	4.5" 20 cpm	6.46	41	50.9, 50.9, 49.1	16.6, 17.3, 16.2	15.7, 15.9, 15.9	1.32, 0.81, 0.73
1G	7	5	28	0.75	4.5" 20 cpm	6.46	41	19.3, 17.5, 17.5	5.6, 5.7, 5.8	13.8, 14.5, 15.0	1.70, 1.16, 1.16
1H	8	5	28	0.75	7.5" 20 cpm	9.9	36	17.5, 17.5, 19.3	5.3, 5.0, 6.4	12.9, 13.0, 13.9	2.04, 1.67, 1.50
1I	9	15	112	1	3" 25 cpm	5.38	25.69	49.1, 49.1, 49.1	18.9, 17.2, 17.8	16.5, 15.2, 15.2	0.78, 1.71, 1.81

Test	Ohmsett Test #	Target Oil Thickness (mm)	Oil dispensed at (gpm)	Spd (kt)	Wave settings	Wave Height (in)	Wave length (ft)	Oil Dispensed (gal)	Est. Oil Thickness (mm)	Avg Sensor Reading (mA)	Std Dev Sensor Reading
1J	10	10	112	1.5	3" 25 cpm	5.38	25.69	31.6, 33.3, 35.1	14.1, 11.5, 12.8	15.3, 14.3, 14.1	2.03, 2.43, 2.58
1K	11	10	112	1.5	none	none	none	33.3, 54.4	10.77, 11.1	15.6, 16.0	0.46, 0.50
1L	12	10	75	1	none	none	none	33.3, 32.8	10.8, 10.2	16.0, 16.0	0.36, 0.38

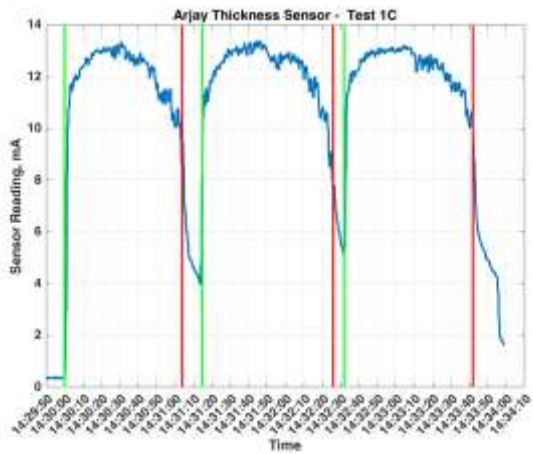
Run 1: 5 mm, 0.75 kt, calm



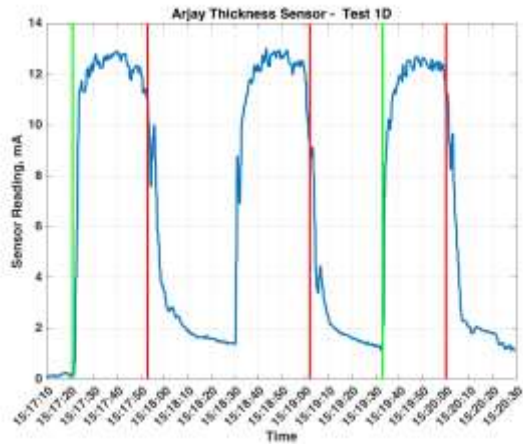
Run 2: 5 mm, 1.25 kt, calm



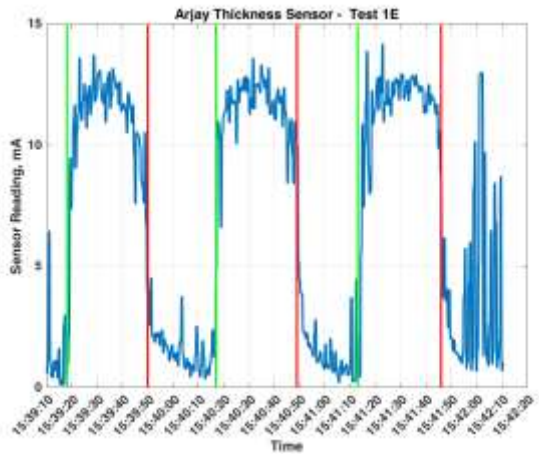
Run 3: 15 mm, 0.75 kt, calm



Run 4: 15 mm, 1.25 kt, calm



Run 5: 15 mm, 1.25 kt, H=5.15, L=25.7



Run 6: 15 mm, 1.25 kt, H=6.45, L=41

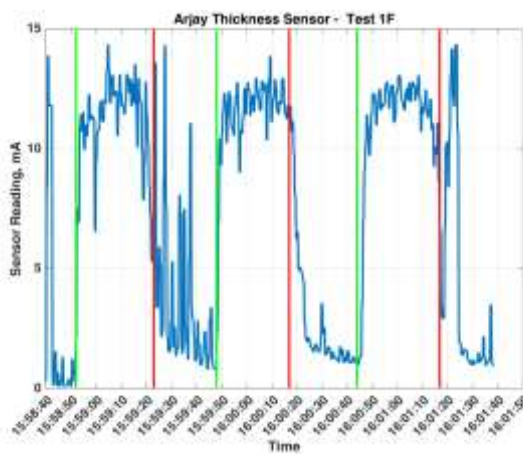
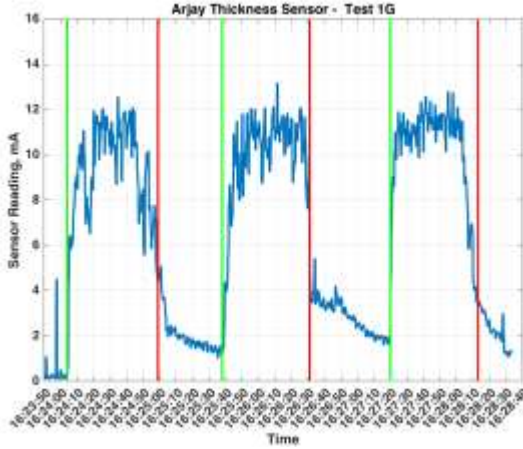
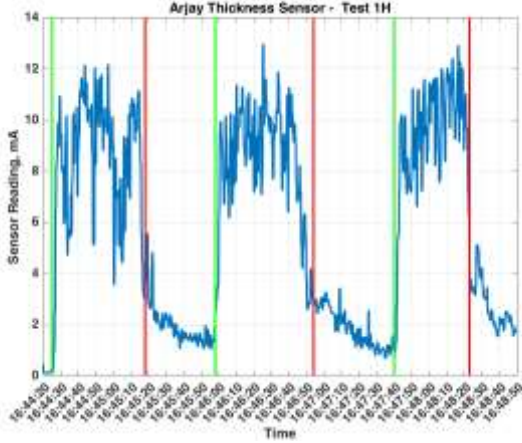


Figure 58: Arjay sensor graphs, tests 1-6.

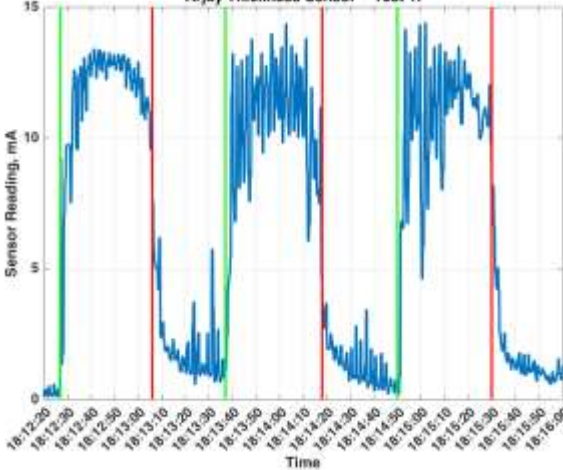
Run 7: 5 mm, 0.75 kt, H=5.73, L=41



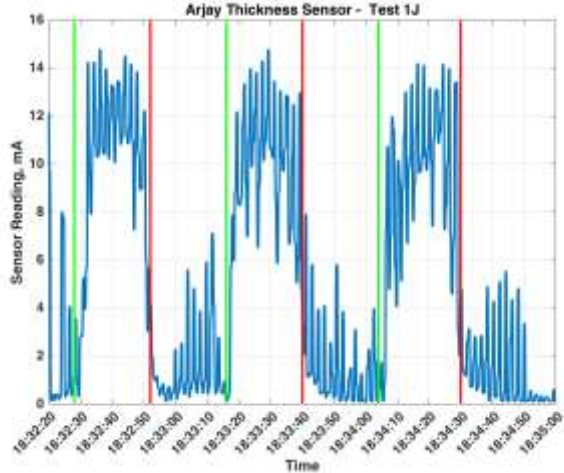
Run 8: 5 mm, 0.75 kt, H=9.65, L=36



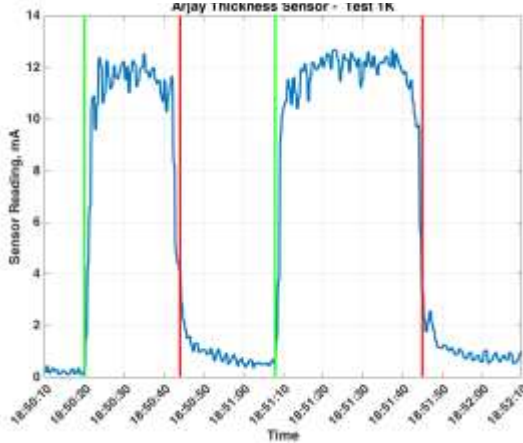
Run 9: 15 mm, 1 kt, H=4.8, L=25.7



Run 10: 15 mm, 1.5 kt, H=4.24, L=25.7



Run 11: 10 mm, 1.5 kt, calm



Run 12: 10 mm, 1 kt, calm

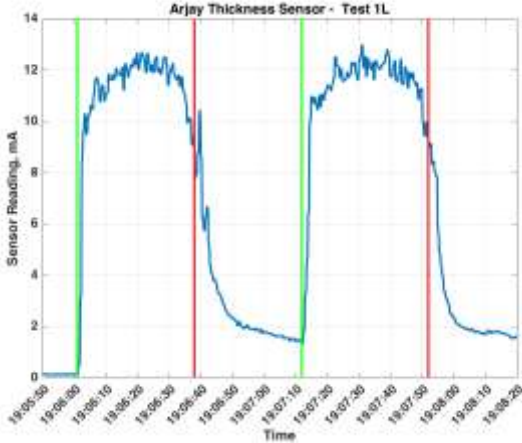


Figure 59: Arjay sensor graphs, tests 7-12.

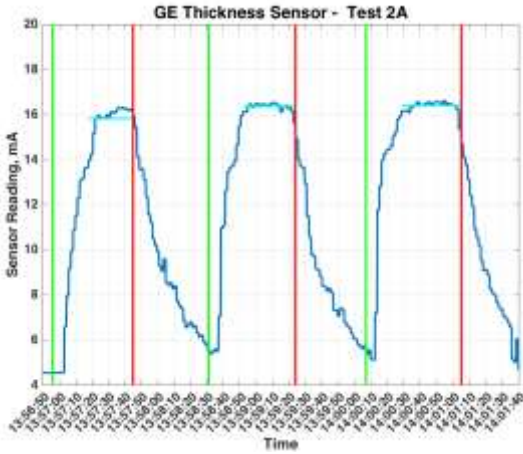
Appendix E. GE Sensor Results

Table 13: GE sensor results.

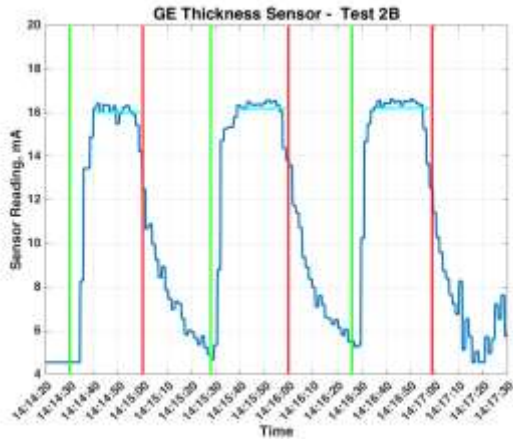
Test	Ohmsett Test #	Target Oil Thickness (mm)	Oil dispensed at (gpm)	Spd (kt)	Wave settings	Wave Height (in)	Wave length (ft)	Oil Dispensed (gal)	Est. Oil Thickness (mm)	Avg Sensor Reading (mA)	Std Dev Sensor Reading
2A	13	5	28	0.75	none	none	none	19.3, 15.8, 21.8	5.6, 3.9, 6.2	15.8, 16.4, 16.4	0.64, 0.14, 0.19
2B	14	5	46.6	1.25	none	none	none	17.5, 19.3, 19.3	4.8, 6.2, 5.9	16.0, 16.2, 16.2	0.44, 0.55, 0.73
2C	15	15	83.9	0.75	none	none	none	49.1, 50.9, 50.9	17.5, 15.6, 15.0	16.5, 16.7, 16.7	0.33, 0.17, 0.20
2D	16	15	139.8	1.25	none	none	none	47.4, 54.4, 47.5	20.6, 20.4, 20	16.5, 16.6, 16.5	0.44, 0.10, 0.49
2E	17	5	46.6	1.25	3" 25cpm	5.38	25.69	17.5, 17.5, 17.5	5.9, 4.7, 4.7	12.2, 11.9, 12.3	1.82, 1.15, 1.76
2F	18	5	46.6	1.25	4.5" 20 cpm	6.46	41	17.5, 17.5, 17.5	5.1, 4.6, 4.7	14.3, 14.4, 14.9	1.32, 1.47, 0.84
2G	19	5	28	0.75	4.5" 20 cpm	6.46	41	19.3, 19.3, 17.5	5.6, 5.5, 4.8	15.0, 15.7, 15.8	0.88, 0.51, 0.51
2H	20	5	28	0.75	7.5" 20 cpm	9.9	36	19.3, 17.5, 21.1	5.8, 5.3, 5.0	14.4, 15.2, 15.8	0.91, 0.87, 0.69
2I	21	10	75	1	none	none	none	35.1, 31.6, 29.8	12.1, 11.5, 9.3	16.3, 16.4, 16.4	0.22, 0.14, 0.11

Test	Ohmsett Test #	Target Oil Thickness (mm)	Oil dispensed at (gpm)	Spd (kt)	Wave settings	Wave Height (in)	Wave length (ft)	Oil Dispensed (gal)	Est. Oil Thickness (mm)	Avg Sensor Reading (mA)	Std Dev Sensor Reading
2J	22	10	112	1.5	none	none	none	33.3, 26.3	10.2, 11.8	15.7, 16.1	0.30, 0.46
2K	23	10	75	1	4.5" 20 cpm	6.46	41	35.1, 35.1, 34.3	12.3, 9.4, 10.4	15.5, 16.2, 16.1	1.20, 0.33, 0.36
2L	24	10	112	1.5	4.5" 20 cpm	6.46	41	27.0, 25.9, 28.0	10.0, 10.5, 10.4	13.6, 14.1, 14.0	1.26, 1.34, 1.71

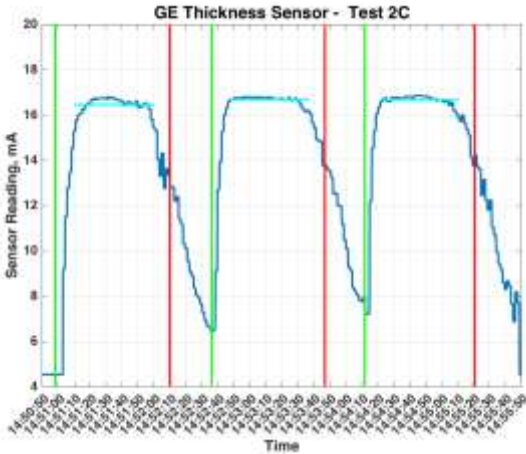
Run 13: 5 mm, 0.75 kt, calm



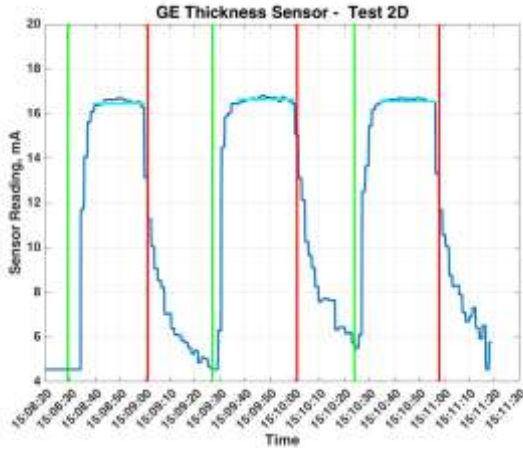
Run 14: 5 mm, 1.5 kt, calm



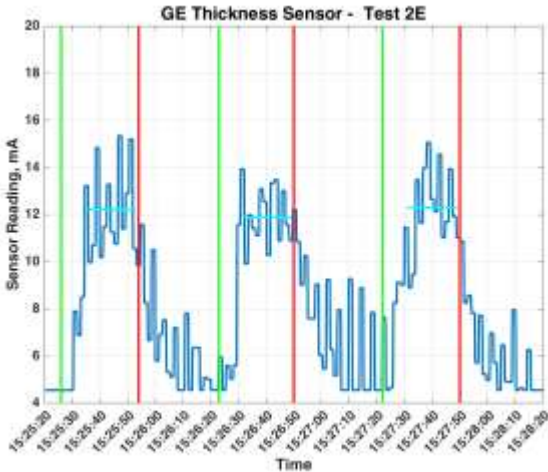
Run 15: 15 mm, 0.75 kt, calm



Run 16: 15 mm, 1.25 kt, calm



Run 17: 5 mm, 1.25 kt, H=5.38, L=25.7



Run 18: 5 mm, 1.25 kt, H=6.46, L=41

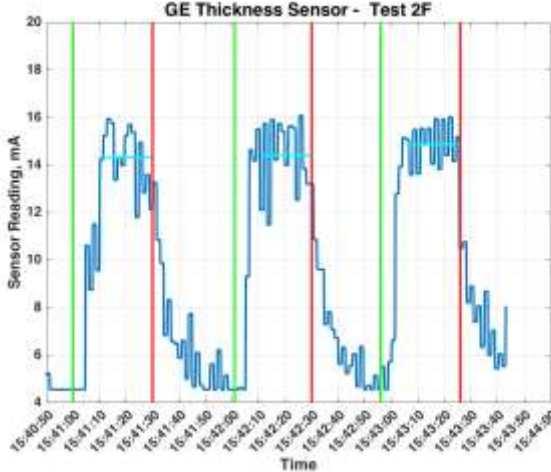
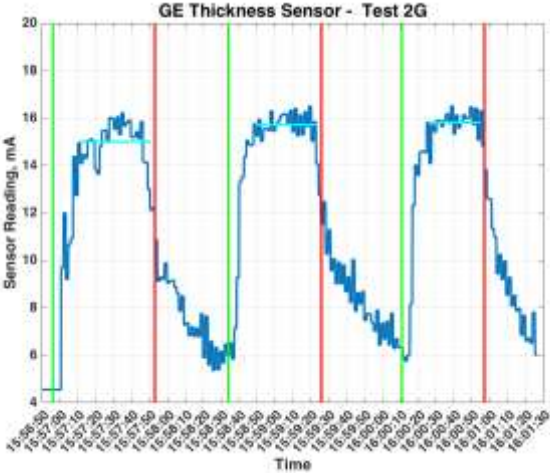
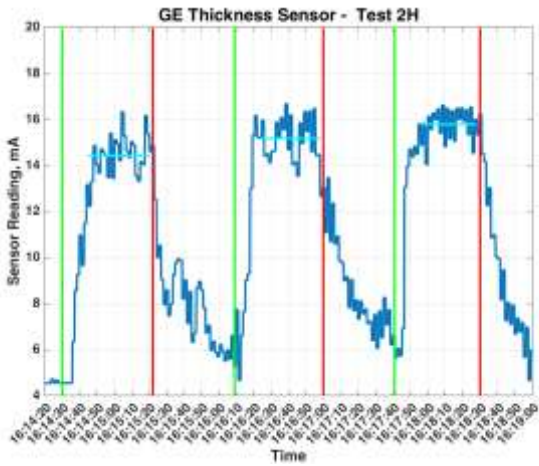


Figure 60: GE sensor graphs, tests 1-6.

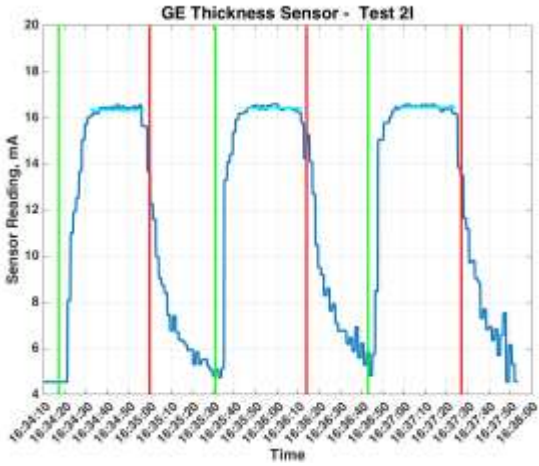
Run 19: 5 mm, 0.75 kt, H=6.26, L=42



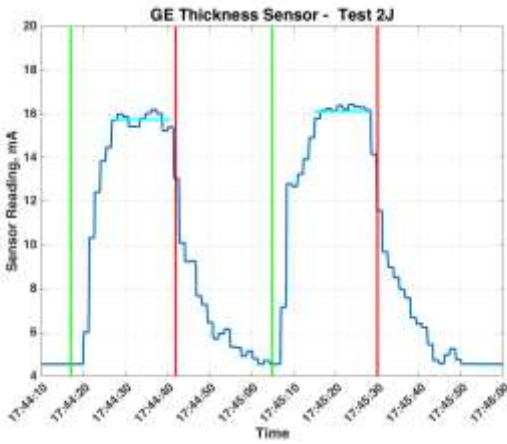
Run 20: 5 mm, 0.75 kt, H=9.9, L=36



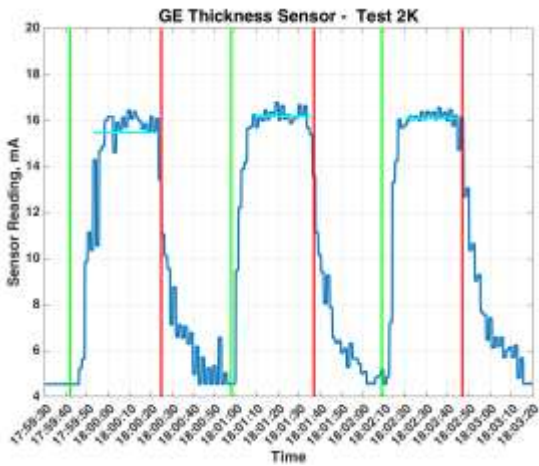
Run 21: 10 mm, 1 kt, calm



Run 22: 10 mm, 1.5 kt, calm



Run 23: 10mm, 1 kt, H=6.28, L=41



Run 24: 10 mm, 1.5 kt, H=6.99, L=41

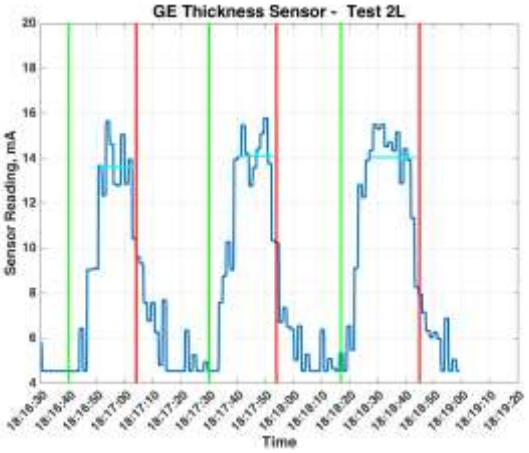


Figure 61: GE sensor graphs, tests 7-12.

Appendix F. IR SENSING

These examples support the efficacy of using thermal imaging detection in oil spill recovery efforts. The first set of examples piggybacked on oil skimming activities during Ohmsett testing in which deposits of oil traveled down a boom chute toward a skimmer. The data collection included both visual and thermal IR images of the alternating regions of oil and water in the chute. The primary conclusion is that the oil and water are clearly distinguishable in the IR data. The Ohmsett skimming examples, appearing as Figures 62 through 65, consist of image pairs (visual on the left and IR on the right) and a graph of the IR temperature (in all of the examples the minimum IR measurement for water outside of the chute was set to be zero; the oil, then, shows as positive temperatures) along two lines in the chute (shown on the IR image as solid and dotted lines; the left to right progression in the graph corresponds to bottom to top in the IR image):

Figure 62 demonstrates the ability of the IR data to discriminate between oil and water. Specifically, the water “hole” in the solid trace is clearly seen in the profile data between points 500 and 800. Further, the wispy appearance (varying oil thickness) of the oil along the solid line lower in the image appears as fluctuations in the temperature as expected. This clear distinction between water and oil in the IR data was consistently repeatable.

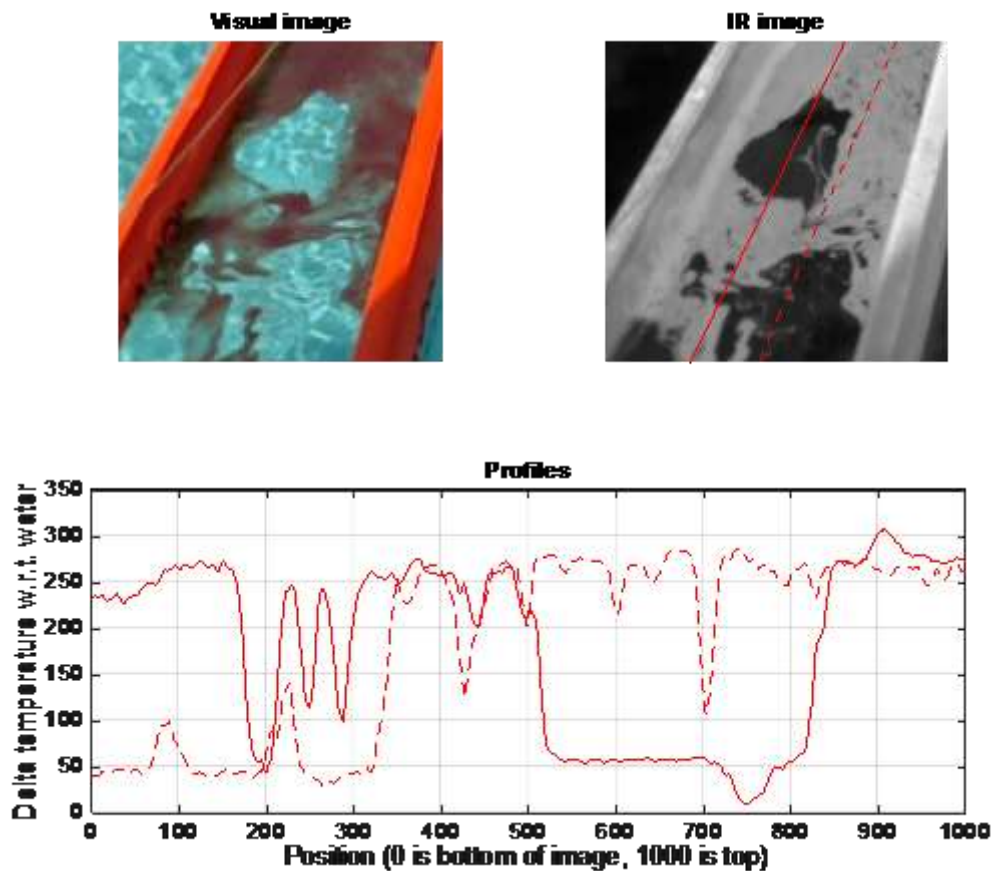


Figure 62: A first example showing that the oil/water interface is clearly reflected in the IR data. Each graph line represents the thermal measurements along the respective line in the IR image.

Figure 63 shows the impact of waves on the IR data collection. The sharp edge of the oil/water barrier toward the top of the image clearly appears in the profiles near position 600. The wave action causes more oscillation in the data as evidenced in the early parts of the profiles. This effect is caused by the reflective surface of the oil/water varying the level of solar radiation captured by the sensor. Averaging over multiple images could reduce/eliminate the noise due to waves.

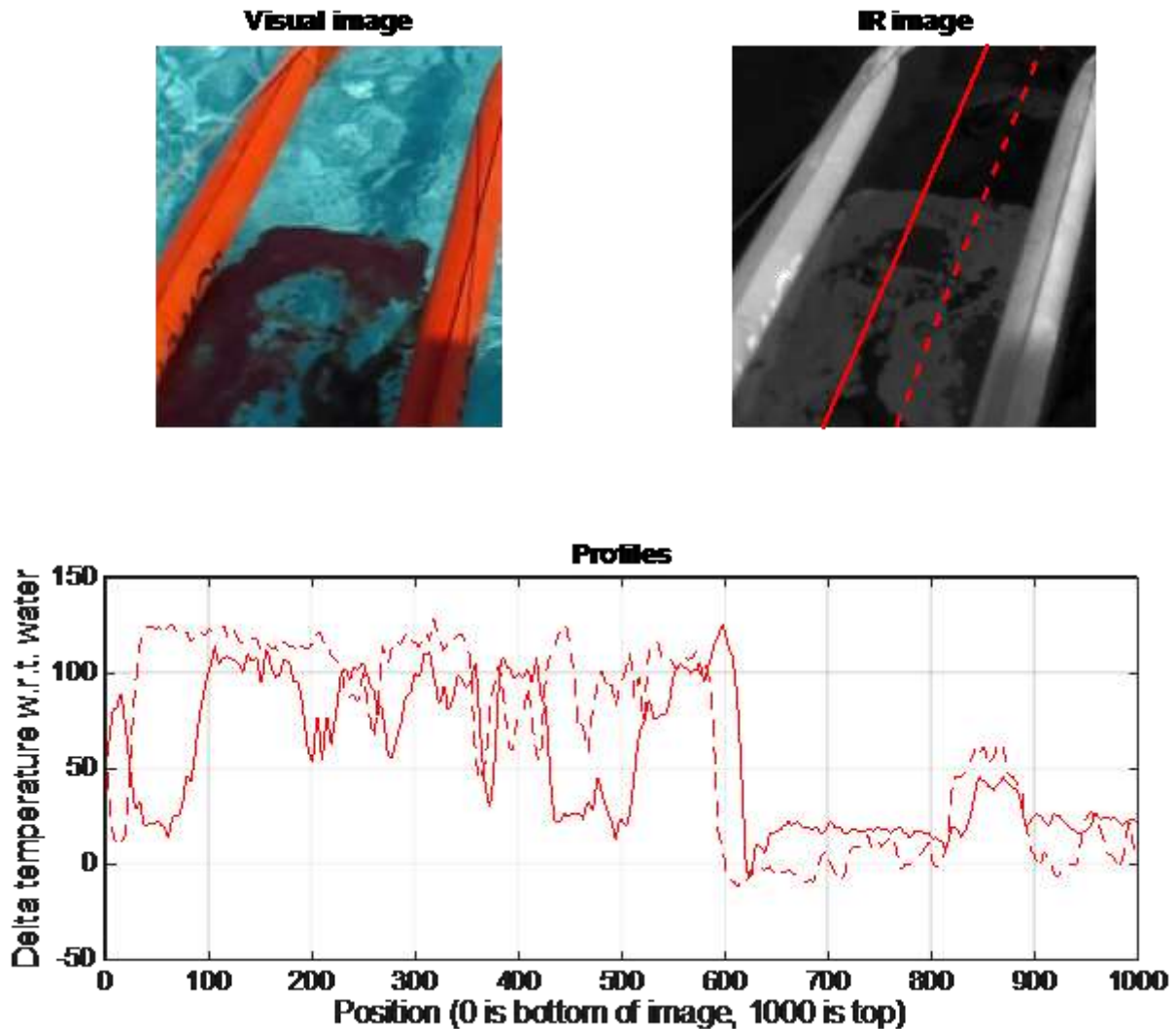


Figure 63: An example showing that while waves make the IR data noisier, the oil/water interface is still evident. Each graph line represents the thermal measurements along the respective line in the IR image.

Figure 64 and Figure 65 are included to suggest how oil thickness impacts the measurement. Figure 64 was a test with (target) 5 mm oil layers while Figure 65 was with (target) 15 mm layers. In this case the difference in thickness is seen as a variation in the IR temperatures; 120 units for 5 mm and 200 units for 15 mm. Unfortunately, the experiments at Ohmsett were not sufficiently controlled to be able to assess the repeatability of this observation.

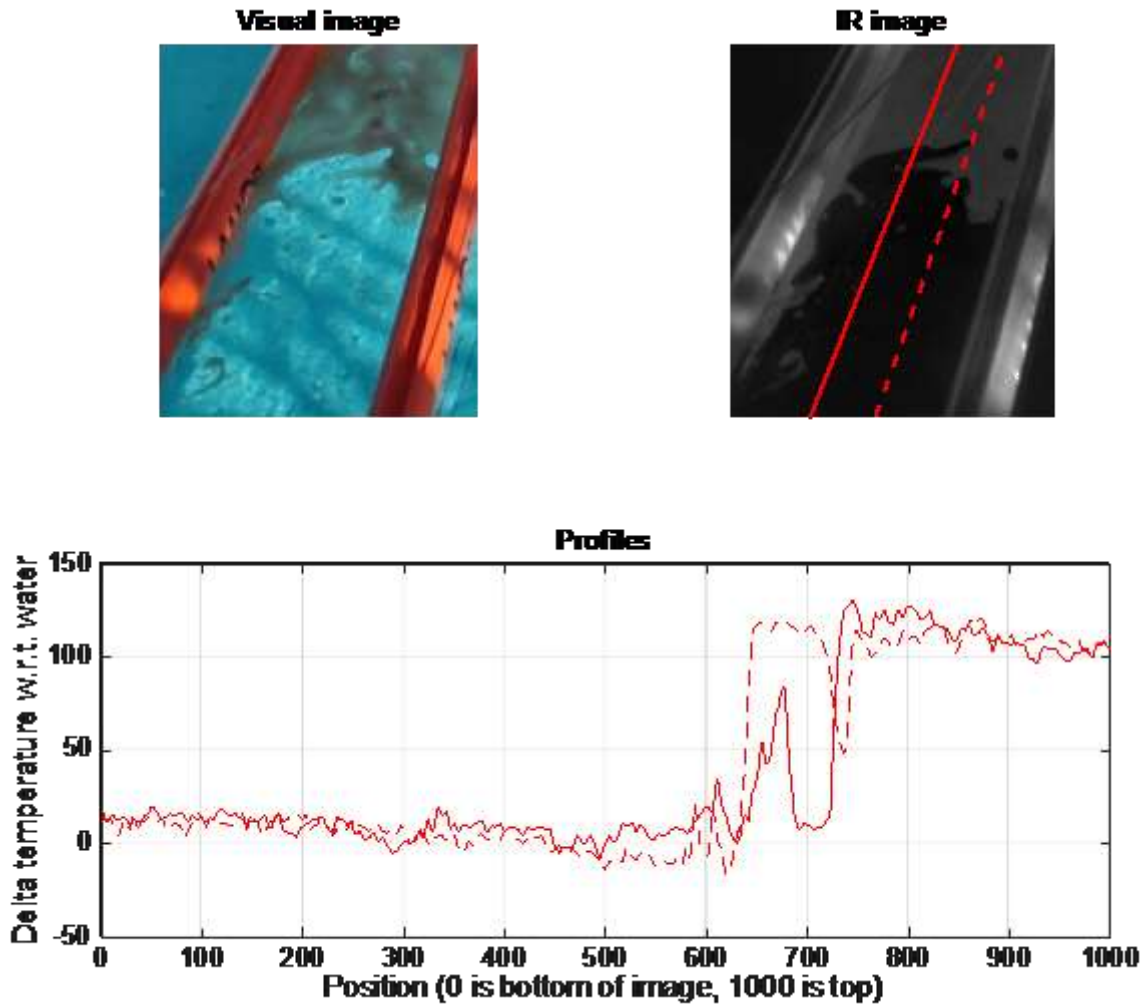


Figure 64: Data for a 5mm oil layer in calm water. Each graph line represents the thermal measurements along the respective line in the IR image.

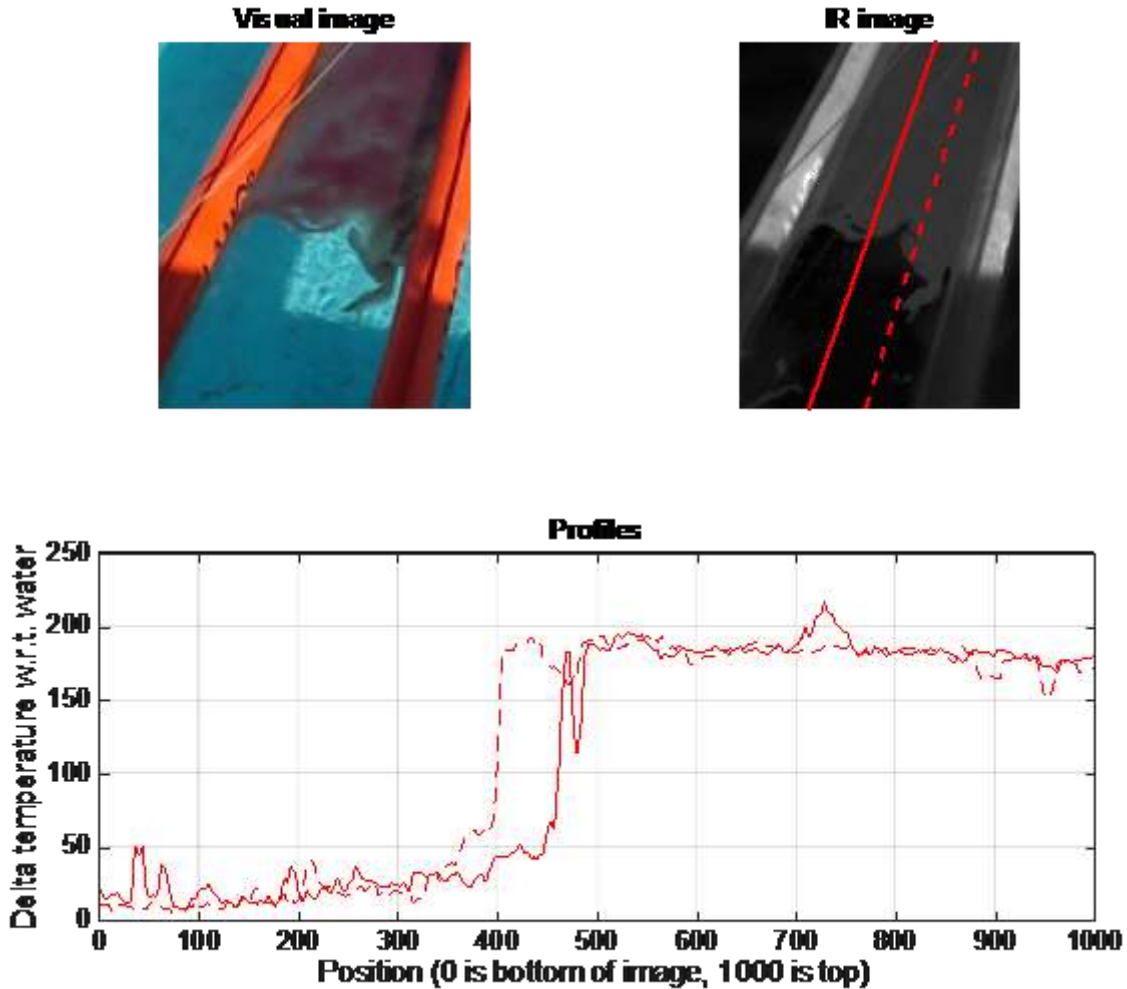


Figure 65: Data for a 15mm oil layer in calm water. Each graph line represents the thermal measurements along the respective line in the IR image.

As oil recovery is performed in all weather conditions, a concern was how the reflection of the sun on the water/oil would impact oil recognition; Figure 66, which consists of two images and one graph, shows one such example:

- A visual of the situation is first, on the top left. The strong reflection of the sun clearly appears in the oil region.
- After some simple processing, and shown on the top right, the IR amplitudes demonstrate that the oil/water temperature difference is still present in the IR image data even though the raw image (not shown) appeared to saturate the sensor. This image also includes horizontal lines to mark the locations of the data profiles shown in the remaining, lower right, graph.
- The graph shows the amplitude of the IR data along the three profile lines. The blue and red profiles show a distinct difference of approximately 400 units between the water (8000 on this scale) and oil (8400). The green profile is included to show that the pipe in the test rigging also appears warmer. Fortunately, advanced image processing techniques

would recognize the narrow spatial profile of the pipe and classify that region as not being oil.

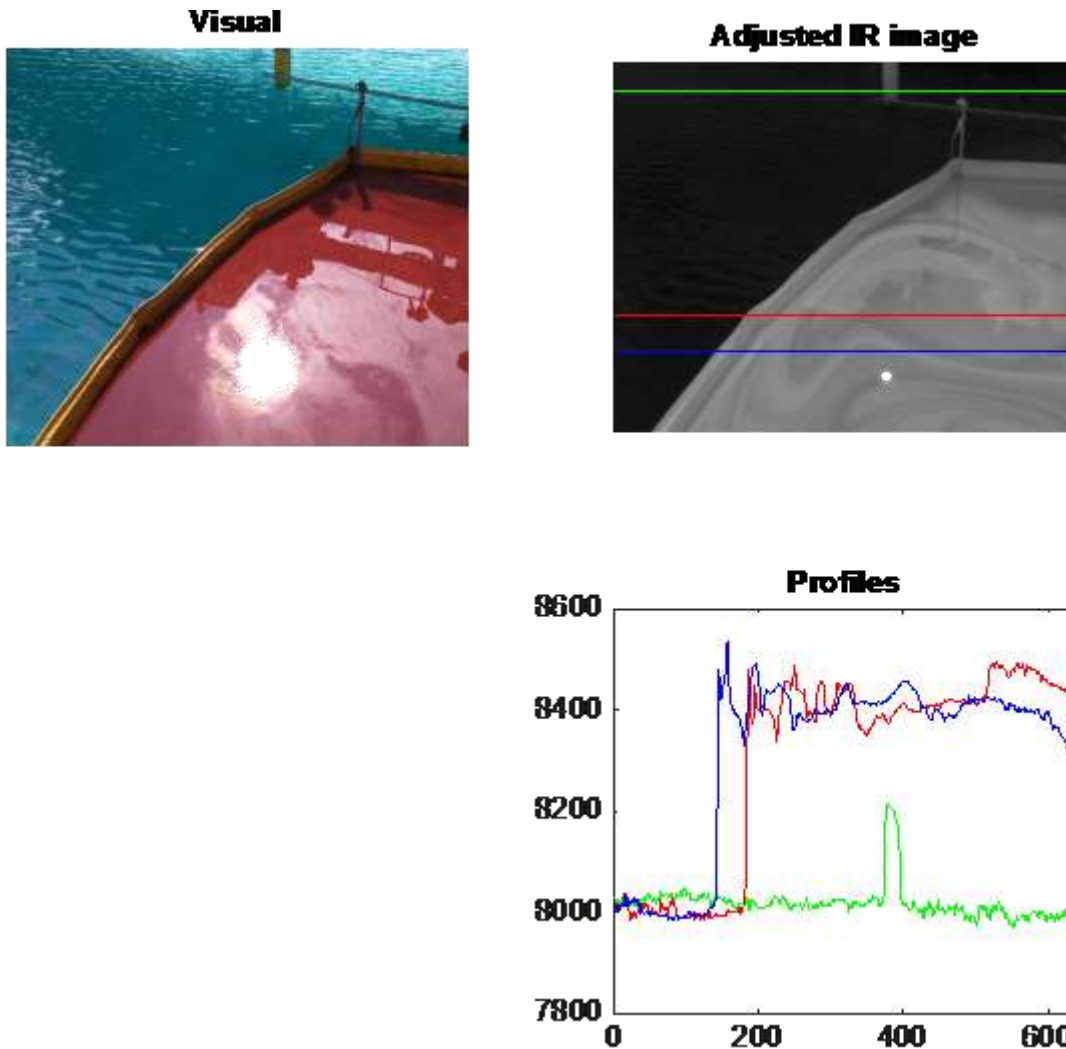


Figure 66: An example with sun reflection. Each line in the graph represents measurements along the respective lines in the adjusted IR image.

Figure 67 shows an example assessing the spatial consistency of the IR data; specifically responding to the question “Did the distance from the IR sensor to the oil impact the ability to sense the oil?” The slight curvature in the data is most likely a cause of distortion from the IR camera lens.

- A visual image of the captured scene is shown on the top left. While a small section of land appears in the lower left, the field of oil mostly fills the image.
- As shown on the top right, the IR image demonstrates that the oil temperature is fairly consistent (the image is a flat gray). To further verify this, four horizontal profiles were selected at varying distances from the IR sensor.
- The graph shows that the amplitude of the IR data along the four profile lines is reasonably constant (the step on the green profile is due to the land portion of that slice).

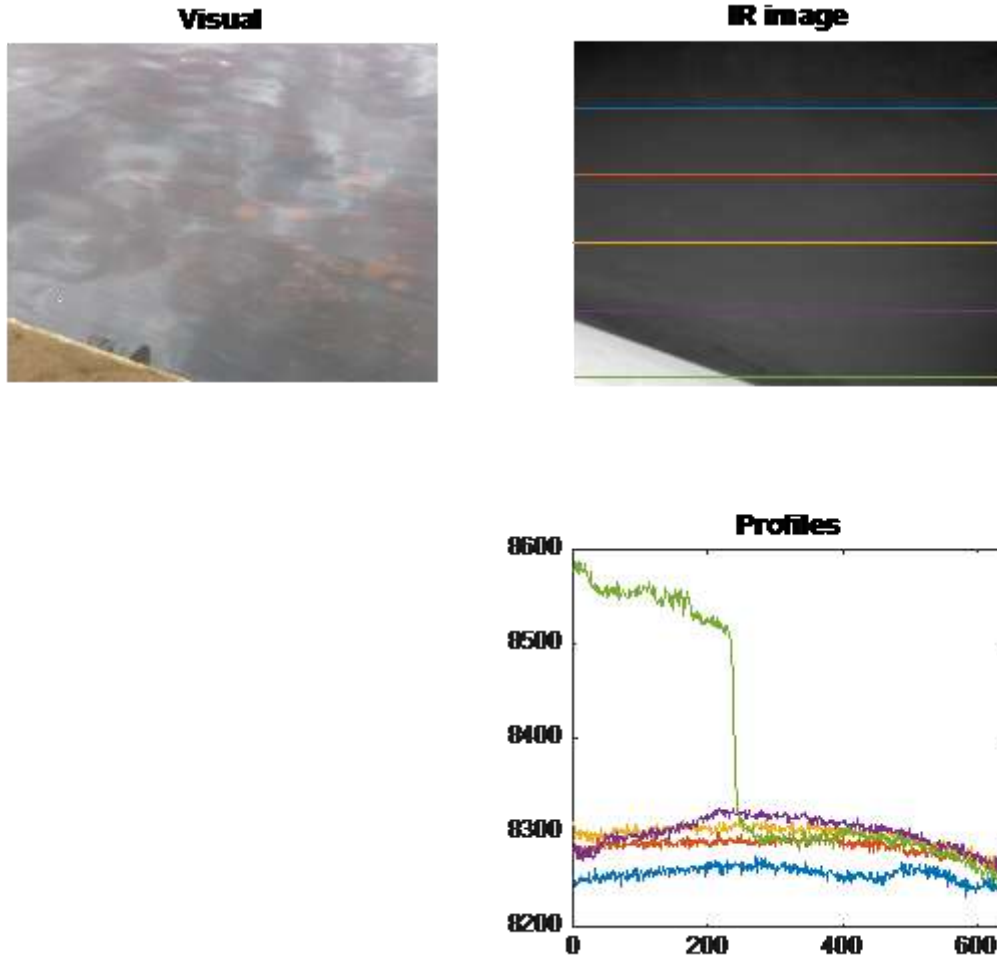


Figure 67: IR profiles versus distance for a relatively uniform oil layer.

The final two Ohmsett examples compared the thermal IR sensor data to that of that of two floating sensors; Figure 68 is for the Arjay sensor and Figure 69 for the GE sensor. In both cases the IR and floating sensor data is scaled/normalized to allow for a visual comparison. The data is from the boom/skimmer configuration of Figure 62 through Figure 65 ; in this case the IR data corresponds to the measurement at a single point close to the floating sensor over the duration of the skimming test (one IR point per image frame in a sequence of images corresponding to 2 or 3 oil regions). In Figure 68 two such deposits are evident in both traces. Figure 69 has three visible oil deposits. Observations were:

- Both sensors (as expected) show equal time duration for the presence of the oil.
- The IR data is “noisier,” especially in periods when no oil is present. One explanation is that it was difficult to keep the IR location constant over the test in that the IR sensor was not located on the skimmer vessel; hence, the sensors constantly moved relative to each other. Another explanation is that there actually was some oil in between the patches and the IR sensor was reacting to this very thin layer.
- The two floating sensors exhibit delay in their respective responses. Both upon entering and exiting the oil regions the depth sensors experience a time delay until the response has stabilized at a constant value. It is likely that this delay on the downward response is

due to oil sticking to the sensor itself. Both the upward and downward delays might be due to an averaging operation within the sensor itself; the IR data is frame by frame with no averaging.

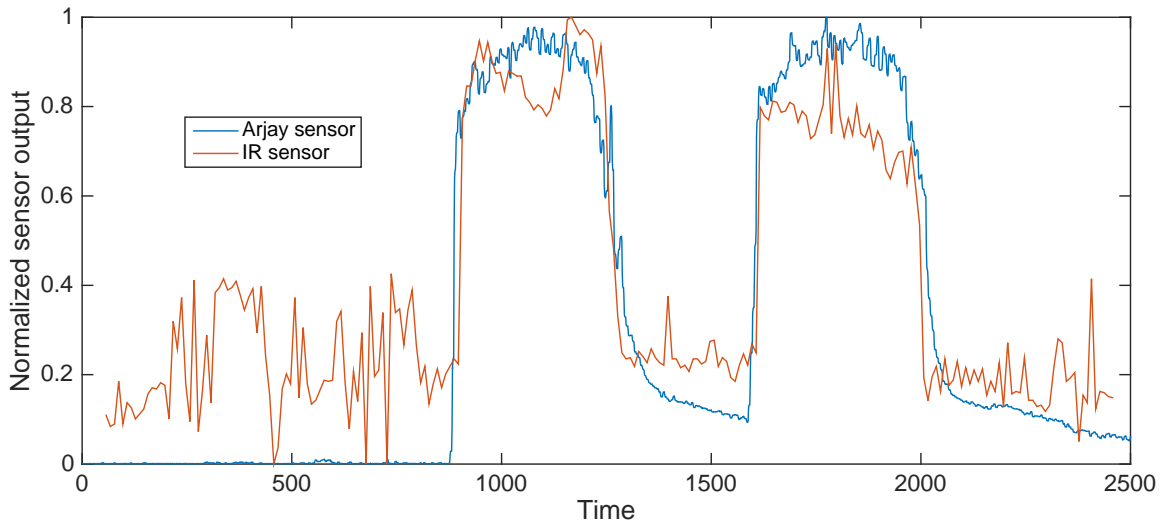


Figure 68: Time sequential data – comparing the normalized IR sensor data to that of the Arjay floating sensor.

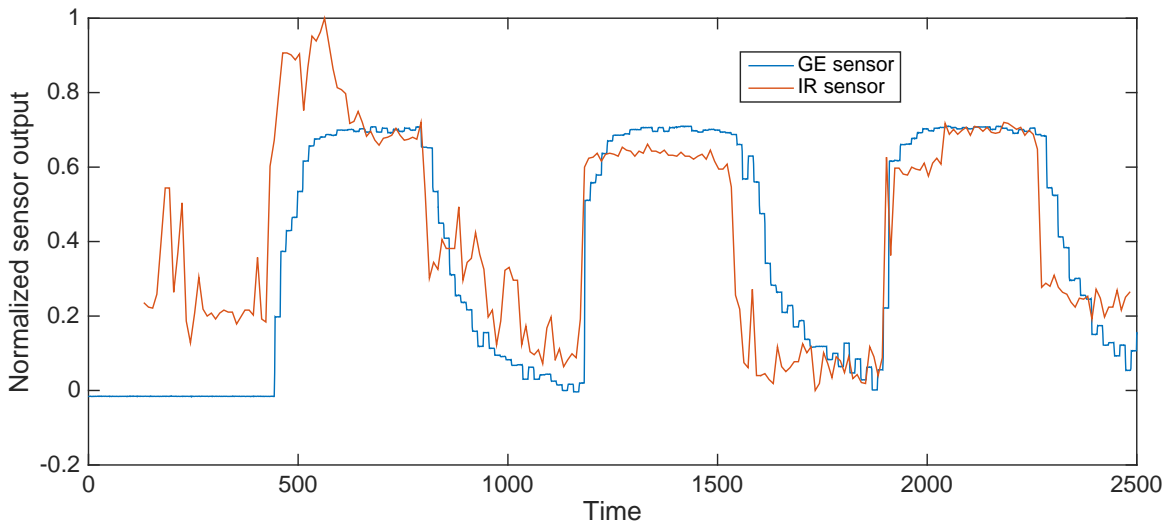


Figure 69: Time sequential data – comparing the normalized IR sensor to that of the GE floating sensor.

To better assess the ability of the IR data to show relative thickness of the floating oil Alion test engineers constructed a simple lab testing setup. In this simple test setup four thin-walled plastic cylindrical containers were suspended in a 100-gallon tub of water. Different amounts of oil were placed within the containers; the resulting depths from left to right were: 5.5 mm, 9.8 mm, 15.3 mm, and 19.7 mm, respectively. A variety of tests were performed to help classify the response of the oil. One such test regimen involved heating the surface of the tank using IR heat lamps pointed with a low angle of incidence to limit any heat reflection towards the lens. Different water temperatures were also considered; in these cases water temperature was

controlled using an aquarium heater at the bottom of the tank. In Figure 70, the red dotted line marks the location of the IR profile, the actual temperature measurements are indicated by the solid red line. It is clear from this profile that the thicker the oil, the higher the IR response. For all of the tests involving IR radiation to the top of the tank the same result was achieved.

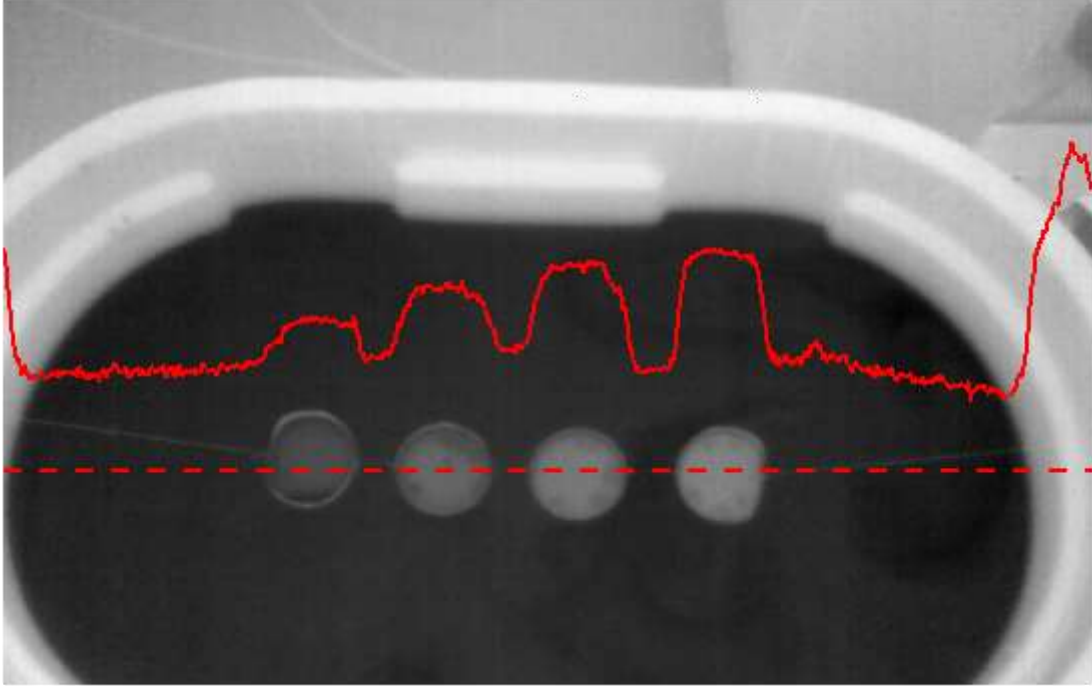


Figure 70: IR image and temperature profile for different thicknesses of oil using IR lamps to heat surface of the tank.

During the lab testing, equilibrium results were also considered. For these tests the water and oil were allowed to reach the same temperature without any radiant surface heating from the heat lamps. Figure 71 through Figure 73 show results of thick and thin oil. The two left containers contain 1 mm of oil while the other two contain 20 mm of oil. Thickness is still distinguishable but with a smaller difference than when heated. Again the distortion of the IR lens is noticeable in the positive and negative slopes at the outside edges of the readings. It is of note that the water remained at the same temperature as the surrounding air during these tests. If cooler air were introduced, we would expect to see the oil actually appear darker (cooler) than the surrounding water [Jha2008]. Figure 73 clearly shows the effect of the lens distortion towards the outer edge of the images. This is an effect that can most likely be compensated for with sensor calibration.

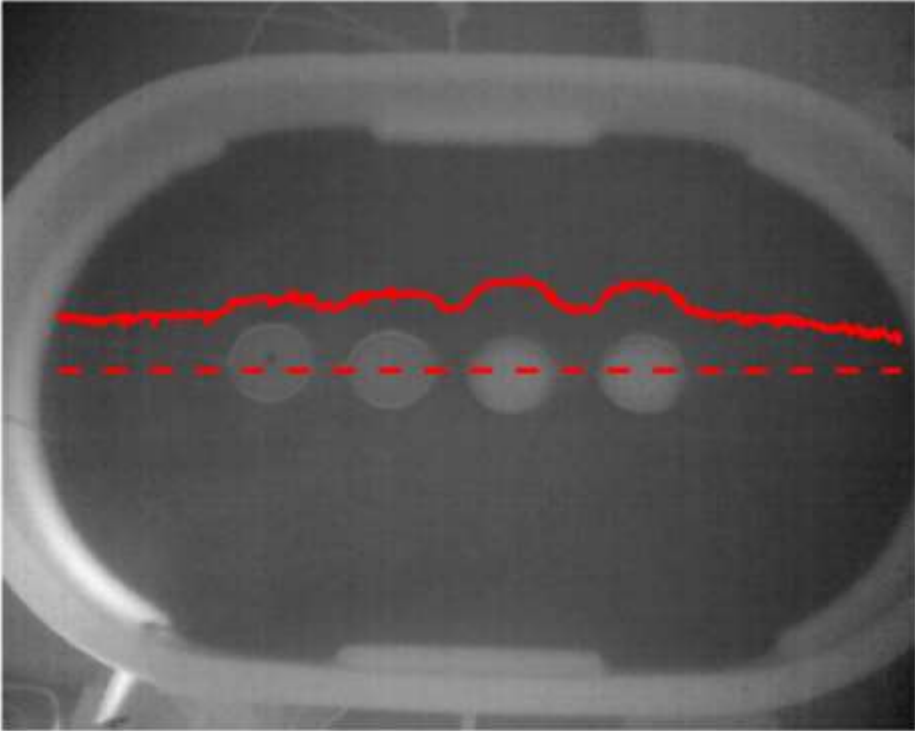


Figure 71: IR image and temperature profile for thick and thin oil at equilibrium.

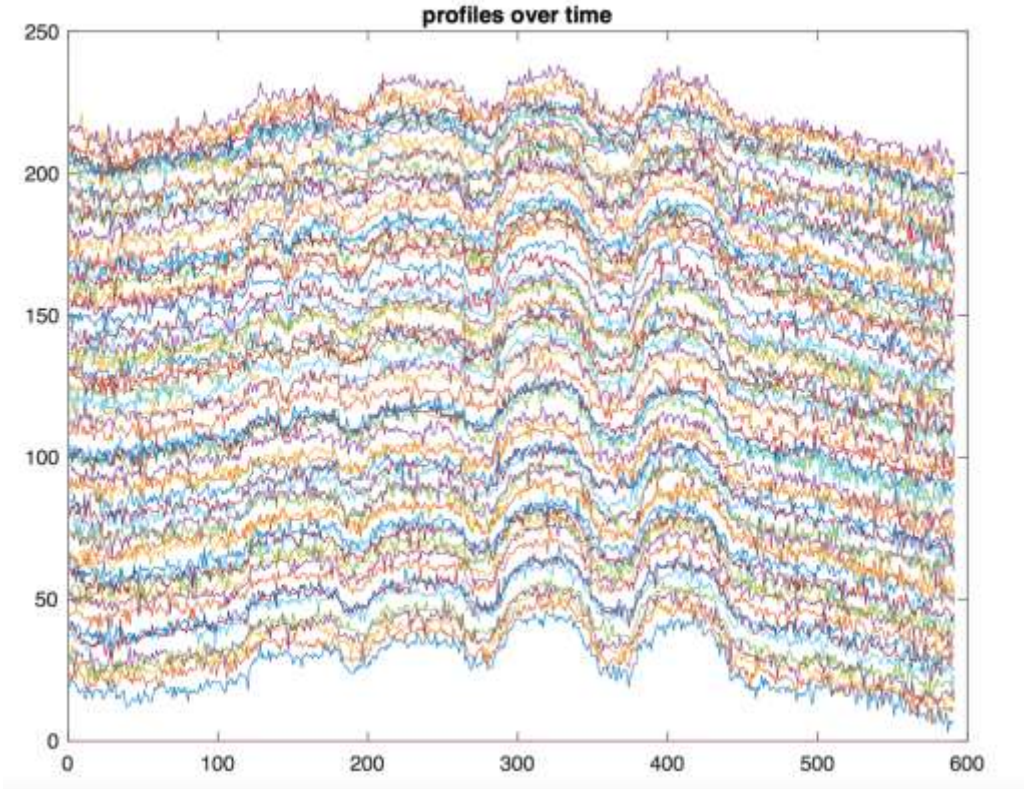


Figure 72: IR image and temperature profiles over time for thick and thin oil at equilibrium.

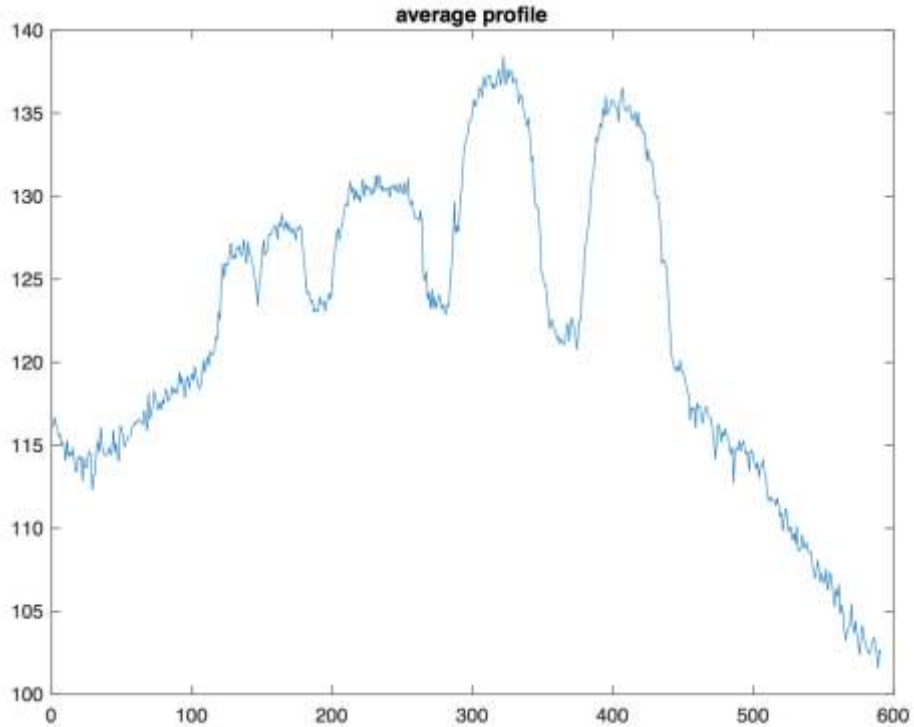


Figure 73: IR image and temperature profile for different thicknesses of oil.

One final test was conducted using Hydrocal outdoors to assess typical environmental conditions of sunlight and shadow. Specifically, the tank with four cylinders of oil (thicker to the right) was moved outdoors with data collection occurring over a 13-hour period; two examples from that test are shown in Figure 74 and Figure 75. In both cases the top image shows a visual of the setup while the bottom image is the IR data superimposed with the location and temperatures along a horizontal profile:

- Figure 74 was from the morning when the tank was in full sunshine. The temperature profile was as expected; large jumps in the IR reading at the oil edges with the amplitude of each jump dependent upon the oil thickness.
- Figure 75 is from late in the afternoon when the tank had been in shadow for some time; as observed in the temperature profile, the oil now appears colder (!) than the oil.

In both instances, the difference between the oil and water is easily recognized, even without any advanced image processing. Given that the IR measurements should be continuous with respect to time, there should have been a point during the day when the water and oil appeared to be of equal temperature; unfortunately, our data collection rate (one frame every 20 minutes) did not catch this instant. This effect was also exacerbated by high winds, which quickly cooled the oil surface.

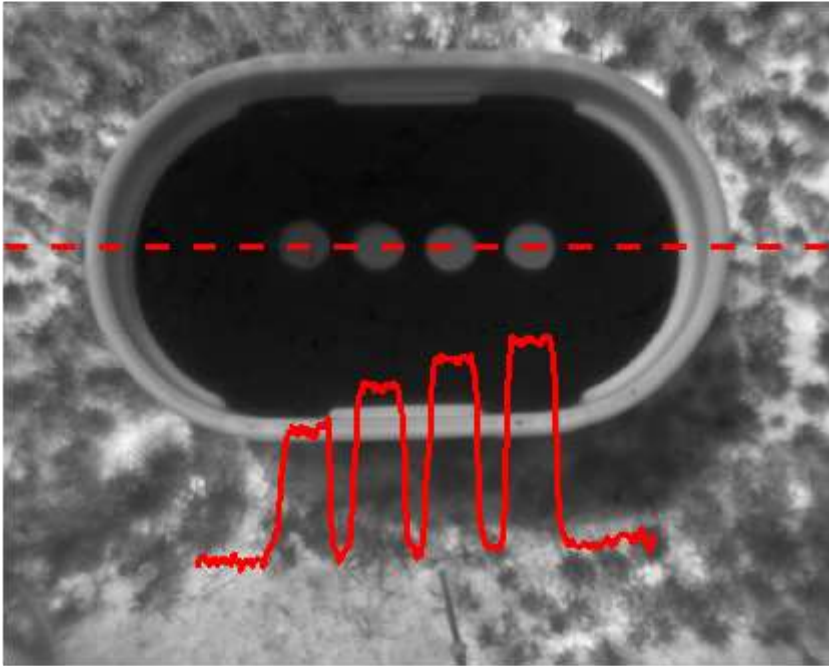


Figure 74: Outdoor data showing typical results: top is visual, bottom is IR with profile location (dotted) and temperature (solid). As previously seen, the oil appears warmer than the water.

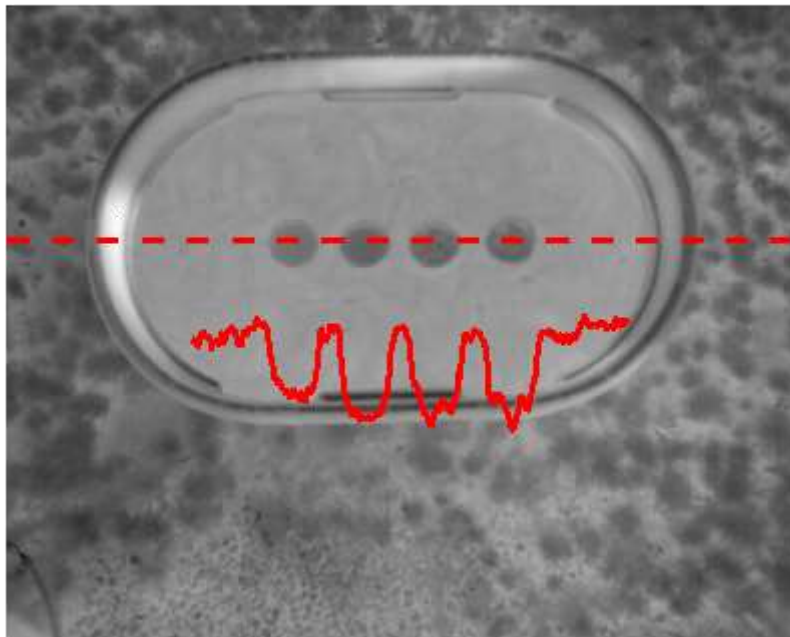


Figure 75: Outdoor data showing (temperature) reversed results: top is visual, bottom is IR with profile location (dotted) and temperature (solid). In this case the water appears to be warmer than the oil due to the lack of solar radiation and cooler surrounding air and wind.

In summary:

1. The experimental results suggest that the IR sensor is effective at locating floating oil and that relative thickness can be sensed. This is clear from Figures 62 - 67.
2. In comparison to the floating sensors, the IR sensor provides additional spatial information; not just the thickness at the sensor location but also for an adjacent area.
3. When properly mounted above the water surface, image processing of the IR data can provide information for navigating the skimmer to stay within the thickest region of an oil spill.
4. Waves and chop did make the IR data noisier; however, this can probably be reduced/eliminated by averaging over multiple IR images.
5. While some variation with distance from the sensor is possible, it seems small. If this is due to lens distortion, it can be measured and corrected for.
6. Surrounding environmental data such as the level of solar radiation, air temperature, water temperature, and wind will need to be taken into account to develop and implement different profiles used for determining the presence and thickness of oil.

These comments, especially numbers 3 and 4, suggest that an IR-based system would have significant performance advantages over the floating sensors – specifically, the ability to sense oil over a larger region and the (likely) insensitivity of the IR process to waves – hence, the use of IR sensors merits additional exploration.